Modeling of Trim Panels in the Energy Finite Element Analysis

by

Seyed-Javid Moravaeji

A dissertation submitted in partial fulfillment
of the requirements for the degree of
Doctor of Philosophy
(Mechanical Engineering)
in The University of Michigan
2008

Doctoral Committee:
Professor Nickolas Vlahopoulos, Co-Chair
Assistant Research Scientist Aimin Wang, Co-Chair
Professor Karl Grosh
Associate Professor Bogdan Epureanu
Associate Research Scientist Matthew P Castanier

To my Family

ACKNOWLEDGEMENTS

Funding support for this research has been provided by NASA in connection with the department of Naval Architecture and Marine Engineering at the University of Michigan. I appreciate the effort Professor Vlahopoulos put into providing this support to me. Also, I am grateful to Dr. Wang for spending long hours with, me discussing different problems that I faced during this work.

I would like to thank Professors Grosh and Epureanu and Dr. Castanier from the Mechanical Engineering department for setting aside their valuable time while serving on my committee. Specially, I would like to express my personal gratitude to Professor Grosh for his invaluable advise and support during my hardest time.

I am in great debt to Mrs. Christine Feak from English Language Institute for providing generous advice on the communication aspects of this work.

Finally, I cannot thank enough my family for their love and support.

TABLE OF CONTENTS

LIST OF FIGURES

Figure

NOMENCLATURE

a: Joint radius
b: Damping between solid and fluid phases of a porous medium
c_i: Wave speed
e: Dilatation
f: Frequency or force
i: unit imaginary $\sqrt{-1}$
k: Wave number
r: Coordinate (cylindrical)
t: Time
u: Displacement
v: Velocity
x, y, z: Coordinates
A, C: Wave amplitude
$\mathcal{A}$: Cross sectional area of a beam D_B, D_I: Plate rigidities
E: Young's modulus
F: Force
$\mathcal{I}_{yy}$: Moment of area of a beam
L: Length or Thickness
M: Moment
P: Porous material Lamè constant, Power
$[Q]$: Wave matrix relating wave amplitudes vector to displacement vector
Q_p, R_p: Porous material constant
R_{ref}: Reflected wave amplitude
$[S]$: Wave matrix relating wave amplitudes vector to force vector
$[T]$: Transfer matrix
U: General displacement vector
X, Y, Z: Coordinate sytem α: Power flow coefficient
γ_0 Specific heats ratio for air
δ_{ij}: Kronecker delta function
ϵ_{ij}: Strain component
ϵ': Foam structural shape factor

ζ: Plate mid-plane coordinate or viscosity of fluid

η: Plate mid-plane coordinate or loss factor

θ: Coordinate (angle in cylindrical) or Incident wave angle

θ_i: Angle of rotation about axis i

κ: Wave number

λ: Lamè's constant

λ_c: A parameter in liquid bulk modulus expression

μ: Lamè's constant (shearing modulus)

ν: Poisson ratio

ξ: Plate mid-plane coordinate

ρ: density

$,\sigma,\sigma_r$: Flow resistivity

σ_{ij}: stress component

τ: Transmission loss

τ_{ij}: Shearing stress component

ϕ: Porosity

ϕ_i: Velocity potential

χ_{ij}: Porous wave number parameter

ψ_i: Velocity (rotational) potential

ω: Rotational frequency

$[\Gamma]$: Matrix relating wave amplitude to velocity/stress vector

Φ: Porosity or velocity potential vector

$[\Upsilon]$: Partial open pore interface matrix

ABBREVIATIONS

B: Bending (waves)
B: Bonded (layered materials)
BC: Boundary Condition
c: closed pore (porosity vector)
EB: Euler Bernoulli
EFEA: Energy Finite Element
f: fluid phase (superscript)
F: Far-field (wave)
FEA: Finite Element Analysis
I: Incoming (wave)
L: Longitudinal (wave)
N: Near-field (wave)
o: Open pore (porosity vector)
O: Out-going (wave)
p: porous (superscript)
s: solid phase (superscript)
T: Torsional (wave)
TF: Transfer Function
TL: Transmission Loss
SEA: Statistical Energy Analysis

ABSTRACT

Modeling of Trim Panels in the Energy Finite Element Analysis

by

Seyed-Javid Moravaeji

Co-Chairs: Nickolas Vlahopoulos and Aimin Wang

Modeling a trim panel is divided into finding the power exchange through two different paths: i) the connection of the outer and inner panels ii) through the layers directly. The vibrational power exchanged through the mounts is modeled as the connection of two parallel plates connected via a beam. Wave matrices representing plates and beams are derived separately; then a matrix method is proposed to solve for the wave amplitudes and hence the vibrational power exchange between the plates accordingly. A closed form formula for the case of connection of two identical plates is derived. For the power transmission loss directly through the layers, first transfer matrices representing layers made of different materials is considered. New matrices for a porous layer are derived. A method of finding the layered structure transfer matrix is proposed. It is concluded that in general a single isotropic layer cannot replace a structure accurately. Finally, on the basis of an equivalent transfer matrix, an optimization process for is proposed to replace the panel by a suitable set of layers.

CHAPTER 1

Introduction

1.1 Research Overview

Noise treating materials have been used very often in many structures to reduce the noise level. The instances where these materials are used are but not limited to cars, air plane fuselage very often these structures consist of layers of treating materials in between the structural elements. Since the treatment materials do not have a significant role in supporting the structure forces, usually the structural elements are joint directly with the treating materials going in between. Therefore, a typical panel treated with noise reduction materials can provide two paths for the sound energy to be transmitted from the generated side to the other side. Hence the noise transmission via the mounts and through the layers of the structure should be considered separately.

The common tool for analyzing a complex system is the traditional finite element. However finite element analysis is not always the right tool for analyzing structures. This is due to the fact, that as the frequency of the vibration increases, finite element method needs a refiner mesh which is computationally more expensive. Also, finite element analysis is a deterministic method while the nature of noise is more appropriate for dealing with the noise transmission in structures [1]. Statistical energy analysis that addresses the analyzing the structural vibration in higher frequency better has been mostly developed by Lyon and his colleagues [2]. In this method, a complex structure is divided into subsystems which have similar modal densities. It is assumed that the vibrational energy of these subsys-

tems (similar to heat conduction) move from sub-systems with less modal densities to other subsystems which have higher modal densities. The main variable in this method is the total energy of a subsystem.The main difficulty with SEA is to find the couplings between the systems. This coupling is set up by coupling loss factors which by themselves are not very straightforward to be determined. Also, if the lumped systems are highly coupled the method loses its accuracy and the lumped subsystems must be redefined [3]. It should be remarked that SEA is rather a very specialized method and unlike the commercially available FEA software does not have a broad number of users.

As an alternative to statistical energy method, "Energy Finite Element" method has been developed to deal with the noise analysis problem; Bernhard's work [4] is one of the pioneers in this area. In energy finite element like the traditional finite element, the structure is broken down to smaller elements. However, the main variable is now the time and space averaged energy densities of the elements. To derive the energy finite element system of quotations, first the governing differential equations of the energy terms one derives from the primitive elements such as no beams and plates. In this process, the near field terms of the incoming waves are ignored. After the waves are ignored the governing equation of the energy densities are found. Finally a finite element formulation is developed to provide a system of equations for the element level [5]. This system of the equations, relates the model energy density vector of the element to the input model power vector and the vector of power flows across the elements. Each element now should be connected to the adjacent elements in such a way that the poser flow stays a continuous function. The averaged power flows of adjacent nodes can be related by a power transmission or joint matrix. At the geometrical or material discontinuities, the energy densities are not necessarily continuous. Validation, formulation, and implementation of this method have been developed in the past years (for example see [6, 7]), the modeling of a trim panel, is mainly concerned with the finding joint matrices for the connections of the panel. The response of the complex structure is obtained by the discretizing the structure into smaller well known elements. The vibrational behavior of simple geometry structures like plates and beams are already well known for instance Cho [8] has derived the formulations for beam and homogenous plates connections. To model a trim panel, two different energy paths should be taken into account: energy

transmitted through the outer and inner layers via mounts and the direct path of energy through the layers.

In this dissertation, the joint matrices for two different paths of noise energy are calculated for the energy finite element. First, the vibration power transmission between two plate elements via a beam or a spring is found; then a method for finding the equivalent element to replace the layered structure between the inner and outer acoustic media is proposed.

1.2 Literature Review

In this section, the existing literature for tools needed to find the power transmission matrix between point connected structure as well as the analysis of layered structure including porous layers, are reviewed. Point Connected Structures The problem of finding the power transmission coefficient between two plates connected through a beam needs the modeling of the plate elements and the beam.

1.2.1 Beam and Plate models

The vibration behavior of the beams have been studied thoroughly for example, Graff [9], Redwood [10], Achenbach [11], Cramer [12] are among the classical books to consider the beam vibration problem.

The simplest model of vibration of a beam is obtained when the beam is considered slender and the shear deformation effect and rotary inertia effects are ignored. As it is often mentioned in classical references, if these effects are added to a general beam model, a more accurate model called Timoshenko beam is obtained. In fact, the most general problem of vibration of a beam is considered by analyzing the vibration of a solid cylinder [9, 10] Such a model can be reduced to an Euler-Beronoulli beam model (which is quite accurate for the present purposes) when the beam is considered slender. Banerjee [13] has derived a more complex dynamic stiffness matrix for a more general pre-twisted Timoshenko beam.

Plate vibrational behavior has also been studied vastly. The common, simple plate model used is the Kirchhoff thin plate. The assumptions and limitations of the thin plate

model can be found in classical plate books like Leissa [15] and Szilard [16]. As the first approximation, only the out of plane or bending vibration of thin plates is considered. The bending motion of a thin plate is governed by a 4th order partial differential equation [12, 15, 16]. The general solution of this partial differential equation in the polar coordinate system can be expressed in terms of the Hankel and or Bessel functions. By means of three dimensional equation of motion, Morfey [17] showed that the in-plane vibration solution for a thin plate also have a very similar form. The in-plane and out-plane displacements of an elastic thin plate can both be expressed in terms of Hankel modal functions. In general, in-plane and out-plane vibration fields of a plate are not decoupled; Ljunggren [18, 19] has shown that a force applied on the origin of the plate that generates both in-plane and out-plane motions. In his work, the displacements and forces are expressed as infinite series which can model plate with any favorable accuracy.

Important quantities which can validate any plate model are different plate impedances since impedance relates forces to the displacements. Different impedances can be calculated for different loadings acting on a plate. A relatively complex in-plane moment impedances has been derived by Dyer which for small arguments is in accordance with the expression given by Crammer [12]. Ljunggren [18, 19] found two torsional impedance expressions for systematical and antisymmetrical modes of a thin plane. Further impedance studies which can verify a plate model can be found in works of Leung [20], Pinnington[21] , and Thomas [23].

Langley and Shorter, derived a model for a thin plate [24]. This model which has been used in this work, basically is a rigid disk inclusion inside can elastic thin plate infinite region. They have related the wave amplitudes of outgoing waves to the displacement and force vectors acting on the origin of the plate.

1.2.2 Porous Materials

A porous medium is modeled as a macroscopic homogeneous continuum which is consisted of two phases in equilibrium: a solid phase and a fluid phase. The solid phase is a porous matrix where the fluid phase fills the pores. The filling fluid can be quite light such as air or heavy like water. The fluid phase may be modeled as a simple inviscid fluid or may

be represented by a more mathematically complicated fluid constitutive law. Compared to the fluid, the solid matrix may be often (specially in higher frequency range and smaller flow resistance) assumed to be rigid [25, 26]. Modeling of porous media is drastically influenced by Biot's work [27]. In his model,it is concluded that a porous media can carry two dilatational waves and one shearing waves. Also there is a mathematical analogy between the thermoelasticity and poroelasticity [26, 29].

The development of poroelasticity was originally motivated from geophysics and studies of soil. Poroelasticity has been successfully used to model material systems in different fields of study such as seismic waves, rock and soil mechanics, sea-bed studies, biomechanics and biomaterial, and noise insulating materials; (e.g. [26]). As an example, elastic porous material theory has been employed to investigate bones. Although compared to the hard component of the bone, the inside fluid has a very small bulk modulus,the dynamic load effects of the fluid cannot be ignored. In other words, a slowly loaded drained bone does not respond much differently from a bone with the fluid inside; however, this is not quite true if the forces are dynamic [26].

A special type of porous material is the noise treatment foam material; in these materials, the fluid phase is simply air. The constitutive law of an open cylindrical shape pores foam material involves seven solid phase constants [28, 25, 30]: porosity; solid phase Poisson's ratio; structural shape factor; flow resistivity; solid phase structural dissipation factor; solid phase Young's modulus; the solid phase density. Deresiewicz and Skalak [41] argued that there are three possible type of contacts for a porous surface; then they derived the mathematical equations for the boundary conditions that describe the surface condition of a porous layer. Gurevich and Schoenberg [42] demonstrated that Deresiewicz and Skalak conditions can be recaptured by replacing the porous surface with a layer of an ideal fluid whose permeability is proportional to the layer thickness as the thickness tends to zero.

Allard and Bolton [28, 30] used this model to express the displacement and force fields of a porous layer in terms of wave amplitudes and these material constraints.

1.2.3 Layered Structures

Very often an infinite layer can be a very suitable model for a structures. Such a layer is like an plate; i.e. the dimension along one axis is very large comparing to the thickness and the variation of the plate along the third axis can be ignored. In many occasions, a structure consists of a stack of such layers. For each layer, once the displacement field of such layer is known, the force field can be derived accordingly. The equations of waves propagating in a layered structure can be determined after applying the boundary conditions at the interfaces of the adjacent layers. To deal with this problem, it is possible to set up a large number of equations (according to Brekhovskikh [31] about four times of the number of layers) and determine the wave amplitudes. Then by substituting the wave amplitudes back into the field equations, the displacement and forces can be calculated. This is the approach used by Bolton [30] and some of Allard's works [33]. However, another method of dealing with a system of layered structures is using a matrix approach [31, 32]. The advantage of using transfer matrices is that once the library of different layer matrices are developed, finding the response of the structure is done much easier and by multiplying a set of matrices instead of solving a large number of equations (at least 4 times the number of layers).

To use the matrix method to reduce a layered structure matrix, Allard [33] have derived a transfer matrix for solid layer; however, their matrix is incorrectly reported for $e^{-i\omega t}$ convention instead of $e^{+i\omega t}$. Network analogy of a solid layer to a electrical block diagram has been introduced by Rudgers [34]. Cerevenka and Challande, and Folds and Loggins [35, 36] have also developed a computational algorithm for the matrix method when the layers are comprised of a combination of fluids and/or solids. Moore and Lyon [37] used the impedance matrix method for analyzing geometrically symmetric panels with and without soft cores, cited that the accuracy is limited when the thickness is (relative to frequency) is large.

Driving a transfer matrix for a porous layer has been first done by Allard and his colleagues [39, 40]. The boundary conditions applied on a layer are not simply enforced by equating the displacement and force fields of two adjacent layer when one of the layers

is porous [41, 42]; they defined different joint matrices to enforce the boundary conditions [33, 28].

A foam layer with a complex model and too many material constants is not easy to deal with. Empirically a foam layer can be replaced by an equivalent layer with a complex companion to the wave speed and density [43, 47]. This model is different from a dissipative fluid model that includes the viscous effects that add an imaginary part to the wave number. Another attempt to replace a foam layer is made by [45]. They retained only one of the main waves by defining an energy criterion and approximated the foam layer by an equivalent un-bonded layer.

1.3 Dissertation Contribution

In this research, the problem of modeling of trim panels in EFEA is considered. The most important part of the modeling is actually finding the vibrational power coefficients for a trim panel. There are two possible vibration energy exchange paths: though the layers and via the supporting mounts.

The vibrational power transmission via mounts is modeled as the power exchange between two infinite plates which are connected via a finite length beam. For the power transmission directly through layers, a matrix method which already exist in the literature is extended for the structures which consist of porous layers. By means of the matrix approach an optimization procedure to replace the layers of trim with new layers is proposed.

The following is a summary of the main contribution of this dissertation:

- A matrix method is developed to study the vibrational behavior of point connected structures. In this method, the structural components are identified by means of two matrices; one relating the displacements vector to the wave amplitude vector and the other one relating the force/moment vector to the wave amplitude vector. These matrices for a beam and a plate element are derived and coded. This approach simplifies the previously reported complicated calculations of the power transmission coefficients for the beams [8] drastically.

- The problem of vibration exchange between two arbitrary plates which are connected via a beam or spring is solved through a more sophisticated method than the impedance method.

- A closed form formula that relates the main bending modes of two identical plates connected via a beam (or spring) is found.

- For the used plate model (a rigid disk inclusion in an infinite annular elastic region) closed form formulas for different plate impedances are found.

- A systematic approach for reducing a layered structure is proposed. In this new approach, layer materials can be fluid, solid, or porous.

- Transfer matrices for common models of layers (fluid, solid, and porous) are derived. Solid layer transfer matrix for the $e^{i\omega t}$ which is reported incorrectly [33] is re-derived. Also, a correction is made to the transfer matrix for a transversely isotropic solid layer by Brekhovskikh [31]. New transfer matrices "bonded bonded" and "unbonded unbonded" for a porous layer are derived in order to make the calculations faster and easier.

- A new layer reduction process is proposed to replace the core layers of a structure which includes a foam layer. This approach can be used to replace a sandwich by three elements in EFEA. It is shown that in general a layered structure cannot be replaced by a single solid isotropic or fluid layer.

1.4 Dissertation Overview

In chapter 2, the dynamic wave matrices which relate the displacements and forces to wave amplitudes are derived for beams and an infinite plates. By using these matrices, the problem of vibration power exchange between a beam perpendicularly connected to an infinite plate is solved and validated. The plate impedances are further compared with the impedances from the existing models.

In chapter 3, the problem of vibrational power exchange between two parallel plates

connected via a beam is solved and validated. A closed form formula is given for a special case of identical plates. Also, the significance of the different wave types are discussed through a numerical problem.

In chapter 4, First the wave equations for a porous media is considered. Then wave equations for fluid and solid layers, as a special case of the porous layer, are found. The boundary conditions for a porous surface is discussed and on the basis of these boundary conditions, transfer matrices for fluid layers, unbonded and bonded solid layers, thin panels, and porous layers are derived.

In chapter 5, a systematic way of expressing the transfer matrix of a sandwich structure between two acoustic media is proposed and the transmission loss calculation is found in terms of the matrices. Further, it is argued that in general a combined layered structure cannot be replaced by a single isotropic layer. Then an optimization procedure for modeling the core layers of a layered structure is proposed.

CHAPTER 2

Modeling of Point Connected Systems

2.1 Introduction

Many structures are consist of components joined that require a very small region. These small area connections may be modeled as joints or point connection. In the following, these point connected structures are modeled and analyzed by combining the vibrational properties of their simple components. The vibration power transmission for these point connected structures can be found and used for EFEA.

The vibrational behavior of structures with simple geometries like plates and beams has already been successfully analyzed. Wave equations for rods, beams, and plates are readily available. Depending on the frequency range, to predict the response of these simple geometry components, simple models may be exploited. When the frequency is not too high the Euler-Bernoulli (EB) model for beams, and the Kirchhoff model for plates can accurately predict the vibrational behavior of the simple components. The frequencies for which these models are suitable, depend on the dimensions of the components; i.e. the wave lengths need to be large enough. This is why when using the traditional finite element analysis (FEA) for studying structures, finer meshes are required as the frequency increases. The traditional FEA is not always the right tool for analyzing structural vibration in higher frequencies since: a) a very fine mesh makes the FEA computationally expensive or even impossible b) the nature of the noise is rather statistical than deterministic; a deterministic computational method cannot provide a very accurate average analysis c) the results will

be sensitive to the structure detail and small changes in the design can lead to results that are unusable [1].

One well-known technique to predict the vibration response in higher frequency ranges is Statistical Energy Analysis (SEA). This method relies on discretizing the structure into groups of similar normal modes which are called subsystems. The energy of each subsystem is the main variable that SEA deals with. Energy flows among the connected subsystems under the assumption that energy travels from a subsystem with a higher average modal energy to a system with a lower energy. This energy flow is very similar to the heat transfer from a higher temperature region to a lower temperature region. In addition to this assumption, SEA assumes that the dissipated energy is proportional to the model energy; finally, as the name suggests, it is assumed that the energy has a statistical nature [2].

The main difficulty with SEA is to find the coupling between the systems. The couplings are established by coupling loss factors which cannot be determined in a very straightforward way. Also, if the lumped systems are highly coupled the method loses its accuracy and the lumped subsystems must be redefined [3]. From a practical point of view, SEA is rather specialized and unlike the commercially available FEA software is not widely used.

One alternative to SEA is the Energy Finite Element Analysis (EFEA) that may be used to analyze the vibration of the structures in the higher frequency range. EFEA main variable is energy density. To drive the EFEA system of equations, first the governing differential equations of the energy terms related to the far field waves are derived for the primitive elements such as beams and plates, as well as the acoustic medium (all are considered lossy) [5]. Then the governing equation of the space and time averaged energy densities, are found for these regions. Finally, a finite element formulation can be developed provides a system of equations for the element level. This system of equations, relates the nodal energy density vector of the element to the input nodal power vector and the vector of power flows across the element. The averaged power flow can be related to the nodal averaged energy densities through a power transmission matrix or joint matrix. The averaged energy densities of the adjacent nodes at the geometrical or material discontinuities are not continuous; however, by applying the power (energy) conservation, the joint matrices that relate the adjacent

nodal energy densities can be determined. At this point, the system of equations can be assembled into a linear system and solved for the energy densities.

In this chapter, first the beam and plate wave matrices are obtained; the wave transmission problem for a semi-infinite beam and an infinite plate connection is solved. Finally, the joint matrix for a vertical beam connected to an infinite plate is found.

2.2 Wave matrices for a slender prismatic beam

The vibration of a beam can be accurately explained via an EB model if the frequency is low enough. A beam can guide three wave types: longitudinal, torsional, and bending. When the frequency is small enough, the first modes of beam vibrations can accurately capture the beam vibration behavior. It is known that these wave types are decoupled when the first modes are only retained [9]. Since two perpendicular planes can have independent bending vibration, two bending waves propagate along the beam's length.

To keep the analysis simple, assume that the shear center of the beam lies on its section neutral axis. To find wave matrices, a Cartesian coordinate system may be chosen such that the Z–axis lies on the central axis of the beam as shown in figure (2.1). Now the goal is to relate the displacements and forces vectors to the wave amplitudes. It should be noted that the displacements vector contains both the linear and the rotational displacements. Also, the forces vector, includes the moments.

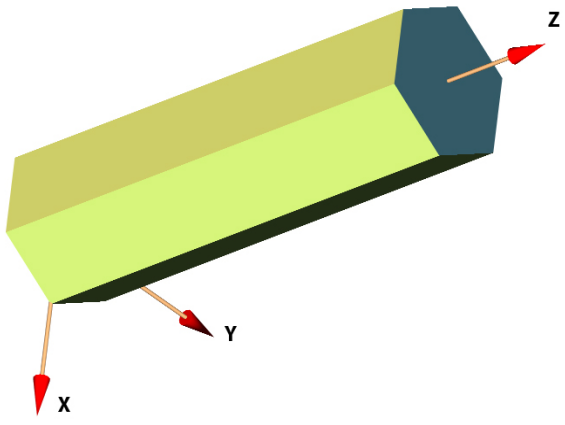

Figure 2.1: Coordinate system chosen for a beam

The governing differential equations of out of plane (bending) first mode wave propagation are of fourth order [9, 12]:

$$\frac{\partial^4 u_j}{\partial z^4}(z) - k_{B_j} u_j = 0, j = X, Y \tag{2.1}$$

while the the longitudinal and torsional waves are governed by second order equations [9, 12]:

$$\frac{\partial^2 u_z}{\partial z^2} - k_L u_z = 0 \tag{2.2}$$

$$\frac{\partial^2 \theta_z}{\partial z^2} - k_T \theta_z = 0 \tag{2.3}$$

The displacement fields for the positive time harmonic convention ($e^{i\,\omega\,t}$) are:

$$u_j(z) = A_{B_j}^{F,O} e^{-i\,k_{B_j} z} + A_{B_j}^{F,I} e^{i\,k_{B_j} z} + A_{B_j}^{N,O} e^{-k_{B_j} z} + A_{B_j}^{N,I} e^{k_{B_j} z}, j = X, Y \tag{2.4}$$

$$u_z(z) = A_L^O e^{-i\,k_L z} + A_L^I e^{i\,k_L z} \tag{2.5}$$

$$\theta_z(z) = A_T^O e^{-i\,k_T z} + A_T^I e^{i\,k_T z} \tag{2.6}$$

where A represents the wave amplitude, the subscripts B,T,L and superscripts F,N,O, and I indicate bending, torsional, longitudinal, far-field, near field, out-going and in-coming waves. The wave numbers are calculated as:

$$k_{B_X} = \sqrt[4]{\omega^2 \frac{\rho \mathcal{A}}{E\,\mathcal{I}_{yy}}} \tag{2.7}$$

$$k_{B_Y} = \sqrt[4]{\omega^2 \frac{\rho \mathcal{A}}{E\,\mathcal{I}_{xx}}} \tag{2.8}$$

$$k_L = \omega \sqrt{\frac{\rho}{E}} \tag{2.9}$$

$$k_T = \omega \sqrt{\frac{\rho(\mathcal{I}_{xx} + \mathcal{I}_{yy})}{\mu\,\mathcal{S}_T}} \tag{2.10}$$

where ρ,E,μ are mass density, Young's modulus, shearing modulus of the beam material and $\mathcal{A}$, $\mathcal{I}_{jj}$ and $\mathcal{S}_T$ are the cross sectional area, area moment about axis j, and the torsional rigidity coefficient of the beam.

Rotations can be computed from the displacements as:

$$\theta_j(z) = (-1)^{\delta_{jy}} \frac{\partial u_j}{\partial z}, \qquad j = x, y \tag{2.11}$$

where δ_{mn} is the Kronecker delta symbol. The displacement and the wave amplitude vectors can be defined as:

$$\{A_B\} = \{A_{BX}^{F,O}, A_{BX}^{F,I}, A_{BX}^{N,O}, A_{BX}^{N,I}, A_{BY}^{F,O}, A_{BY}^{F,I}, A_{BY}^{N,O}, A_{BY}^{N,I}, A_L^O, A_L^I, A_T^O, A_T^I\}^T \tag{2.12}$$

$$\{U_B\} = \{u_x, u_y, u_z, \theta_x, \theta_y, \theta_z\}^T \tag{2.13}$$

The following matrix relation between the displacement and wave amplitude vectors can be established:

$$\{U_B\} = [Q_B]\{A_B\} \tag{2.14}$$

By means of (2.4) - (2.6) matrix $[Q_B]$ is determined as:

$$[\,Q_B\,](z) = \begin{bmatrix} Q_{11} & Q_{12} & Q_{13} & Q_{14} & 0 & 0 & 0 & 0 & 0 & 0 & 0 & 0 \\ 0 & 0 & 0 & 0 & Q_{25} & Q_{26} & Q_{27} & Q_{28} & 0 & 0 & 0 & 0 \\ 0 & 0 & 0 & 0 & 0 & 0 & 0 & 0 & Q_{37} & Q_{38} & 0 & 0 \\ 0 & 0 & 0 & 0 & Q_{45} & Q_{46} & Q_{47} & Q_{48} & 0 & 0 & 0 & 0 \\ Q_{51} & Q_{52} & Q_{53} & Q_{54} & 0 & 0 & 0 & 0 & 0 & 0 & 0 & 0 \\ 0 & 0 & 0 & 0 & 0 & 0 & 0 & 0 & 0 & 0 & Q_{6,11} & Q_{6,12} \end{bmatrix} \tag{2.15}$$

The nonzero elements of the above matrix are computed as:

$$Q_{11} = e^{-i\,k_{BX}\,z}, Q_{12} = e^{i\,k_{BX}\,z}, Q_{13} = e^{-\,k_{BX}\,z}, Q_{13} = e^{\,k_{BX}\,z}$$

$$Q_{25} = e^{-i\,k_{BY}\,z}, Q_{26} = e^{i\,k_{BY}\,z}, Q_{27} = e^{-k_{BY}\,z}, Q_{28} = e^{\,k_{BY}\,z}$$

$$Q_{37} = e^{-i\,k_L\,z}, Q_{38} = e^{i\,k_L\,z}, Q_{6,11} = e^{-i\,k_T\,z}, Q_{6,12} = e^{i\,k_T\,z}$$

By means the simple beam theory which is in fact the first mode expansion of the exact theory of elasticity, it is possible to relate the forces and moments to the waves amplitude

vector. Define the forces vector as:

$$\{F_B\} = \{F_x, F_y, F_z, M_x, M_y, M_z\}^T \tag{2.16}$$

The relationship between the vectors is:

$$\{F_B\} = [S_B]\{A_B\} \tag{2.17}$$

with:

$$[\,S_B\,]_{(z)=}\begin{bmatrix} S_{11} & S_{12} & S_{13} & S_{14} & 0 & 0 & 0 & 0 & 0 & 0 & 0 & 0 \\ 0 & 0 & 0 & 0 & S_{25} & S_{26} & S_{27} & S_{28} & 0 & 0 & 0 & 0 \\ 0 & 0 & 0 & 0 & 0 & 0 & 0 & 0 & S_{37} & S_{38} & 0 & 0 \\ 0 & 0 & 0 & 0 & S_{45} & S_{46} & S_{47} & S_{48} & 0 & 0 & 0 & 0 \\ S_{51} & S_{52} & S_{53} & S_{54} & 0 & 0 & 0 & 0 & 0 & 0 & 0 & 0 \\ 0 & 0 & 0 & 0 & 0 & 0 & 0 & 0 & 0 & 0 & S_{6,11} & S_{6,12} \end{bmatrix} \tag{2.18}$$

where the nonzero elements of the above matrix are found as:

$$S_{11} = i\,E\,\mathcal{I}_{yy}\,k_{BX}^{\,3}\,e^{-i\,k_{BX}\,z}, S_{12} = -i\,E\,\mathcal{I}_{yy}\,k_{BX}^{\,3}\,e^{i\,k_{BX}\,z}, S_{13} = -E\,\mathcal{I}_{yy}\,k_{BX}^{\,3}\,e^{-\,k_{BX}\,z},$$

$$S_{14} = E\,\mathcal{I}_{yy}\,k_{BX}^{\,3}\,e^{\,k_{BX}\,z},\ S_{27} = i\,E\,\mathcal{I}_{xx}\,k_{BY}^{\,3}\,e^{-i\,k_{BY}\,z}, S_{28} = -i\,E\,\mathcal{I}_{xx}\,k_{BY}^{\,3}\,e^{i\,k_{BY}\,z},$$

$$S_{37} = i\,E\mathcal{A}\,e^{-i\,k_L\,z}, S_{38} = -i\,E\mathcal{A}\,e^{i\,k_l\,z}, S_{6,11} = -i\,\mu\,e^{-i\,k_T\,z}, S_{6,12} = i\,\mu\,e^{i\,k_T\,z}$$

$$S_{45} = -E\,\mathcal{I}_{yy}\,k_{BX}^{2}\,e^{-i\,k_{BX}\,z}, S_{12} = -i\,E\,\mathcal{I}_{yy}\,e^{i\,k_{BX}\,z}, S_{13} = E\,\mathcal{I}_{yy}\,e^{-\,k_{BX}\,z}, S_{14} = -E\,\mathcal{I}_{yy}\,e^{\,k_{BX}\,z}$$

The mathematical problem of wave propagation in a beam is well-posed; hence, once there is sufficient number of proper boundary conditions (BC's), the wave, displacement and force fields can be uniquely determined.

The matrices corresponding to the semi-infinite beams can be recovered by eliminating the columns of the matrices which are related to the incoming field waves (even numbered columns); these matrices will be designated by an ∞ superscript from now on. With proper re-ordering, the semi-infinite beam matrices are the same as those available in the literature

[12, 9, 24]. Moreover by extracting the columns related to the incoming far-field waves (i.e. second, sixth, tenth, and twelfth columns), the excitation matrices (labeled by superscript "in") can be obtained.

The time power flows of the wave types are needed for the final calculations. The far field averaged power flows have the following general form [8]:

$$\langle P_j^l \rangle = \alpha_j^l \, \omega |A_j|^2 \,, \qquad\qquad j = B, L, T, S \tag{2.19}$$

where P_j^l is the power flow associated with the wave type j (Bending, Longitudinal, or Torsional) in the structure labeled l; $|A_j|$ is the absolute value of the wave amplitude of wave type j; $\langle \cdot \rangle$ is the average of the quantity over time and the wave length; and α_j for different wave types found to be [14]:

$$\alpha_j^{Beam} = \begin{cases} E\, I_{BB}\, k_B^3 & \text{if j = B (Bending wave type)} \\ \frac{1}{2}\, E\, \mathcal{A}\, k_L & \text{if j = L (Longitudinal wave type)} \\ \frac{1}{2}\, \mu\, S_T\, k_T & \text{if j = T (Torsional wave type)} \end{cases} \tag{2.20}$$

2.3 Wave matrices for a thin plate

The goal of this section is to find matrices which relate displacement and force vectors to the wave amplitude vector by using the proper modifications to the work of Langley and Shorter [24]. It is assumed that the thin plate is comprised of two regions: a rigid small disk (distinguished by its origin) and the rest of the plate (which is considered elastic and follows the Kirchhoff's model). A cylindrical coordinate system is attached to the center of the rigid disk with the Z–axis perpendicular to the plate. A conjugate Cartesian coordinate system may also be defined with same the Z–axis and X–axis on the mid plane defined by $z = 0$ as shown in figure 2.2. The displacements and forces of the disk origin are related to the wave amplitudes of the elastic region by enforcing the compatibility and equilibrium of the regions.

It has been shown that the out of plane motion of a thin elastic plate is governed by

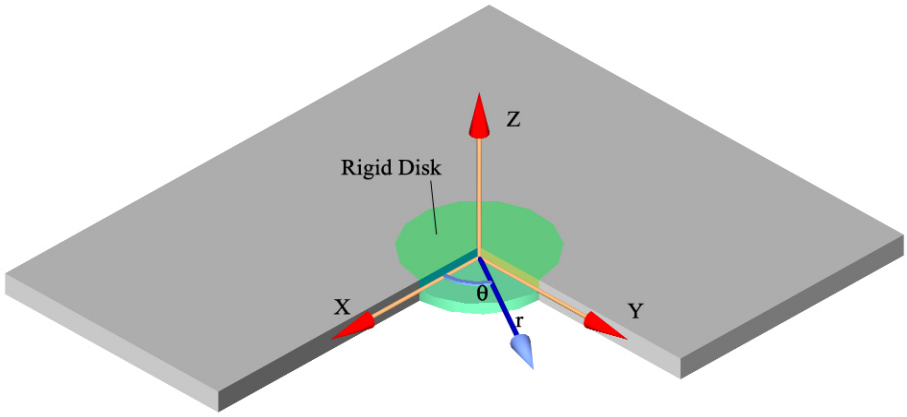

Figure 2.2: Coordinate systems chosen for an infinite plate

[15]:

$$\nabla^4 u_z - k_B^4 u_z = 0 \tag{2.21}$$

k_B is the bending wave number of the thin plate. It is found from the dispersion relation as [12, 24, 9, 15]:

$$k_B = \sqrt{\omega}\sqrt[4]{\frac{\rho L}{D_B}} \tag{2.22}$$

where ρ, L,D_B are mass density (per volume), thickness, and the flexural rigidity of the plate, respectively. The flexural rigidity for a thin plate is computed as:

$$D_B = \frac{EL^3}{12\left(1-\nu^2\right)} \tag{2.23}$$

where ν is the Poisson's ratio of the thin plate's material. In a cylindrical coordinate system can be expressed as [15]:

$$u_z(r,\theta) = \sum_{j=0}^{\infty}\left(u_{B_j}^{F,O} + u_{B_j}^{F,I} + u_{B_j}^{N,O}\right) \tag{2.24}$$

with:

$$u_{B_j}^{F,O} = \left(A_{BC_j}^{F,O}\cos j\theta + A_{BS_j}^{F,O}\sin j\theta\right) H_j^{(2)}(k_B r) \tag{2.25a}$$

$$u_{B_j}^{N,O} = \left(A_{BC_j}^{N,O}\cos j\theta + A_{BS_j}^{N,O}\sin j\theta\right) H_j^{(2)}(-i\,k_B r) \tag{2.25b}$$

$$u_{B_j}^{X,I} = \left(A_{BC_j}^{X,I}\cos j\theta + A_{BS_j}^{F,I}\sin j\theta\right) H_j^{(1)}(k_B r) \tag{2.25c}$$

$H_j^{(l)}(.)$is Hankel function of type l ($l = 1, 2$) and order j. With the convention $e^{i\,\omega\,t}$, type 1 is associated with incoming (or exciting) waves while type 2 represents outgoing solutions [17]. The incoming near-field wave terms are neglected due to the radiation condition for the infinite domain. Further more, it has been shown that two in-plane potentials ϕ and ψ [17] governed by:

$$\nabla^2\phi - k_L^2\phi = 0 \tag{2.26}$$

$$\nabla^2\psi - k_S^2\psi = 0 \tag{2.27}$$

can be used to find the the in-plane displacements as:

$$u_r = \frac{\partial\psi(r,\theta)}{\partial r} + \frac{1}{r}\frac{\partial\phi(r,\theta)}{\partial\theta} \tag{2.28a}$$

$$u_\theta = \frac{1}{r}\frac{\partial\psi(r,\theta)}{\partial\theta} - \frac{\partial\phi(r,\theta)}{\partial r} \tag{2.28b}$$

k_L is the same as the longitudinal wave number for the beam and the shearing wave number is $k_S = \sqrt{\frac{\mu}{\rho}}$ (μ is the Lamè's constant). From equations (2.28a) and (2.28b) it is seen that the in-plane displacements are of higher orders (the derivative of Hankel functions are taken) comparing to the bending displacements; therefore, the near-field terms can be neglected. The potentials have the same generic form as (2.24):

$$\phi(r,\theta) = \sum_{j=0}^{\infty}\left(\phi_{L_j}^{F,O} + \phi_{L_j}^{F,I}\right),\ \psi(r,\theta) = \sum_{j=1}^{\infty}\left(\psi_{T_j}^{F,O} + \psi_{T_j}^{F,I}\right)$$

where the terms are:

$$\phi_{L_j}^{F,O} = \left(A_{LC_j}^{F,O}\cos j\theta + A_{LS_j}^{F,O}\sin j\theta\right)\frac{H_j^{(2)}(k_L r)}{k_L} \tag{2.29a}$$

$$\phi_{L_j}^{I,O} = \left(A_{LC_j}^{F,I}\cos j\theta + A_{LS_j}^{F,I}\sin j\theta\right)\frac{H_j^{(1)}(k_L r)}{k_L} \tag{2.29b}$$

$$\psi_{T_j}^{F,O} = \left(A_{TC_j}^{F,O}\cos j\theta + A_{TS_j}^{F,O}\sin j\theta\right)\frac{H_j^{(2)}(k_T r)}{k_T} \tag{2.29c}$$

$$\psi_{T_j}^{I,O} = \left(A_{TC_j}^{F,I}\cos j\theta + A_{TS_j}^{F,I}\sin j\theta\right)\frac{H_j^{(1)}(k_T r)}{k_T} \tag{2.29d}$$

Following Langley and Shorter's work [24], only up to the first modes will be retained and the higher order modes will be truncated. The forces and moments acting on the annulus interface of the elastic region is determined by integrating the proper components of the shearing force flow and the moment rate along the peripheral cylindrical interface of the regions.

In the complete plate model, the contact of the component and the plate is assumed to be a rigid disk as shown in figure . The origin of this disk is considered as the point of the connection i.e. where the external forces are exerted. The peripheral displacements of the disk can be expressed in terms of the linear and rotational displacements of the disk origin. Enforcing the compatibility and the equilibrium between the area of contact of the disk and the elastic region, the displacement vector of the joint can be related to the wave amplitudes of the elastic part of the plate. The plate joint force vector as (2.16) and the general plate joint displacement are defined as:

$$\{U_P\} = \{u_x, u_y, u_z, \theta_x, \theta_y, \theta_z, 0, 0, 0, 0, 0\}^T, \tag{2.30}$$

The incoming displacement and force vectors are defined similarly and designated by superscript "in". Also, define the wave amplitude vectors as:

$$\{A_P\} = \{A^{F,O}_{B_0}, A^{F,O}_{B_C}, A^{F,O}_{B_S}, A^{N,O}_{B_0}, A^{N,O}_{B_C}, A^{N,O}_{B_S}, A^{F,O}_{L_C}, A^{F,O}_{L_S}, A^{F,O}_{T_0}, A^{F,O}_{T_C}, A^{F,O}_{L_S}\}^T, \tag{2.31}$$

$$\{A^{in}_P\} = \{A^{in}_{B_0}, A^{in}_{B_C}, A^{in}_{B_S}, A^{in}_{L_C}, A^{in}_{L_S}, A^{in}_{T_0}, A^{in}_{T_C}, A^{in}_{L_S}\}^T, \tag{2.32}$$

Similar to what is done for the beams,the $[Q]$ matrices that relate the displacement to the wave amplitude vector are determined as:

$$\{U_P\} \;\; = [Q_P]_{(11\times 11)} \{A_P\}, \qquad \{U^{in}_P\} \;\; = [Q^{in}_P]_{(11\times 8)} \{A^{in}_P\}$$

The nonzero entries of the above matrices are found to be:

$$Q_{P_{1,7}}=Q_{P_{2,8}}=H_0^{(2)}(ak_L)-\frac{H_1^{(2)}(ak_L)}{a},\ Q_{P_{1,11}}=-Q_{P_{2,10}}=\frac{H_1^{(2)}(ak_S)}{a},Q_{P_{3,1}}=H_0^{(2)}(ak_B),$$
$$Q_{P_{3,4}}=H_0^{(2)}(-iak_B),\ Q_{P_{4,3}}=-Q_{P_{5,2}}=\frac{H_1^{(2)}(ak_B)}{a},\ Q_{P_{4,6}}=-Q_{P_{5,5}}=\frac{H_1^{(2)}(-iak_B)}{a},$$
$$Q_{P_{6,9}}=k_S\,Q_{P_{1,11}},\ Q_{P_{7,7}}=-Q_{P_{8,8}}=H_0^{(2)}(ak_L)-\frac{2H_1^{(2)}(ak_L)}{ak_L},Q_{P_{11,1}}=-k_BH_1^{(2)}(ak_B),$$
$$Q_{P_{7,11}}=Q_{P_{8,10}}=-H_0^{(2)}(ak_S)+\frac{2H_1^{(2)}(ak_S)}{ak_S},\ Q_{P_{9,2}}=Q_{P_{10,3}}=k_BH_0^{(2)}(ak_B)-\frac{2H_1^{(2)}(ak_B)}{a},$$
$$Q_{P_{9,5}}=Q_{P_{10,6}}=-ik_BH_0^{(2)}(-iak_B)-\frac{2H_1^{(2)}(-iak_B)}{a},\ Q_{P_{11,4}}=ik_BH_1^{(2)}(-iak_B)$$

and

$$Q^{in}_{P_{1,4}}=Q^{in}_{P_{2,5}}=H_0^{(1)}(ak_L)-\frac{H_1^{(1)}(ak_L)}{a},\ Q^{in}_{P_{1,8}}=-Q^{in}_{P_{2,7}}=\frac{H_1^{(1)}(ak_S)}{a},$$
$$Q^{in}_{P_{3,1}}=H_0^{(1)}(ak_B),\ Q^{in}_{P_{4,3}}=-Q^{in}_{P_{5,2}}=\frac{H_1^{(1)}(ak_B)}{a},\ Q^{in}_{P_{6,6}}=k_S\,Q^{in}_{P_{1,8}}$$
$$Q^{in}_{P_{7,4}}=-Q^{in}_{P_{8,5}}=H_0^{(1)}(ak_L)-\frac{2H_1^{(1)}(ak_L)}{ak_L},Q^{in}_{P_{7,8}}=Q^{in}_{P_{8,7}}=-H_0^{(1)}(ak_S)+\frac{2H_1^{(1)}(ak_S)}{ak_S},$$
$$Q^{in}_{P_{9,2}}=-Q^{in}_{P_{10,3}}=k_BH_0^{(1)}(ak_B)-\frac{2H_1^{(1)}(ak_B)}{a},\ Q^{in}_{P_{11,1}}=-k_BH_1^{(1)}(ak_B)$$

The force vectors acting on the origin of the disk may be expressed in terms of the wave amplitude vectors through $[S]$ matrices:

$$\{F_P\}=\left[S_P\right]_{(6\times11)}\{A_P\},\qquad \{F_P^{in}\}=\left[S_P^{in}\right]_{(6\times8)}\{A_P^{in}\}$$

Define:

$$\begin{aligned} d_0 &= 2\,\pi\,aD_B, \qquad\qquad d_1=\frac{6d_0}{L^2},\\ g(\kappa,j,l) &= \frac{i}{2}d_0\kappa^2\left[2H_1^{(j)}\left((-i)^la\kappa\right)-i^j\,a\,\kappa\,H_0^{(j)}\left((-i)^la\kappa\right)\right]\end{aligned}$$

Most of the entries are zero; the nonzero elements of $[S]$ are:

$$\begin{aligned} S_{P_{1,7}} &= S_{P_{2,8}}=2d_1\,k_LH_1^{(2)}(ak_L),\ S_{P_{1,11}}=-S_{P_{2,10}}=d_1(1-\nu)k_SH_1^{(2)}(ak_S),\\ S_{P_{3,1}} &= d_0{k_B}^3H_1^{(2)}(ak_B),\ S_{P_{3,4}}=id_0{k_B}^3H_1^{(2)}(-i\,ak_B),\ S_{P_{4,3}}=g(k_B,2,0),\\ S_{P_{4,6}} &= g(k_B,2,1),\ S_{P_{6,9}}=\frac{2d_1(1-\nu)}{i\,d_0\,{k_S}^2}\,g(k_S,2,0)\end{aligned}$$

The elements of $[S_P^{in}]$ that are not zero are:

$$\begin{aligned} S_{P_{1,4}}^{in} &= S_{P_{2,5}}^{in} = k_L H_1^{(1)}(ak_L),\ S_{P_{1,8}}^{in} = -S_{P_{2,7}}^{in} = d_1(1-\nu)k_S H_1^{(1)}(ak_S), \\ S_{P_{3,1}}^{in} &= -i\,d_0 H_0^{(1)}(ak_B),\ S_{P_{4,3}}^{in} = -S_{P_{5,2}}^{in} = g(k_B,1,0), S_{P_{6,6}}^{in} = \frac{2d_1(1-\nu)}{i\,d_0\,{k_S}^2}\,g(k_S,1,0) \end{aligned}$$

The impedances for the plate model can readily be obtained from the above matrices. Without the loss of generality, it can be assumed that $[Q_P]$ is invertible. This assumption makes it possible to express the wave amplitude vector in terms of the displacement and hence velocity vector. Therefore:

$$\begin{aligned} \{F_P\} = [S_P]_{(6\times 11)}\,\{A_P\} &= [S_P]_{(6\times 11)}[Q_P]^{-1}_{(11\times 11)}\,\{U_P\} \\ (i\,\omega)\begin{bmatrix}[Z_P]_{(6\times 6)}\\ \cdots\cdots\\ [{Z_P}^*]_{(5\times 6)}\end{bmatrix} &= [S_P]_{(6\times 11)}[Q_P]^{-1}_{(11\times 11)} \end{aligned} \tag{2.33}$$

The last 5 rows of the displacement vector are filled with 0. Therefore the bottom matrix adds no new information; while the top useful matrix gives the plate impedance matrix as:

$$Z_{1,1} = Z_{2,2} = \frac{S_{P_{1,7}}Q_{P_{7,11}} - S_{P_{1,11}}Q_{P_{7,7}}}{i\,\omega\,(Q_{P_{1,7}}Q_{P_{7,11}} - Q_{P_{1,11}}Q_{P_{7,7}})} \tag{2.34}$$

$$Z_{3,3} = \frac{S_{P_{3,1}}Q_{P_{11,4}} - S_{P_{3,4}}Q_{P_{11,1}}}{i\,\omega\,(Q_{P_{3,1}}Q_{P_{11,4}} - Q_{P_{11,1}}Q_{P_{3,4}})} \tag{2.35}$$

$$Z_{4,4} = Z_{5,5} = \frac{S_{P_{4,3}}Q_{P_{9,5}} - S_{P_{4,6}}Q_{P_{9,2}}}{i\,\omega\,(Q_{P_{4,3}}Q_{P_{9,5}} - Q_{P_{4,6}}Q_{P_{9,2}})} \tag{2.36}$$

$$Z_{6,6} = \frac{S_{P_{6,9}}}{i\,\omega\,Q_{P_{6,9}}} \tag{2.37}$$

Since the disk is rigid and the plate is isotropic, the forces applied on the center of the disk, solely induce the motions on the direction of the applied force. In other words, the impedance matrix is diagonal with no horizontal direction preference. Mathematically, since the nonzero entries of the [S] and [Q] matrices appear in the same places, the forces of one direction do not excite any other direction displacements. Ljunggren [**?**] has shown that generally this is not true and every loads can lead into both in-plane and out of plane

displacements (except for the torsional moment that only generates a tangential in-plane displacement).

As for the beam model, the time averaged power flows of each wave type has the form of (2.19). Langley and Shorter [14] calculated the power flow for a diffusive field as:

$$\alpha_{jl}^{Plate} = \begin{cases} 4\,\rho\,Lk_j & \text{if l} = 0 \\ 2\,\rho\,Lk_j & \text{if l} = \text{C,S} \end{cases} \tag{2.38}$$

where j indicates the wave type (i.e. bending, longitudinal, or shearing).

2.4 A semi-infinite beam connection to an infinite plate

In this section, the power exchange between an infinite plate and a semi-finite slender beam is considered. The straightforward method developed here, is different from the calculations suggested by Langley and Shorter [24] and is easily extendable to finite component cases.

Consider a semi-infinite prismatic beam connected to an infinite thin plate as shown in figure 2.3. For simplicity, the beam is perpendicular to the plate and the Z–axis (normal to the plate) passes through the shear center of the beam. Otherwise, by means of rotation matrices, the Z–axes of the beam and plate should be expressed in a global common coordinate system.

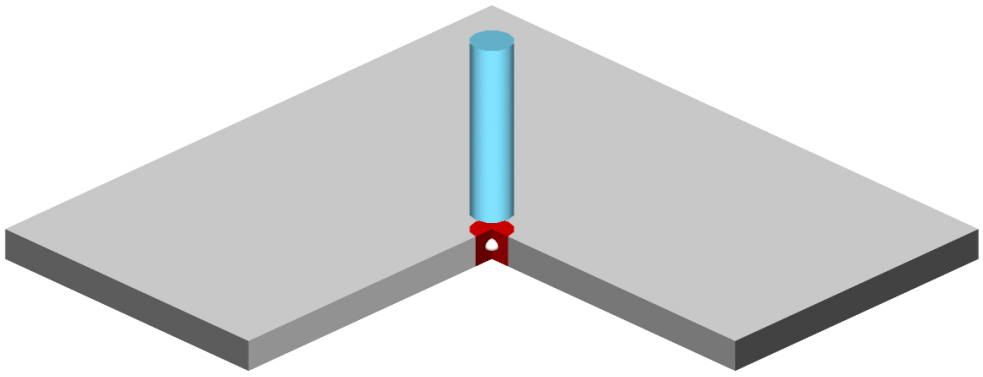

Figure 2.3: Connection of a semi-infinite beam to an infinite plate

The beam displacement vector should be modified in size to comply with the plate dis-

placement vector size. This is simply done by adding five zero rows to the beam displacement vectors and the $[Q]$ matrices as:

$$\{U_B^*\}_{11\times1} \triangleq \begin{Bmatrix} \{U_B\}_{6\times1} \\ \hdashline \{\mathbf{0}\}_{5\times1} \end{Bmatrix},\ \{U_B^{in^*}\}_{11\times1} \triangleq \begin{Bmatrix} \{U_B^{in}\}_{6\times1} \\ \hdashline \{\ \mathbf{0}\ \}_{5\times1} \end{Bmatrix} \tag{2.39}$$

and

$$[Q_B^*]_{11\times6} \triangleq \begin{bmatrix} [Q_B^\infty]_{6\times6} \\ \hdashline [\ 0\ ]_{5\times6} \end{bmatrix},\ [Q_B^{in^*}]_{11\times6} \triangleq \begin{bmatrix} [Q_B^{\infty\,in}]_{6\times6} \\ \hdashline [\ 0\ ]_{5\times6} \end{bmatrix} \tag{2.40}$$

In order to find the wave amplitudes and hence the power transmitted, the compatibility of the displacements and the equilibrium of the forces can now be combined in a global system. The kinematic of the joint ($\{U_B^*\} = \{U_P\}$) gives:

$$[Q_B^*]\{A_B^\infty\} - [Q_P]\{A_P\} = [Q_P^{in}]\{A_P^{in}\} - [Q_B^{in^*}]\{A_B^{\infty\,in}\} \tag{2.41}$$

The dynamic equilibrium ($\{F_B\} - \{F_P\} = \{\mathbf{0}\}$) leads to:

$$[S_B]\{A_B^\infty\} + [S_P]\{A_P\} = -[S_P^{in}]\{A_P^{in}\} - [S_B^{in}]\{A_B^{\infty\,in}\} \tag{2.42}$$

The wave amplitudes are found after solving the following global system of equations:

$$\begin{bmatrix} [Q_B^*] & -[Q_P] \\ [S_B] & [S_P] \end{bmatrix} \begin{Bmatrix} \{A_B^\infty\} \\ \hdashline \{A_P\} \end{Bmatrix} = \begin{bmatrix} [Q_P^{in}] \\ -[S_P^{in}] \end{bmatrix} \{A_P^{in}\} - \begin{bmatrix} [Q_B^{in^*}] \\ [S_B^{in}] \end{bmatrix} \{A_B^{\infty\,in}\} \tag{2.43}$$

The above system of equations has multiple inputs and should be solved for each incoming wave type of the plate and beam separately. For practical configurations, it may be assumed that the left hand side matrix is not singular (therefore invertible). The columns of the right hand side input matrices correspond to the incoming wave type sitting on the same number row as the column number. Using this fact, it is possible to solve the system of equations only once. Moreover, to calculate power transmission coefficients, the input wave amplitudes are usually taken unity. Therefore, the input vectors can be replaced by identity matrices with appropriate sizes. The system of equations are then solved to find the system response to incoming waves from the beam and the incoming waves from the plate separately. In this

way, the final answer will be in a matrix form. The columns of the solution matrix (for each component) represent the induced wave amplitude by the unit incoming wave with the same row number as the wave amplitude vector. Each row of the solution matrix corresponds to the responses of one wave type. Therefore:

$$\begin{Bmatrix} \{\boldsymbol{A_B^\infty}\} \\ \cdots\cdots \\ \{\boldsymbol{A_P}\} \end{Bmatrix} = \begin{cases} \begin{bmatrix} [Q_B^*] & -[Q_P] \\ [S_B] & [S_P] \end{bmatrix}^{-1} \begin{bmatrix} [Q_P^{in}] \\ -[S_P^{in}] \end{bmatrix} & \text{for plate incoming waves} \\ -\begin{bmatrix} [Q_B^*] & -[Q_P] \\ [S_B] & [S_P] \end{bmatrix}^{-1} \begin{bmatrix} [Q_B^{in^*}] \\ [S_B^{in}] \end{bmatrix} & \text{for beam incoming waves} \end{cases} \tag{2.44}$$

It should be noted that $\{\boldsymbol{A_B^\infty}\}$ and $\{\boldsymbol{A_P}\}$ are now matrices rather than vectors. These matrices contain the each wave amplitude response to the incoming waves row-wise and wave amplitude vectors to a particular incoming wave column-wise.

The power transmission coefficient for one wave type is calculated by finding ratio the power flow associated with that wave type to the power flow corresponding to the incoming wave. Equation (2.19) should be used to calculate the power flows for different wave types. For instance, an incoming longitudinal wave in beam is transmitted as a symmetrical bending wave in the plate. Using the identity matrix input method, the power reflection coefficient is the square of the absolute value of the beam longitudinal wave outgoing amplitude and the power transmission coefficient is the absolute value of the plate symmetric bending wave amplitude times $\left|\frac{\alpha_{B_0}^{Plate}}{\alpha_B^{Beam}}\right|$.

2.5 Validations

In this section, numerical examples are used to validate the matrices and the method. First, the obtained impedance expressions are compared to the well-known reported impedances. Second, the numerical example used by Langley and Shorter [24] is replicated to show the consistency between the methods.

2.5.1 Impedance verification

As equation (2.33) shows, impedances contain the information from both the $[S]$ and $[Q]$ matrices. Therefore, matching the impedances from the current method to those available in the literature, indicates those matrices are pertinent. For small argument values the models are more or less identical. The relevant impedances from the work by Ljunggren [18, 19] in the current notation are:

$$Z_{1,1} = \frac{4\,\mu\,L^3 {k_B}^2}{3(1-\nu)\,\omega}\left(H_0^{(2)}(ak_B) - \frac{2i}{\pi}K_0(ak_B)\right)^{-1} \tag{2.45}$$

$$Z_{3,3} = \frac{16\,\mu\,L}{\omega}\left(\frac{(1-\nu)\sin ak_L}{ak_L}H_0^{(2)}(ak_L) + \frac{2\sin ak_S}{ak_S}H_0^{(2)}(ak_S)\right)^{-1} \tag{2.46}$$

$$Z_{6,6}^{\ sym} = \frac{8\,\mu\,La}{\omega k_S H_1^{(2)}(ak_S)} \tag{2.47}$$

A relatively complex in-plane moment impedance for a thin plate has been reported by Dyer [22]; the small argument approximation for this impedance is given as Cremer [12]:

$$Z_{4,4} = \frac{16D_B}{\omega}\left(1 - \frac{4i}{\pi}\ln 0.9ak_S\right)^{-1} \tag{2.48}$$

The graphs in figures (2.4)-(2.13) show the in-plane force and bending moment impedances; as can be seen there is good agreement with the current and existing expressions. However, when it comes to the normal force impedance, the results are somewhat different; because the small contact area can be considered either soft or rigid. For torsional impedance, it is seen that the current analysis is identical to Ljunggren [18, 19] so called "symmetrical loading" results; but as he explains, the "antisymmetrical" solution should be added to it. If both parts are taken into account, despite the agreement of the trends, the impedances difference is about a factor of 2. For more information, the relevant references such as Ljunggren [18, 19], Leung and Pinnington [20], Dyer [22], Cremer [12] and, Thomas [23] can be consulted.

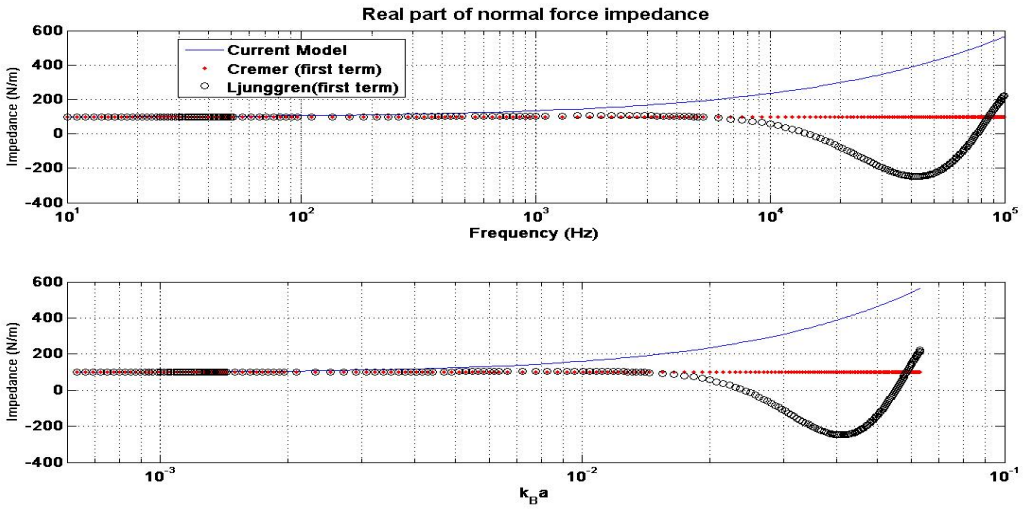

Figure 2.4: Real part of vertical force (bending) impedance

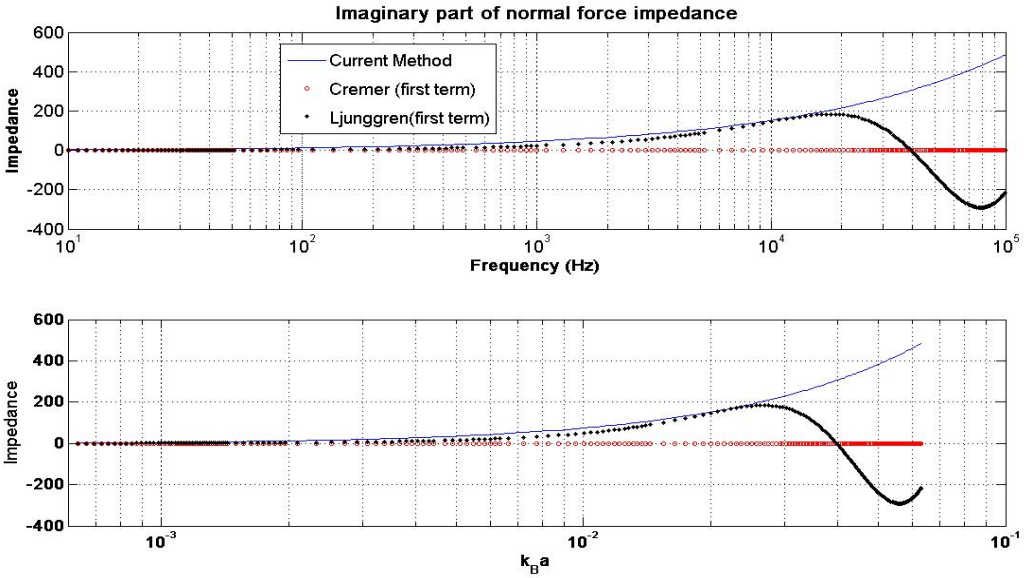

Figure 2.5: Imaginary part of vertical force (bending) impedance

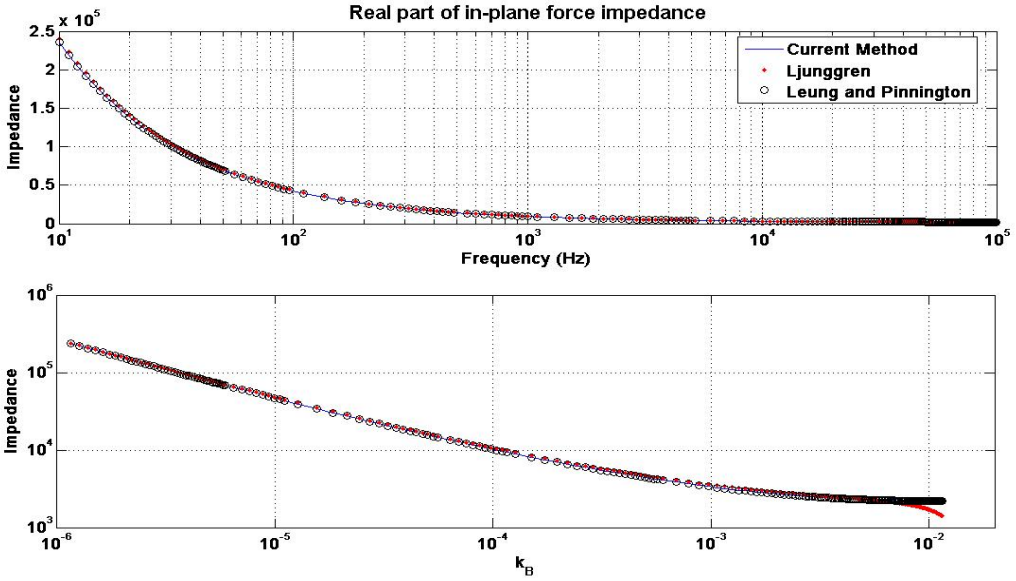

Figure 2.6: Real part of in-plane force impedance

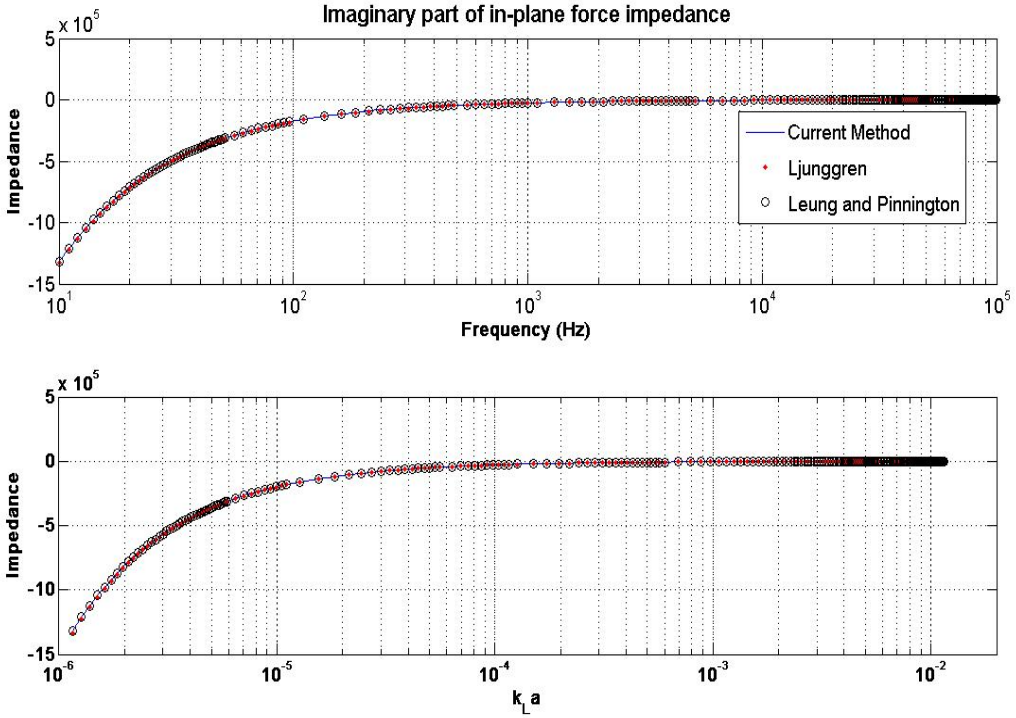

Figure 2.7: Imaginary part of in-plane force impedance

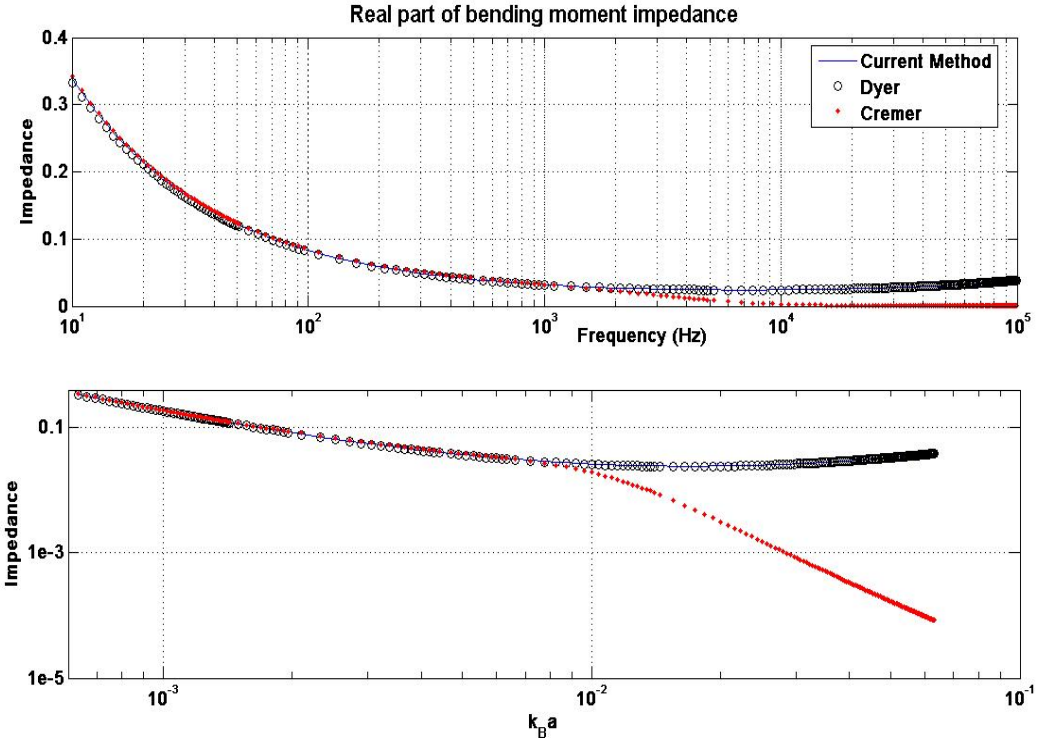

Figure 2.8: Real part of the bending moment impedance

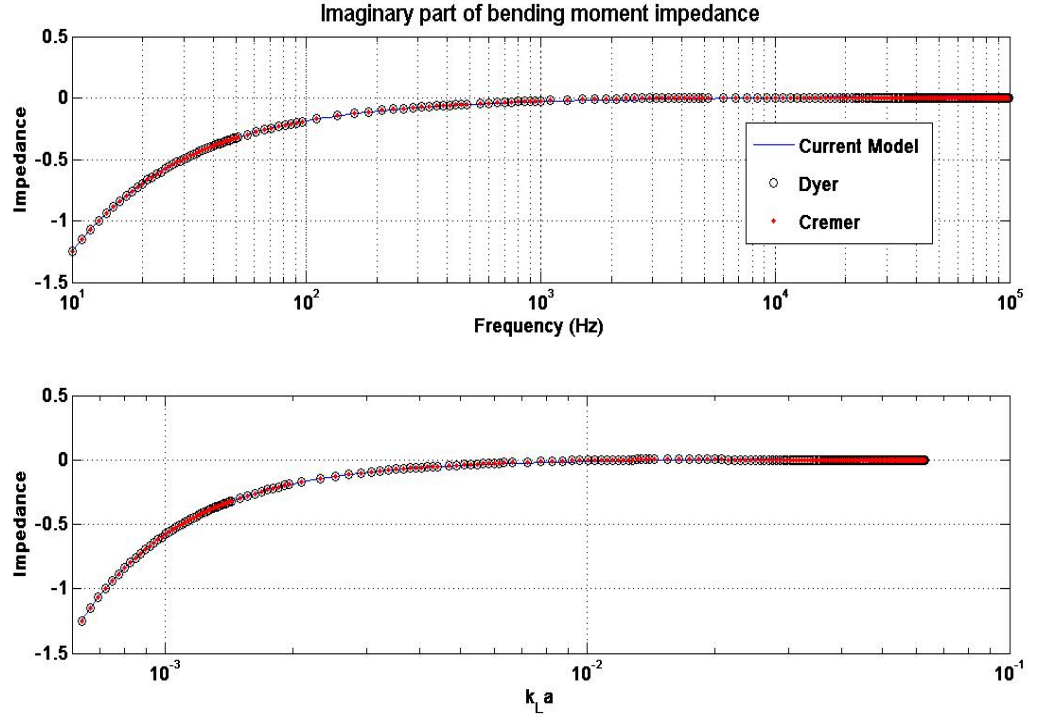

Figure 2.9: Imaginary part of the bending moment impedance

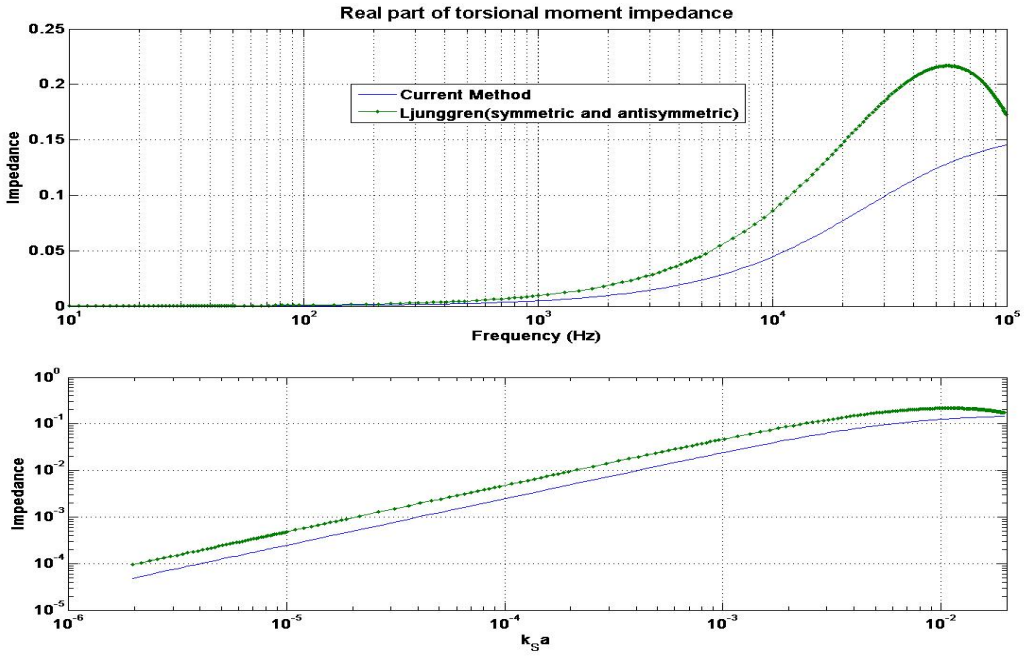

Figure 2.10: Real part of the twisting moment impedance

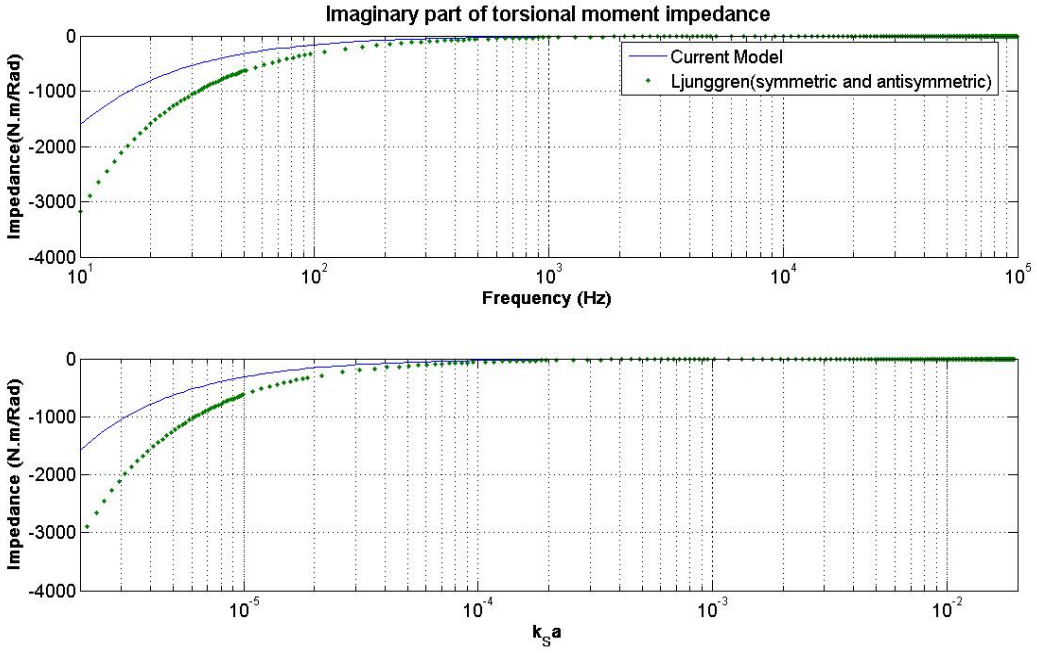

Figure 2.11: Imaginary part of the twisting moment impedance

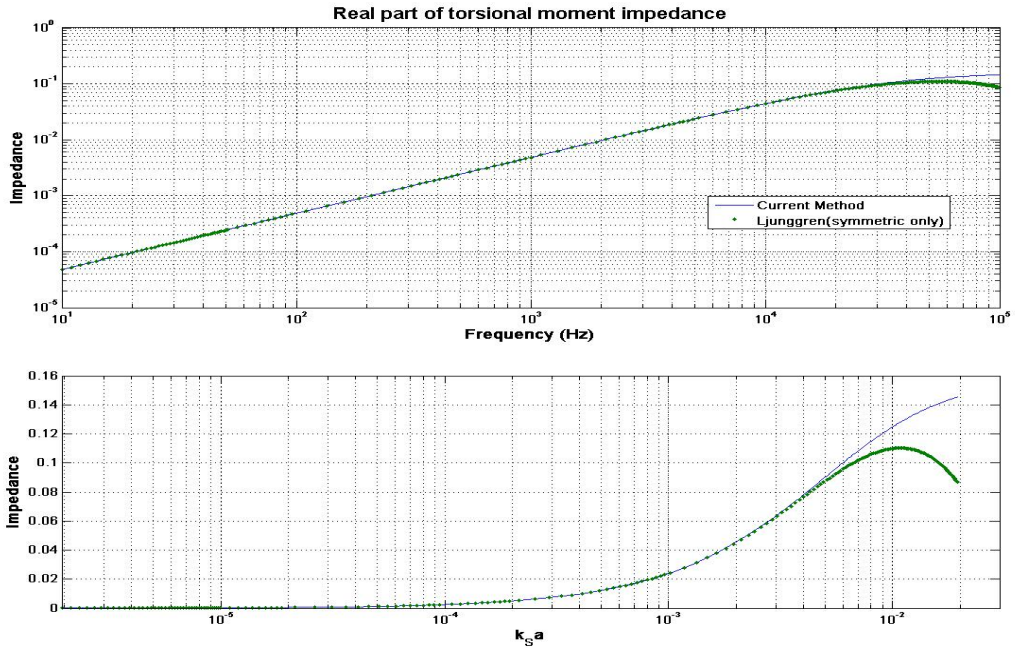

Figure 2.12: Real part of the twisting moment impedance for a symmetric mode

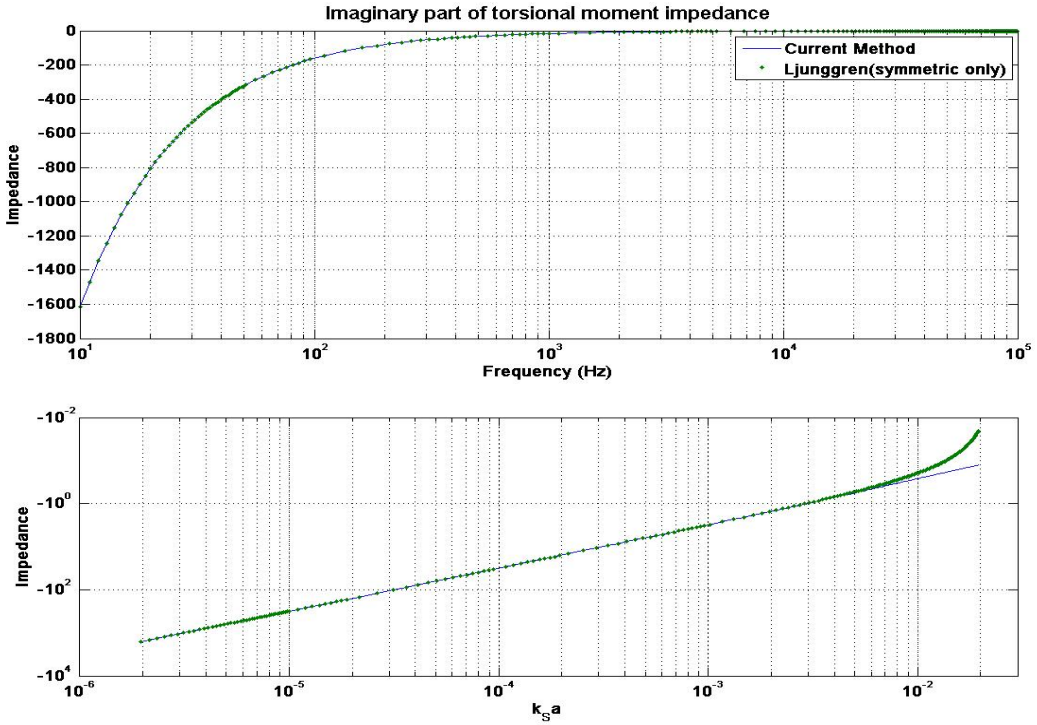

Figure 2.13: Imaginary part of the twisting moment impedance for a symmetric mode

2.5.2 Plate and beam system examples

Here, the replication of the result example from Langley and Shorter [24] (originally Lyon [46]) is considered as the numerical validation.

A large thin aluminum ($\rho = 2700kg/m^3, E = 7.1GPa, \nu = 0.3$) plate with a thickness of 3.175 mm is considered as the infinite plate. A strip from the same plate with a width of 38.1 mm is connected perpendicularly to the center of the plate as shown in the figure (2.14).

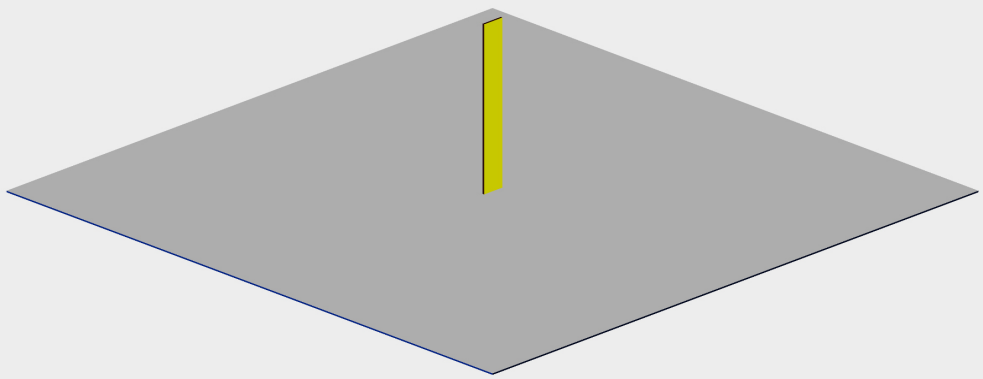

Figure 2.14: A semi-infinite rectangular beam and a plate example

The radius of the joint is actually a free parameter. Remembering that the beam has a rectangular cross section, the joint size can be chosen either as the radius of the largest circle that can be inscribed in the rectangle as shown in figure (2.15) or the radius of the circle with the same area.

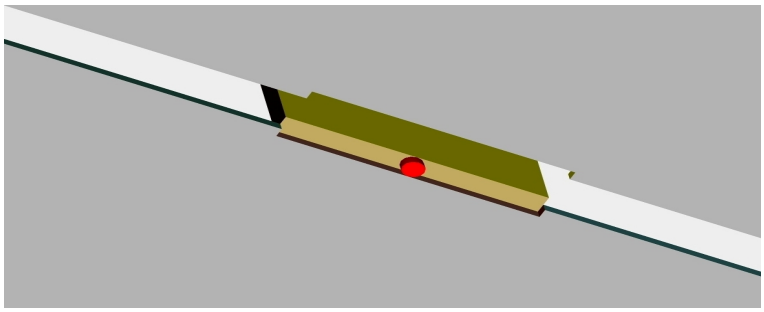

Figure 2.15: Inscribed circle can be chosen as the rigid joint disk

The nonzero power transmission coefficients are plotted in figures (2.16) to (2.19) over a frequency range of 0.1-10 kHz. The X–axis beam excitation graph is the same as reported

Langley and Shorter [24]. It is interesting to note that an incoming wave in the beam excites at most only one mode of each wave types at most. An incoming plate symmetric bending wave excites only a longitudinal wave in the beam and an incoming symmetric torsional wave in the plate causes a purely torsional motion in the beam. The other incoming wave in the plate, excites exactly one mode of the bending, longitudinal, and torsional wave types.

Another interesting property of the response is the reciprocity. This is another check for the correctness of the method. The reflection and transmission coefficients of two specific wave types (one in the beam and the other one in the plate) are the same. For instance, the transmission coefficient of an incoming longitudinal wave in the beam is equal transmission coefficient of an incoming symmetric bending wave in the plate.

The transmission and reflection coefficients obtained for these joint radii when the incoming waves are torsional, longitudinal, and the stiffer bending side of the beam waves do not change much. Naturally, the contact area (or the energy passage) for the joint with a larger radius (equivalent circle for this case) is larger and therefore, the transmission coefficients are higher. However, for the flexible side of the beam the main transmission coefficient (plate bending coefficient) and the reflection coefficient (the X–axis) are quite sensitive to the choice of this parameter. The reason is that the order of plate impedance changes with respect to the beam flexible side impedance and it is known from the 1 DOF energy transmission theory (for instance Lyon[2]) the relative order of the impedances of two point connected structures plays a very important role in the energy exchange between the components. Figures (2.20)-(2.23) show the sensitivity of the power coefficients to the chosen joint sizes.

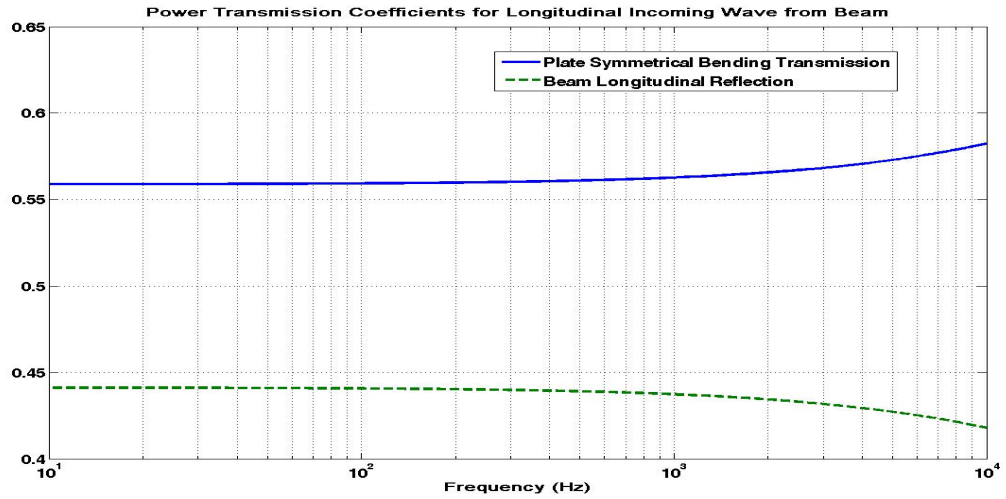

Figure 2.16: Beam longitudinal incoming wave power coefficients

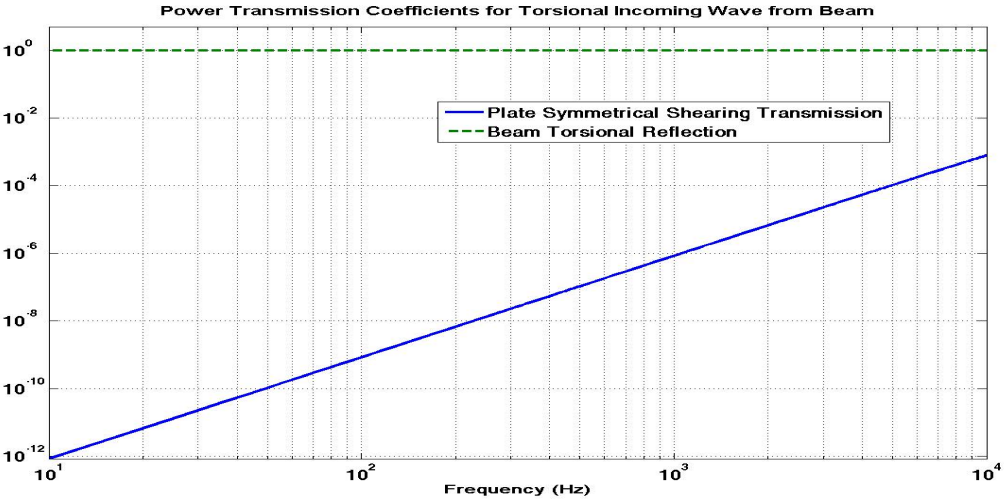

Figure 2.17: Beam shearing incoming wave power coefficients

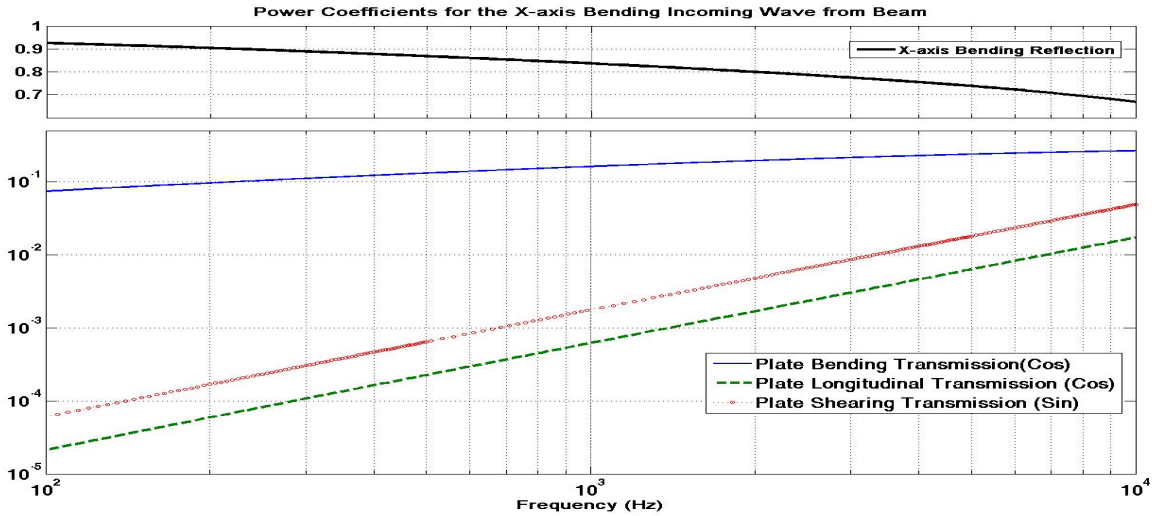

Figure 2.18: Beam X direction bending wave power coefficients

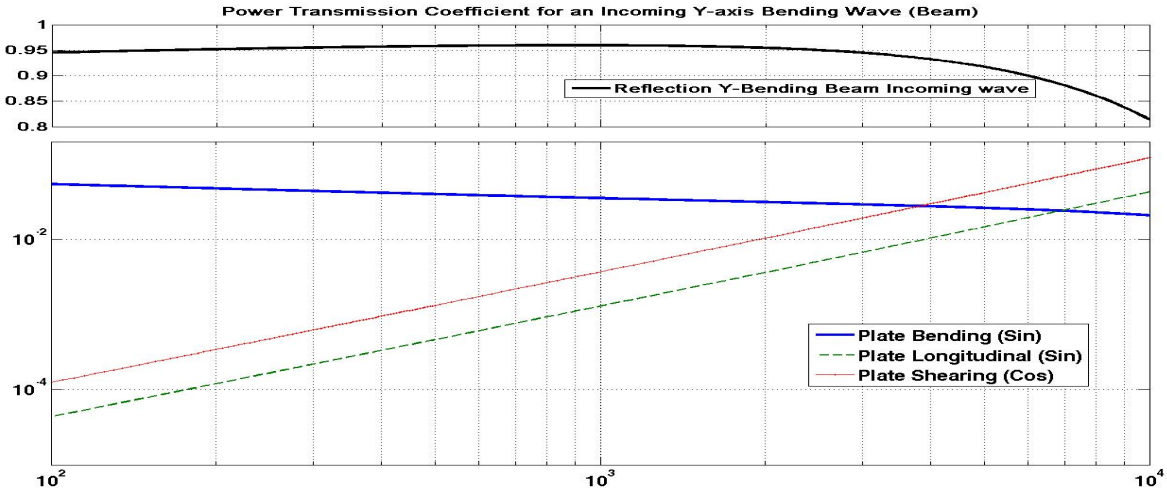

Figure 2.19: Beam Y direction incoming bending wave power coefficients

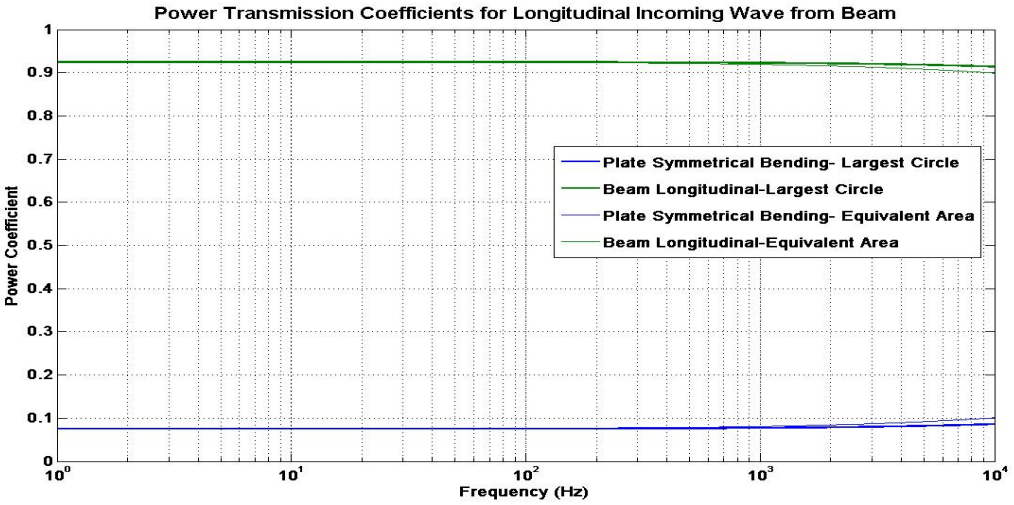

Figure 2.20: Sensitivity of the longitudinal power coefficients to the joint radius

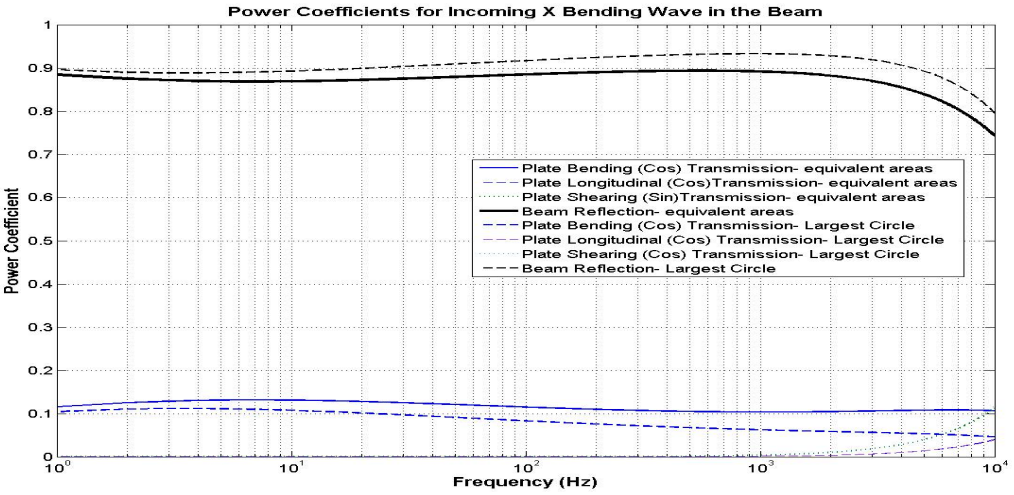

Figure 2.21: Sensitivity of the X-bending power coefficients to the joint radius

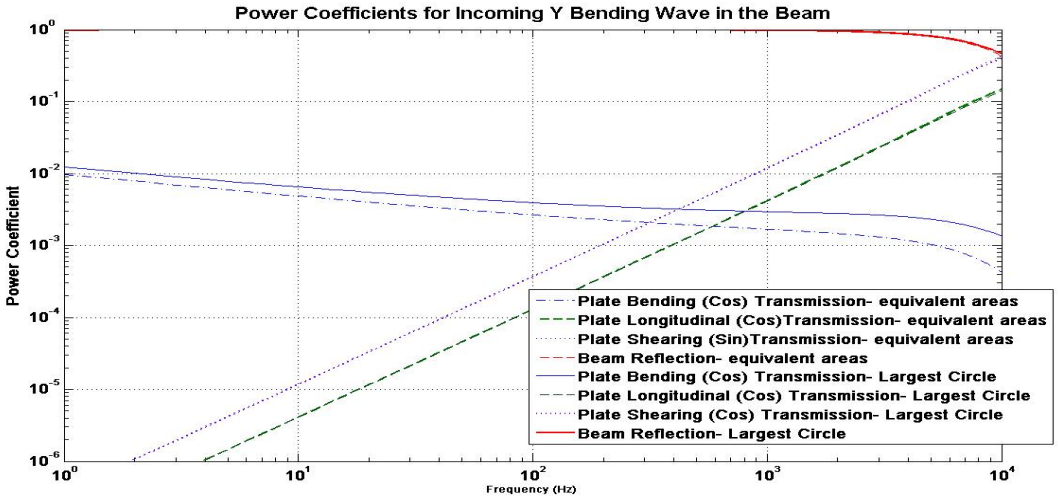

Figure 2.22: Sensitivity of the Y-bending power coefficients to the joint radius

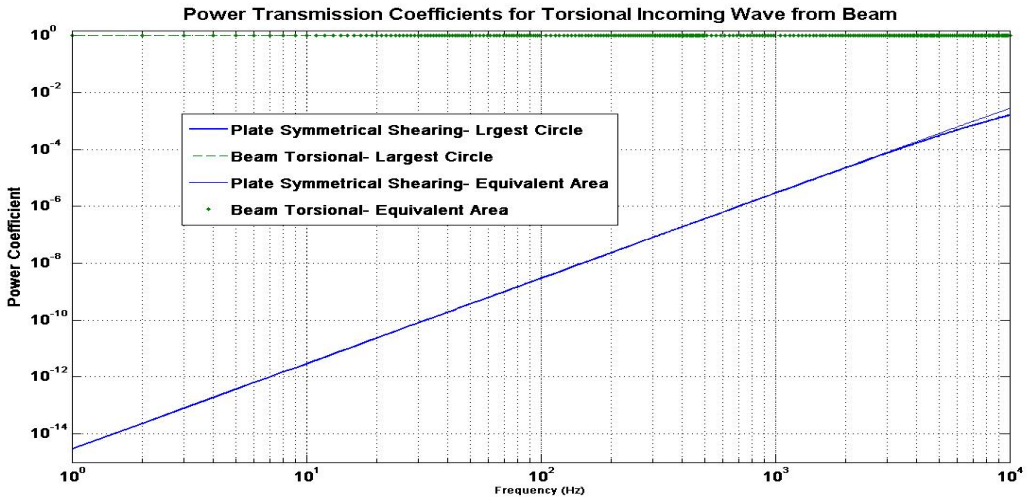

Figure 2.23: Sensitivity of the shearing power coefficients to the joint radius

CHAPTER 3

Vibration Power Transmission Coefficient between two Parallel Plates via a Beam

3.1 Introduction

Many structures can be considered as a system of layers of different materials which are secured in between an outer and an inner panel. To support the structural forces, these panels must be connected to one another directly. Usually one panel is riveted or welded to mounts which are themselves are fixed to the other panel. Vibrational power and energy, hence the noise, can now be exchanged between such two panels via the connection and independently from the layers in between the panels. A system of two parallel plates and one beam can serve as a model for finding the power swapped between the panels. For instance, in a typical aeroplane fuselage, the inside panel is supported on small mounts which are themselves are fixed to the outer plate. The treatment material, and air gaps (air plate like layers) are secured between theses panels. However, the powers transmitted through the layers of such a sandwich are analyzed in the next chapter.

In this chapter, first the matrices developed in the previous chapter are assembled together in order to find the wave fields in the components of the structure, then the power transmission coefficients are found. These power coefficients can be used in EFEA for analyzing a more complex structure. Further, numerical examples are solved to show the applicability of the method. The method is validated by comparing the calculations to a 1 degree of freedom spring connection; also the energy conservation is checked by finding the

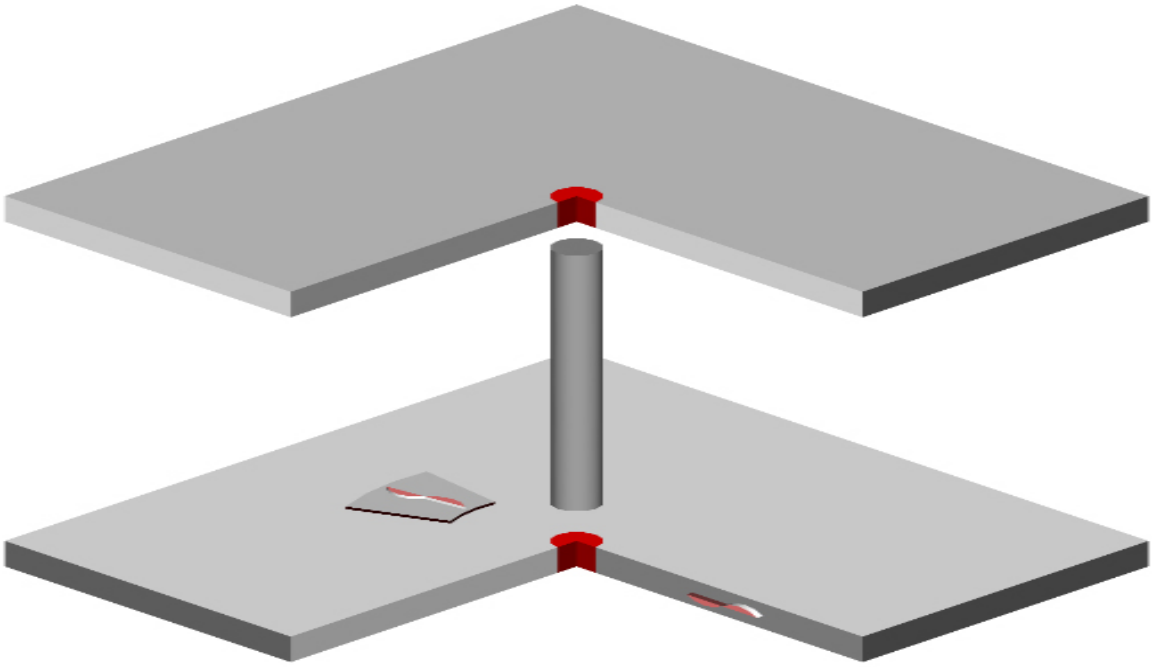

Figure 3.1: Connection of two parallel plates via a beam

sum of the power transmission coefficients.

3.2 Waves in a two connected plates system

Consider two infinite parallel thin plates that are connected to each other via a finite length slender beam. Each tip of the beam is assumed to be fully connected to one point of each plate as shown in the figure (3.1). To keep the problem solution form simple, without the loss of generality, it may be assumed that the beam is perpendicular to both plates. This assumption eliminates a few intermediate steps of rotating the coordinate systems.

Using the models developed in the previous chapter, it is seen that there exist 34 unknown outgoing wave amplitudes in the structure. Each plate model includes 11 wave amplitudes; the beam model also adds an extra set of 12 wave amplitudes. The excitation of each plate can be done through any of 8 incoming different waves which is similar to the problem of connection of an infinite plate and a semi-infinite beam. The plates can be different in material and geometry, therefore, they are designated by 1 (bottom plate) and 2 (top plate). The global coordinate system can arbitrary be placed on the origin of

the bottom plate; there is no preference of the coordinate system and the final result is invariant. Since the plates are thin, the plate matrices are independent of z; however, the top plate coordinate system should be reflected about the top mid plane in order to match with the global coordinate system.

The beam displacement vector is defined by equation (2.13) and the force and wave amplitude vectors relation stay unchanged as equation (2.17). Since the beam length is finite, unlike the semi-infinite beam case, all the 12 columns of beam matrices are retained. The beam displacement vector is modified by means of equation (2.22) and the $[Q]$ matrix has to be altered (just like the case of a semi-infinite beam and infinite plate) accordingly as:

$$[Q_B^{**}]_{11\times 12} \triangleq \begin{bmatrix} [Q_B]_{6\times 12} \\ \hdashline [\ 0\ ]_{5\times 12} \end{bmatrix} \tag{3.1}$$

The compatibility enforcement at $z = 0$ results in:

$$[Q_B^{**}]\{A_B\} - [Q_{P_1}]\{A_{P_1}\} = [Q_{P_1}^{in}]\{A_{P_1}^{in}\} \tag{3.2}$$

In the absence of extra joint forces, the equilibrium of the dynamic forces at $z = 0$ leads to:

$$[S_B]\{A_B\} + [S_{P_1}]\{A_{P_1}\} = -[S_{P_1}^{in}]\{A_{P_1}^{in}\} \tag{3.3}$$

The continuity of the second joint displacement and the dynamic equilibrium of the acting forces leads into similar equations. However, instead of reorienting the second plate coordinate system to match the global system, the compatibility and equilibrium conditions applied to the second joint can be modified accordingly as:

$$\{U_B^*\}_{(z=L_B)} = -\{U_{P_2}\} \tag{3.4}$$

$$\{F_B\}_{(z=L_B)} = \{F_{P_2}\} \tag{3.5}$$

Now (3.4) and (3.5) may be expressed in terms of the wave amplitude vectors. The set of the new equations along with (3.2) and (3.3) can be assembled into a global linear system where the unknown quantities are the wave amplitudes of the plates and the finite length

beam. The global system of equations is obtained as:

$$\begin{bmatrix} -[Q_{P_1}] & [\mathbf{0}] & [Q_B^{**}]_{z=0} \\ [S_{P_1}] & [\mathbf{0}] & [S_B]_{z=0} \\ [\mathbf{0}] & [Q_{P_2}] & [Q_B^{**}]_{z=L_B} \\ [\mathbf{0}] & -[S_{P_1}] & [S_B]_{z=L_B} \end{bmatrix} \begin{Bmatrix} \{A_{P_1}\} \\ \cdots\cdots\cdots \\ \{A_{P_2}\} \\ \cdots\cdots\cdots \\ \{A_B\} \end{Bmatrix} = \begin{bmatrix} [Q_{P_1}^{in}] \\ -[S_{P_1}^{in}] \end{bmatrix} \begin{Bmatrix} A_{P_1}^{in} \end{Bmatrix} - \begin{bmatrix} [Q_{P_2}^{in}] \\ -[S_{P_2}^{in}] \end{bmatrix} \begin{Bmatrix} A_{P_2}^{in} \end{Bmatrix} \tag{3.6}$$

The above linear system gives the wave amplitudes in the plates and also the beam. Mathematically, the above linear system can be singular; however, for a system with realistic and appropriate physical parameters, the existence of the solution can be taken for granted.

In order to find the power transmitted form one plate to the other plate, only the plates far-field wave amplitudes are needed. Hence, the near field terms as well as those corresponding to the beam will be discarded. Like the problem of the connection of a semi-infinite beam and an infinite plate system, the above linear system has two inputs: the excitation from the top plate and the excitations from the bottom plate. To find the responses of each excitation, the incoming wave amplitude vectors can be replaced by an 8×8 identity matrix. The solution matrix for each plate excitation, contain the induced wave amplitude vectors from different incoming wave types column-wise; row-wise, it gives the values of each wave type to different excitations.

Once the wave amplitudes are found; the power flows associated with each plate wave type can be calculated by means of equation (2.19). The ratios of the power flows corresponding to each wave type to an incoming wave type power flow, give the power transmission coefficients.

3.2.1 Validation for a special case

In this section a special case of the general problem is considered. The plates can be totally different in material and the geometry; but when the plates are identical, the symmetric bending mode transmission can be expressed by a relatively simple formula. This formula is comparable to the power transmission coefficient obtained for the plates

when they are connected via a spring.

3.2.2 Symmetric Mode transmission

As a special case, when the plates are identical in material and geometry, the calculations are not too messy and a compact closed form solution for the structure response can be obtained. For the sake of brevity, normal forces acting on the plates origins and the out of plane displacements of the joints can be designated by F and u, respectively. The global coordinate system can be fixed on the bottom plate origin and subscripts 1 and 2 refer to the bottom (exciting side) plate and the top (receiving side) plate correspondingly. Keeping the 0 bending mode only, the out of plane displacements of the plate origins for a unit amplitude incoming wave can be written as:

$$u_1 = Q_{P_{3,1}} A_1 + Q^{in}_{P_{3,4}} A_1^n + Q^{in}_{P_{3,1}} \tag{3.7}$$

$$u_2 = -Q_{P_{3,1}} A_2 - Q^{in}_{P_{3,4}} A_2^n \tag{3.8}$$

where A_1,A_1^n,A_2,and A_2^n are the bending wave amplitudes (the index corresponds to the plate number and n designates the near field). Also:

$$Q_{P_{11,1}} A_1 + Q^{in}_{P_{11,4}} A_1^n + + Q^{in}_{P_{11,1}} = 0 \tag{3.9}$$

$$Q_{P_{11,1}} A_2 + Q^{in}_{P_{11,4}} A_2^n = 0 \tag{3.10}$$

Similarly, the normal forces acting on the plates joints are calculated as:

$$F_1 = S_{P_{3,1}} A_1 + S^{in}_{P_{3,4}} A_1^n + S^{in}_{P_{3,1}} \tag{3.11}$$

$$F_2 = -S_{P_{3,1}} A_2 - S^{in}_{P_{3,4}} A_2^n \tag{3.12}$$

The minus signs are needed to convert the direction of the top plate Z–axis to the global coordinate system.

Alternative to the exponential form, the beam longitudinal displacement field can be

expressed (in terms of sine and cosine functions instead of the exponentials) as:

$$u_z(z) = \cos k_L z \, A_1^B + i \, \sin k_L z \, A_2^B \tag{3.13}$$

The axial force is now calculated as:

$$F_z(z) = -E\mathcal{A} \frac{\partial u_z}{\partial z} = (E\mathcal{A} \, k_L \, \sin k_L z) \, A_1^B + (-i \, E\mathcal{A} \, k_L \, \cos k_L z) \, A_2^B \tag{3.14}$$

The connection of the beam and the plates dictates the equality of the beam axial displacement and the plate out of plane displacement plate origin. Moreover, the longitudinal forces on the tips of the beam balance the normal forces acting on the origins of the plates. Therefore, the compatibility and equilibrium conditions on the joints give the following set of equations:

$$\begin{cases} Q_{P_{3,1}} \, A_1 + Q^{in}_{P_{3,4}} A_1^n + Q^{in}_{P_{3,1}} - \, A_1^B = 0 \\ Q_{P_{11,1}} \, A_1 + Q^{in}_{P_{11,4}} A_1^n + + Q^{in}_{P_{11,1}} = 0 \\ S_{P_{3,1}} \, A_1 + S^{in}_{P_{3,4}} A_1^n + S^{in}_{P_{3,1}} - i \, E\mathcal{A} \, k_L \, \cos k_L L_B \, A_2^B = 0 \\ Q_{P_{3,1}} \, A_2 + Q^{in}_{P_{3,4}} A_2^n - \cos k_L L_B \, A_1^B - i \, \sin k_L L_B \, A_2^B = 0 \\ S_{P_{3,1}} \, A_2 + S^{in}_{P_{3,4}} A_2^n - E\mathcal{A} \, k_L \, \sin k_L L_B \, A_1^B + i \, E\mathcal{A} \, k_L \, \cos k_L L_B \, A_2^B = 0 \\ Q_{P_{11,1}} \, A_2 + Q^{in}_{P_{11,4}} A_2^n = 0 \end{cases} \tag{3.15}$$

The reflected (A_1) and transmitted (A_2) wave amplitudes can be obtained from the above equations. The transmitted wave amplitude is computed as:

$$A_2 = \frac{E\mathcal{A} k_L Q_{P_{11,4}}}{\sin k_L L_B} \frac{P_1 - P_2}{P_3 + P4 - (E\mathcal{A} k_L)^2} \tag{3.16}$$

where P_1 to P_4 are:

$$P_1 = \frac{Q^{in}_{P_{3,1}}(S_{P_{3,1}}Q_{P_{11,4}}-S_{P_{3,4}}Q_{P_{11,1}})-Q^{in}_{P_{11,1}}(S_{P_{3,1}}Q_{P_{3,4}}-S_{P_{3,4}}Q_{P_{3,1}})}{(Q_{P_{3,1}}Q_{P_{11,4}}-Q_{P_{11,1}}Q_{P_{3,4}})^2} \tag{3.17}$$

$$P_2 = \frac{S^{in}_{P_{3,1}}}{Q_{P_{3,1}}Q_{P_{11,4}}-Q_{P_{11,1}}Q_{P_{3,4}}} \tag{3.18}$$

$$P_3 = \frac{2E\mathcal{A}k_{_L}}{\tan k_{_L}L_{_B}}\frac{S_{P_{3,1}}Q_{P_{11,4}}-S_{P_{3,4}}Q_{P_{11,1}}}{Q_{P_{3,1}}Q_{P_{11,4}}-Q_{P_{11,1}}Q_{P_{3,4}}} \tag{3.19}$$

$$P_4 = \left(\frac{S_{P_{3,1}}Q_{P_{11,4}}-S_{P_{3,4}}Q_{P_{11,1}}}{Q_{P_{3,1}}Q_{P_{11,4}}-Q_{P_{11,1}}Q_{P_{3,4}}}\right)^2 \tag{3.20}$$

Equation (3.16) can also be expressed in terms of the plate impedance ($Z^{P}_{3,3}$) as:

$$A_2 = \frac{\frac{E\mathcal{A}k_{_L}}{i\,\omega\,\sin k_{_L}L_{_B}}Z^{P^*}}{Z^{P2}_{3,3}+\frac{2E\mathcal{A}k_{_L}}{i\,\omega\,\tan k_{_L}L_{_B}}Z^{P}_{3,3}-\left(\frac{E\mathcal{A}k_{_L}}{\omega}\right)^2} \tag{3.21}$$

where Z^{P^*} is:

$$Z^{P^*} = \frac{Q_{P_{11,4}}Q^{in}_{P_{3,1}}Z^{P}_{3,3}}{Q_{P_{3,1}}Q_{P_{11,4}}-Q_{P_{11,1}}Q_{P_{3,4}}} - \frac{Q_{P_{11,4}}Q^{in}_{P_{11,1}}(S_{P_{3,1}}Q_{P_{3,4}}-S_{P_{3,4}}Q_{P_{3,1}})}{i\,\omega\,(Q_{P_{3,1}}Q_{P_{11,4}}-Q_{P_{11,1}}Q_{P_{3,4}})^2} + \frac{S^{in}_{P_{3,1}}Q_{P_{11,4}}}{i\,\omega\,(Q_{P_{3,1}}Q_{P_{11,4}}-Q_{P_{11,1}}Q_{P_{3,4}})} \tag{3.22}$$

As the beam longitudinal wave number approaches to 0, the above formula reduces to:

$$A_2 = \frac{\frac{Z^{P^*}}{Z_{Spring}}}{\frac{Z^{P}_{3,3}}{Z_{Spring}}+\left(\frac{Z^{P}_{3,3}}{2Z_{Spring}}\right)^2} \tag{3.23}$$

The plates are assumed to be identical, hence, the power transmission coefficient is simply reduced to $|A_2|^2$.

To verify that the symmetric bending mode of the full matrix solution generates the same results as the closed formula for this special case, the solutions of both methods are compared for following numerical examples:

- Steel plates (Young's modulus: 200 GPa, Poisson's ratio: 0.32, density 7850 kg/m^3)

of 5 mm in thickness and a steel connecting beam of length 5 cm with a circular cross section of radius 5 mm.

- Two 1 mm aluminum plates (Young's modulus: 70 GPa, Poisson's ratio: 0.35) and a circular connecting aluminum beam of length 10 cm and of radius 1 cm.

As it is seen from the figures (3.2) and (3.3) the matrix solution is identical to the calculations from the closed form formula. Also, it is notable that the stiffer the beam is, the larger the transmission coefficient will be. This perfectly makes sense since it means that the more rigidly connected plates exchange their vibrational energy easier. Also, it is seen that the small argument expansion for the trigonometric functions are acceptable for the practical structural configurations.

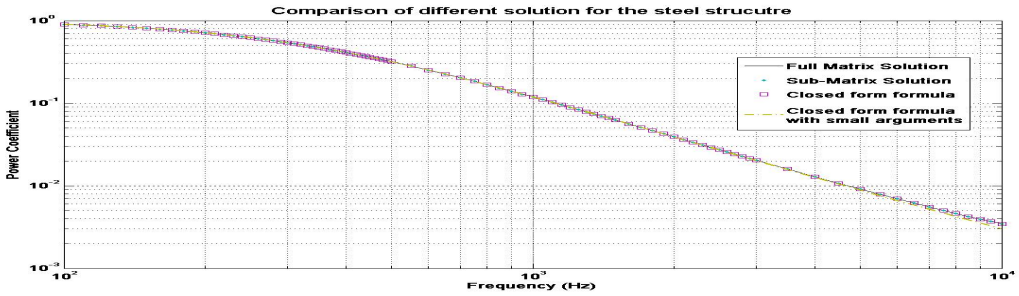

Figure 3.2: Verification of the matrix method for a special case (two steel plates connected via an steel beam

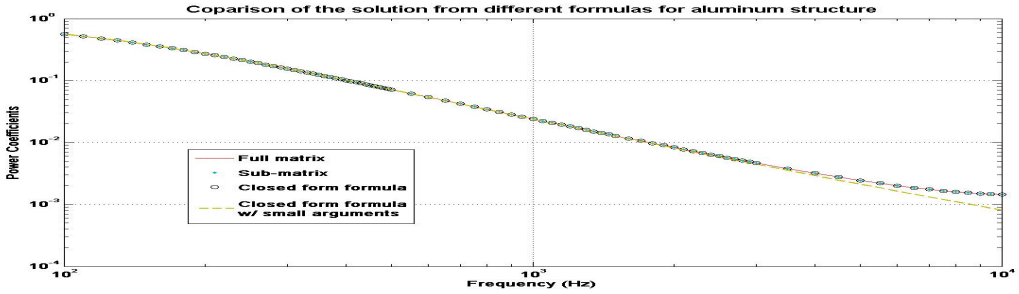

Figure 3.3: Verification of the matrix method for a special case (two aluminum plates connected via an aluminum beam)

3.2.3 Plates connected via a spring

The power transmission between two point connected subsystems can be obtained by means of their impedances. It is known that the power transmission coefficient for two mechanical subsystems with mechanical impedances Z_1 and Z_2 can be calculated as (Lyon [2]):

$$\tau_{sys} = \frac{4\,\Re(Z_1 Z_2)}{|Z_1 + Z_2|^2} \tag{3.24}$$

where $\Re$ indicates the real part of a complex number.

A spring impedance is calculated from the Hooke's law as:

$$Z_{_{Spring}} = \frac{S_{_{Spring}}}{i\,\omega} = i\,Z_{_S} \tag{3.25}$$

where $S_{_{Spring}}$ is the spring stiffness which is a purely imaginary complex number.

To take advantage of this formula, it is possible to consider the spring and one of the plates as one subsystem. The impedance of the plate and spring can be found by combining two impedances which are connected in series. Hence:

$$Z_{_{SP}} = \frac{Z_P Z_{_{Spring}}}{Z_P + Z_{Spring}} = \frac{i\,Z_P Z_S}{Z_P + i\,Z_S} \tag{3.26}$$

where $Z_{_{SP}}$ is the impedance of the combined plate and spring subsystem. $Z_{_P}$ (which according to the classical formula is a real number) is the plate normal force impedance. Combining equations (3.24) and (3.26):

$$\tau_{sys} = \frac{4\,\Re(Z_{P_2}\frac{i\,Z_{P_1}Z_S}{Z_{P_1}+i\,Z_S})}{\left|Z_{P_2} + \frac{i\,Z_{P_1}Z_S}{Z_{P_1}+i\,Z_S}\right|^2} = \frac{4Z_{P_1}Z_{P_2}}{\left(\frac{Z_{P_1}Z_{P_2}}{Z_S}\right)^2 + (Z_{P_1}+Z_{P_2})^2} \tag{3.27}$$

If both plates have identical properties, the above formula will reduce to:

$$\tau_{sys} = \frac{1}{1 + \left(\frac{Z_P}{2Z_S}\right)^2} \tag{3.28}$$

The spring model also implies that if the spring is chosen very stiff relative to the plate,

the power transmission coefficients will be close to one. this is in accordance with the close formula insight. However the pitfall of the spring model is that one can argue that the energy path from one plate to another can be considered as a series of three subsystems: plate, spring, plate. The average energy transmitted from a plate to the spring will be zero sice the impedance of a plate is a real number and the spring impedance is purely imaginary; therefore, (3.24) suggests that no power exchange can take place.

3.2.4 Comparison of the spring and beam model

In this section a very light beam and a spring model results are compared. These formulas have similar forms; however, the existing model for the connection of the plates through a light spring can not capture the effect of the finite length of the spring and is indifferent to the distance of the plates which is in general not right.

A light beam can be considered as a spring. This can be shown by evaluating equations (3.13) and (3.14) at z=0. It is possible to eliminate the wave constants and find the kinematic and constitutive laws for beam longitudinal vibration. Therefore:

$$u_{_z}(0) = u_0 = A_1^{^B} \tag{3.29a}$$

$$F_{_z}(0) = F_0 = -i\,E\mathcal{A}\,A_2^{^B} \tag{3.29b}$$

Substituting the wave constants found from equations (3.29) into equations (3.13) and (3.14), the displacements and the forces can be related directly as:

$$u_{_L} = (\cos k_{_L}L_{_B})\;u_0 + \left(-\frac{\sin k_{_L}L_{_B}}{E\mathcal{A}\,k_{_L}}\right)F_0 \tag{3.30a}$$

$$F_{_L} = (E\mathcal{A}\,k_{_L}\sin k_{_L}L_{_B})\,u_0 + (\cos k_{_L}L_{_B})\;F_0 \tag{3.30b}$$

A common assumption for a light spring model is that the forces acting on the tips of a light spring are equal and opposite. Moreover, a linear spring, follows the Hooke's law; therefore

the analogous displacement and force equations for a light spring model are:

$$u_{_L} = u_0 - \frac{1}{S_{_{Spring}}} F_0 \tag{3.31a}$$

$$F_{_L} = F_0 \tag{3.31b}$$

An inspection of the equations (3.30) and (3.31) reveals that as the density of a beam approaches to 0, the beam wave number also tends to 0: $k_{_L} = \omega \sqrt{\frac{\rho}{\mu}} \rightarrow 0$. This shows that the beam model actually reduces into light a spring that has an equivalent stiffness of $\frac{E\mathcal{A}}{L_{_{Sp}}}$, where $L_{_{Sp}}$ is the length of the spring. A close exam reveals that in the limit, as the density of the beam approaches to 0, power transmission coefficient obtained from equation (3.16) reduces to equation (3.28) only if the absolute values of the plate and spring impedances are close. In other words, this shows that the complete model can capture more aspects of the power transmission than the well known simple spring model.

3.2.5 Breaking down the model to two plates and two semi-infinite beams

Another way to estimate the power transmitted from one plate to another plate is by decomposing the structure into two subsystems in a different way. This time, one plate and a semi-infinite beam can be considered as a subsystem.

The power exchange expression of equation (3.24) can be used to find the energy transmitted from the source plate to a semi-infinite beam as:

$$\tau_{_{Plate \rightarrow Beam}} = \frac{4\Re(Z_{_{Beam}} Z_{_{Plate}})}{|Z_{_{Beam}} + Z_{_{Plate}}|^2} \tag{3.32}$$

The impedance of a semi-infinite beam at its tip can easily be computed as:

$$Z_{_{Beam}} = \frac{F_{_{Beam}}(0)}{i\,\omega\, u_{z_{Beam}}(0)} = \frac{-E\mathcal{A}\frac{\partial u_z}{\partial z}(0)}{u_z(0)} = \frac{E\mathcal{A}k_{_L}}{\omega} = E\mathcal{A}\sqrt{\frac{\mu}{\rho}} \tag{3.33}$$

As it is seen the impedance of a semi-infinite beam at the tip is constant.

Now the structure can be considered as a combination of two parts, each containing a plate and a semi-infinite beam. The plates are identical. Hence, from energy reciprocity,

the power transmitted from the plate to the beam is equal to the power transmitted from the beam to the plate. Therefore, the overall power transmission of the system is computed by squaring the power transmission from one of the plates to the assumed semi-infinite beam. Recalling that the classical plate impedance is a real constant, the overall power transmission is obtained as:

$$\begin{aligned} \tau_{Plate1\rightarrow Plate2} &= \frac{16 Z_{Beam}^2 Z_{Plate}^2}{(Z_{Beam}+Z_{Plate})^4} \\ \tau_{Plate1\rightarrow Plate2} &= \frac{1024\, D_{Plate} L_{Plate} E_{Beam}^2 \mu_{Beam} \mathcal{A}_{Beam}^2 \frac{\rho_{Plate}}{\rho_{Beam}}}{\left(8\sqrt{D_{Plate} L_{Plate} \rho_{Plate}} + E_{Beam}\mathcal{A}\sqrt{\frac{\mu_{Beam}}{\rho_{Beam}}}\right)^4} \end{aligned} \tag{3.34}$$

Since both of the impedances are constant, the power transmission estimation from this simple model is constant. Obviously the estimation is not accurate enough to model the power exchange between two parallel plates.

3.2.6 Comparison of the methods by numerical examples

In this section, through two numerical examples, the power transmission coefficient between two identical plates are obtained and compared for the different models. These models are: power exchange by only considering the symmetrical bending mode of the plate vibration (both the closed form formula and matrix method); modeling the connection as a spring; and the impedance method. For each example, a specific value for the spring stiffness (or the spring equivalent to the beam) is considered and the power coefficients are computed afterwards. For the first numerical example, the spring constant is around 10 kN/m and for the second one, the spring constant is set around 100 kN/m. For each one, the beam properties are varied in such a way that the equivalent spring impedance remains unchanged. The power transmission coefficient resulting from different beam properties are then compared to those resulting from the spring model and the simple model with the constant power coefficient (two subsystems each including a semi-infinite beam and an infinite plate). For both cases, the plates are assumed to be identical steel plates (with a Young's Modulus of 200 GPa, mass density of 7850 kg/m^3, and a Poisson's ratio of 0.32). The plates thicknesses are both 1mm. Furthermore it is assumed that the plates are large

enough to be modeled as infinite thin plates. Studied cases for each spring constant are:

- case 1: The light beam as a benchmark.
- case 2: Length and the Young's modulus of the beam are increased by a factor of 5; (therefore the equivalent stiffness remains the same).
- case 3: Length and the Young's modulus of the beam are reduced by a factor of 5.
- case 4: The radius of the cross section and the length are increased by a factor of 5 and the Young's modulus of the beam and is reduced by a factor of 5.

As the first example, a spring with a stiffness value around 10 kN/m is considered (the mass density value is selected very small because a very light beam represents a spring). An equivalent stiffness (which is calculated from $\frac{E\mathcal{A}}{L_{Sp}}$) around this value can be obtained by choosing the following properties: E = 12.73 MPa (Young's Modulus), ν= 0.3 (the Poisson's ratio), radius of the cross section of the Beam: 5 mm, and the original length is considered 10 cm. The following graphs shown in figure (3.4) the results obtained for this example.

For the second example, the spring stiffness value will be 10 times larger than the first example; i.e.: around 100 kN/m. To get an equivalent stiffness for the beam, the properties are chosen as: E = 63.65 MPa (Young's Modulus), ρ = 1e-6 kg/m^3 (the mass density value is selected very small because a very light beam represents a spring), ν= 0.3 (the Poisson's ratio), radius of the cross section of the Beam: 1 cm, and the original length is considered 20 cm. Figure (3.5) shows the results obtained for different cases of this example.

It is observed that in general the spring model predicts less energy exchange in lower frequencies comparing to the more involved light beam model. This is due to the fact that unlike the spring model, the power exchange happens through whole cross section of the beam not through just one point. Also the spring results are not sensitive to the length provided that the stiffness remains the same; this simplification is not in accordance with the fact that a length is important in such structures. Another observation is that for lower frequency range, the light beam model is not sensitive to property variations if the

equivalent stiffness remains constant; however, a shorter flexible beam (case 4) deviates from the benchmark faster and blocks more energy transmission in higher frequencies.

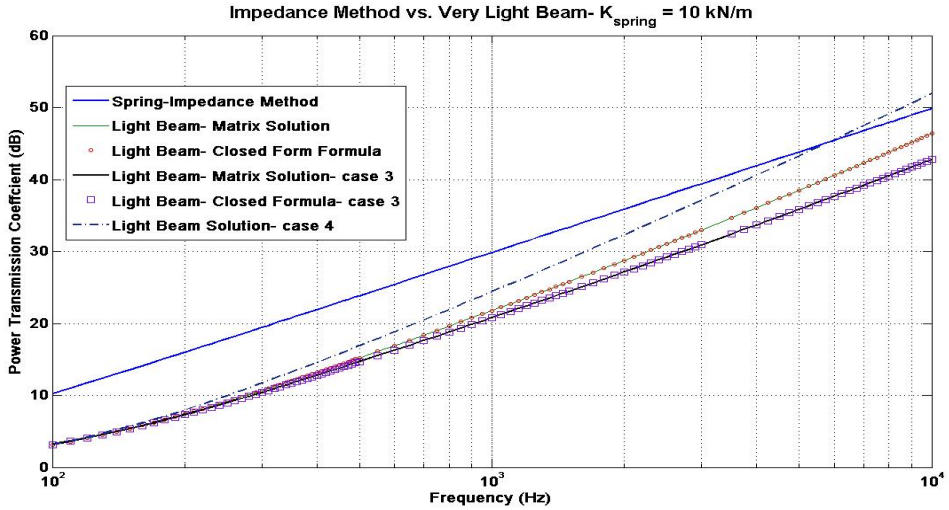

Figure 3.4: Verification of the matrix method for a special case (two steel plates connected via an steel beam

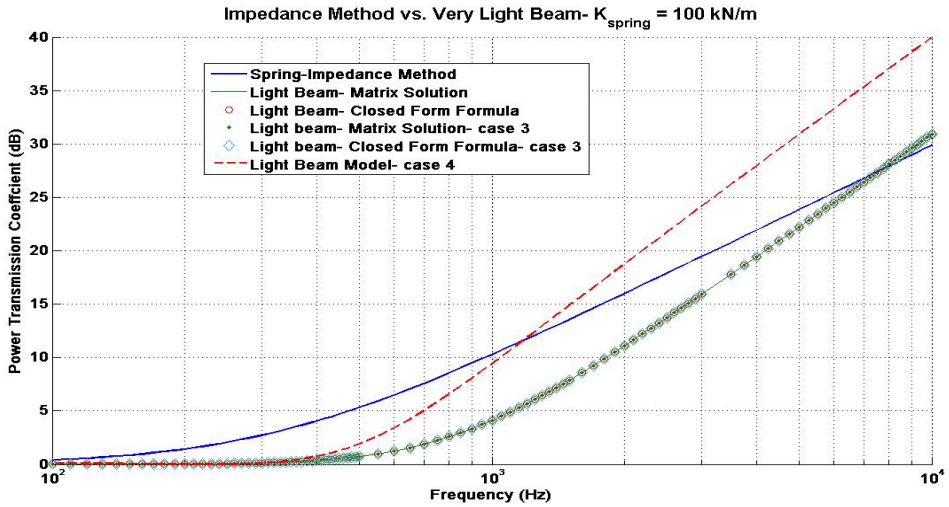

Figure 3.5: Verification of the matrix method for a special case (two aluminum plates connected via an aluminum beam)

3.3 Vibrational Power Transmission found by beam model- a case study

In this section, the previous semi-infinite beam and plate system is converted to a finite length beam that connects two identical plates. The plates are thin (3.175 mm thickness) and from aluminum ($\rho = 2700kg/m^3, E = 7.1GPa, \nu = 0.3$). The beam is a strip of width 38.1 mm from the plates. The beam is attached perpendicularly to the parallel plates. The beam length is chosen as 5cm.

In this numerical example, the beam properties along the lateral axes are different. Therefore, it is possible to compare the effect of the beam along the X and Y axes.

An incoming wave can potentially lead into 8 transmission and 8 reflection coefficients. For this example, the nonzero coefficients are plotted in figures (3.6) to (3.13) over a frequency range of interest which is 0.1-10 kHz.

It is observed that an incoming plate symmetric bending wave only excites longitudinal wave in the beam and an incoming symmetric torsional wave in the plate causes a purely torsional motion in the beam. The other incoming wave in the plate, exactly excite one mode of the bending, longitudinal, and torsional wave types. This is due to the fact that the matrix is a first order expansion of independent modes.

Another interesting property of the response is the reciprocity which is another check for the correctness of the method. The reflection and transmission coefficients of two specific wave types (one in the beam and the other one in the plate) are the same. For instance, the transmission coefficient of an incoming symmetric bending wave in one plate is the same as the transmission coefficient of an incoming symmetric bending wave from the plate (since an incoming symmetric bending wave in one plate only excites a symmetric bending wave in the other plate). This is also true for a symmetric torsional wave. Like the semi-infinite beam case, an incoming wave in one of the plates at most excites one mode of each wave types in the other plate (i.e. at most exactly excite one mode of the bending, one mode of the longitudinal wave, and one mode of the torsional wave). The reciprocity of the energy paths is also retained.

The energy conservation can be maintained only if the sum of the power coefficients are

equal to 1. For instance, the following criterion can be defined to determine the accuracy

$$accuracy = \max_{frequency} (|1 - max\sum \tau_{ij}|, |1 - min\sum \tau_{ij}|)$$

For this example, the sum of the coefficients for each in-coming wave is 1 with an accuracy of 10^{-12}.

For this problem, the symmetric bending mode is the main mechanism of vibration power exchange between the plates. Like the previous case of similar plates, as the frequency increases, the power transmission coefficient drops and more of the wave is reflected. On the other extreme, the symmetric shearing mode is of least significance. Although some finite length effect is observed; but since usually a frequency averaging is employed in determining the final result, the resonance is not importance. A symmetric mode can only excite symmetric mode of the same wave type in the plates.

Cosine bending mode is the next important mode in this problem; however, it is ignorable when the frequency is less than 5 kHz. A cosine bending (longitudinal) mode only excite cosine bending and longitudinal modes and sine shearing modes of the plates. The sine modes of bending (longitudinal) waves excite only the sine modes of the bending and longitudinal waves and the cosine shearing waves. Shearing waves, however, can excite the same mode of shearing waves and the opposite mode type of the other wave types.

In general, the bending wave types have more contribution in power exchange and the shearing waves are of least importance.

Finally it is seen that a stiffer beam, reflects more in-plane waves and permits less power exchange. This is the reason that a much smaller transmission coefficients are found along the stiffer side of the beam.

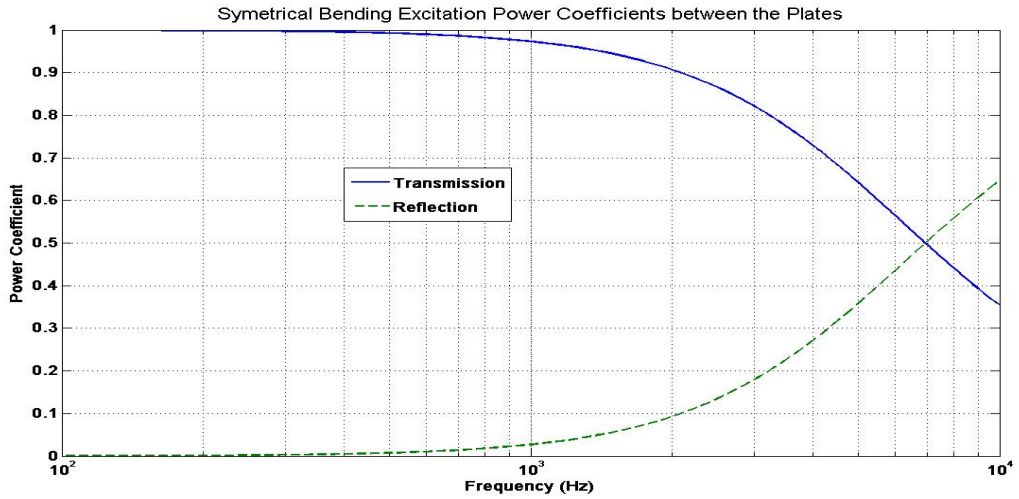

Figure 3.6: Power transmission coefficients for a symmetric bending mode

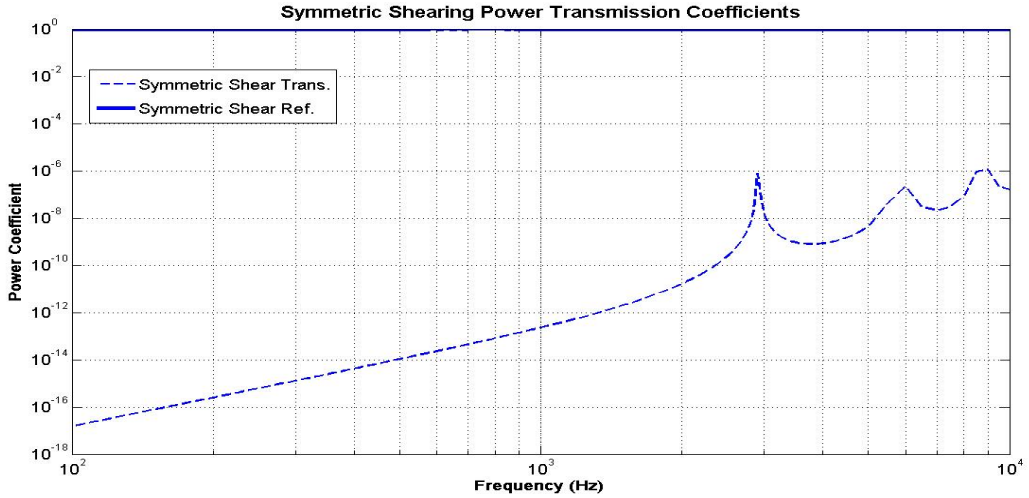

Figure 3.7: Power transmission coefficients for a symmetric shearing mode)

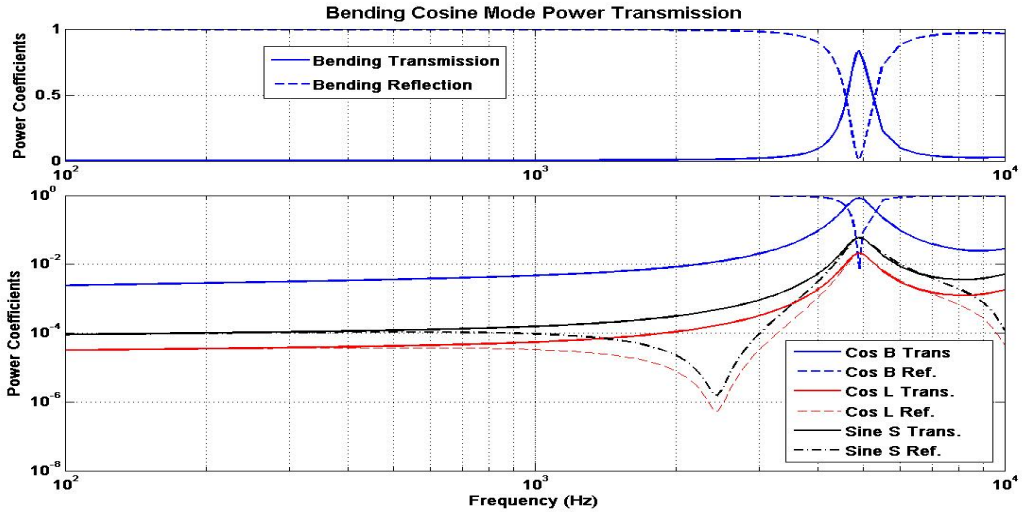

Figure 3.8: Power transmission coefficients for a cosine bending mode

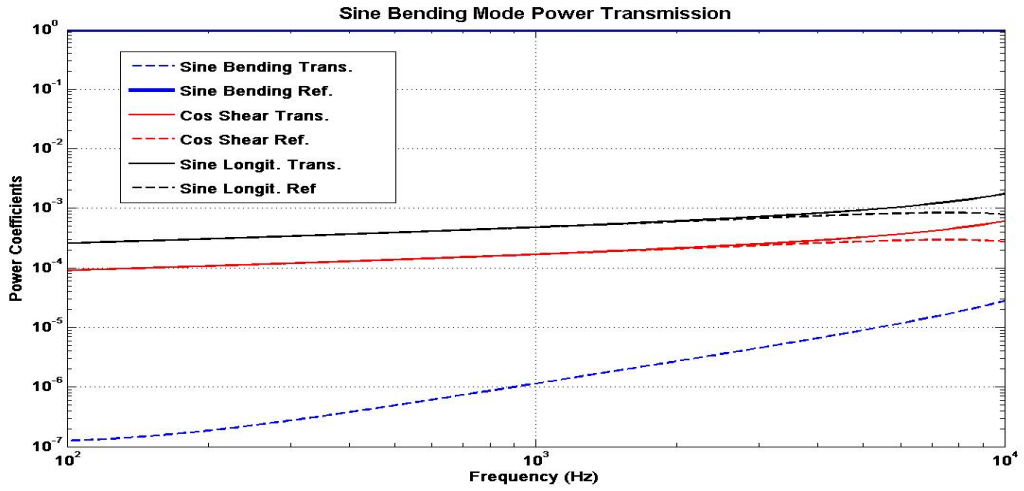

Figure 3.9: Power transmission coefficients for a sine bending mode

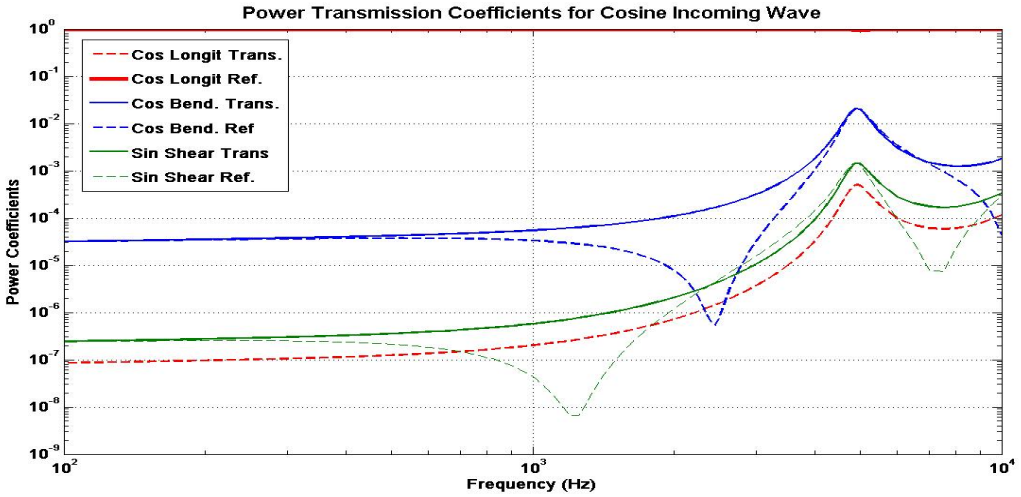

Figure 3.10: Power transmission coefficients for a cosine longitudinal mode

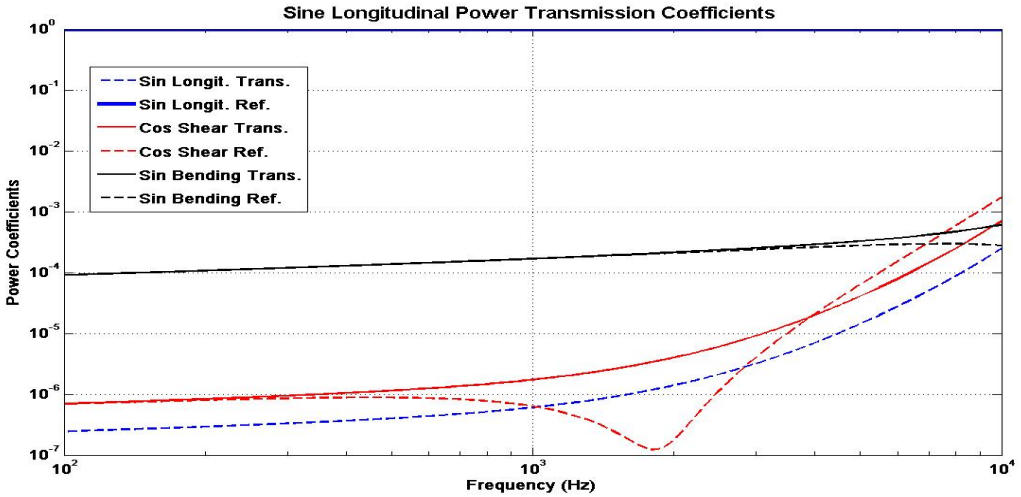

Figure 3.11: Power transmission coefficients for a sine longitudinal mode

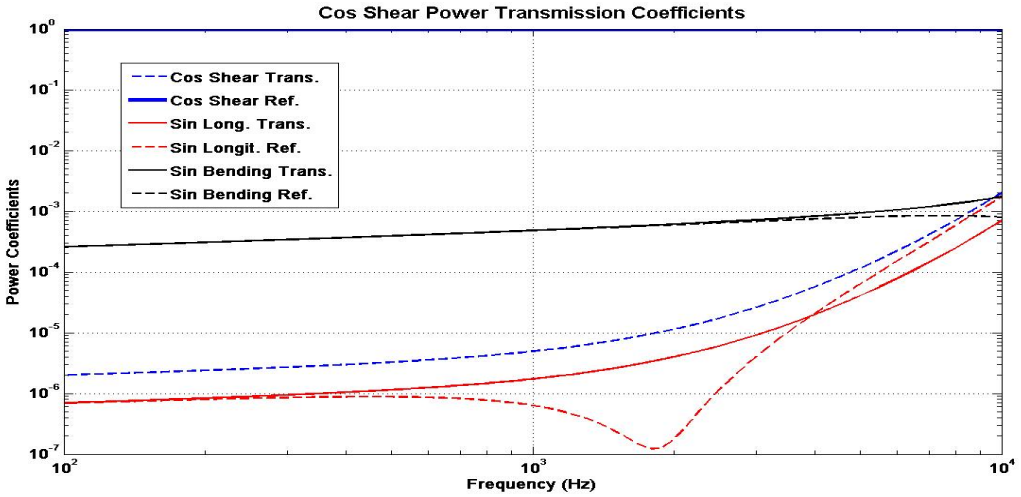

Figure 3.12: Power transmission coefficients for a cosine shearing mode

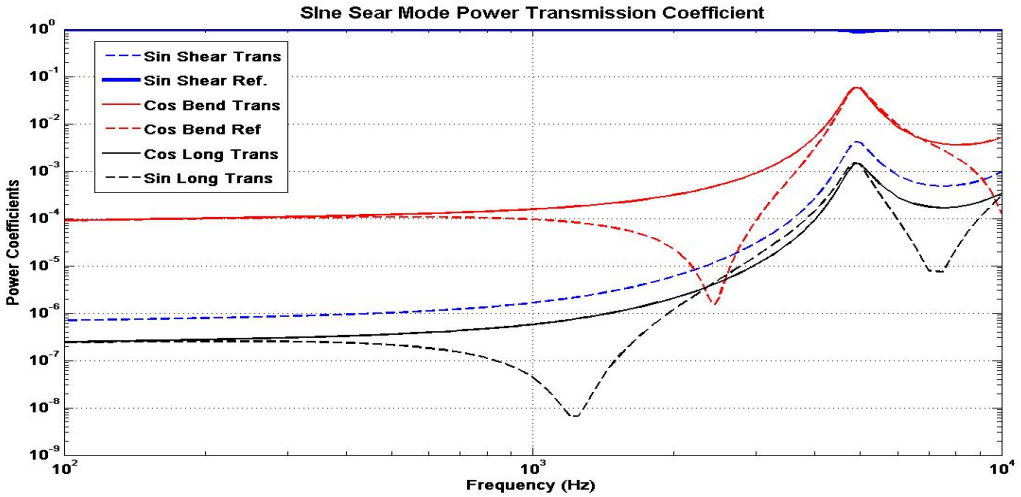

Figure 3.13: Power transmission coefficients for a sine shearing mode

CHAPTER 4

Analysis of Layered Structures

4.1 Introduction

Many structures in daily life are made of layers of material. For instance, if an aircraft fuselage is sectioned, the outer panel, noise treatment material, and inner panel which are possibly separated with some air gaps can be recognized. Such structures are commonly modeled as layers of materials with infinite width and finite depth. Below, a matrix method is developed to analyze such structures. This analysis will be used in next chapter for modeling a sandwich structure by element suitable for EFEA.

In this chapter, first the matrices for an infinite layer of porous material is derived form the plain wave equations. Then, the matrices for a solid layer, a thin plate, and a layer of plate like fluid are derived by considering special case of the complete porous material model. Also, a more general case of a solid layer whose material is only isotropic transversely is given. The boundary conditions are applied to find a library of matrices for different surface conditions.

4.2 Porous medium wave equations

A porous medium is considered to be a continuum consisting of two phases in equilibrium: a solid phase and a fluid phase. The solid phase is a porous matrix where the fluid phase fills the pores.

Porous materials are commonly assumed to be homogenous and isotropic due to the

complexity of the model and the difficulties of obtaining the material constants. The filling fluid can be quite light such as air or heavy like water. The fluid phase may be modeled as a simple inviscid fluid or may be represented by a more mathematically complicated fluid constitutive law. Since both fluid and solid phases are in dynamic equilibrium, the deformation of a porous material makes the fluid in between the pores to diffuse.

Compared to the fluid, the solid matrix may be often assumed to be rigid [25] and [26]; poroelasticity on the other hand, takes into account deformability of the solid component. Poroelasticity approaches the rigid matrix representation when the flow resistance of the pores is very small and the frequency range is quite high [26]. Poroelasticity theory was originally developed in response to the seminal work of Biot in 1950's [27]. Biot accounted for the inertia and viscous influences through interactions of the fluid by using a Lagrangian model [28]. Assuming this model, he devised two types of wave equations that govern the motion particle of the system of porous materials. He also concluded that there is a mathematical analogy between the thermoelasticity and poroelasticity [26] and [29].

The development of poroelasticity was originally motivated from geophysics and studies of soil. Poroelasticity has been successfully used to model material systems in different fields of study such as seismic waves, rock and soil mechanics, sea-bed studies, biomechanics and biomaterial, and noise insulating materials; e.g. [26]. As an example, elastic porous material theory has been employed to investigate bones. Although compared to the hard component of the bone, the inside fluid has a very small bulk modulus,the dynamic load effects of the fluid cannot be ignored. In other words, a slowly loaded drained bone does not respond much differently from a bone with the fluid inside; however, this is not quite true if the forces are dynamic [26].

The general form of the governing equations of motion for a porous medium saturated by a fluid has been derived by Biot [27] as:

$$\sigma^s_{ij,j} - b(\dot{u}^s_i - \dot{u}^f_i) + F^s_i = \rho_{11}\ddot{u}^s_i + \rho_{12}\ddot{u}^f_i \tag{4.1}$$

$$\sigma^f_{,i} + b(\dot{u}^s_i - \dot{u}^f_i) + F^f_i = \rho_{12}\ddot{u}^s_i + \rho_{22}\ddot{u}^f_i \tag{4.2}$$

In the above equations, σ's represent the stresses, superscripts indicate the components (i.e.

"f" for fluid and "s" for solid), subscripts ($i, j = x, y, z$) identify the directions, ρ_{11}, ρ_{12}, and ρ_{22} are densities that incorporate inertial interactions of the fluid and solid phases, b is a damping constant which is a function of the permeability, fluid phase viscosity, and the porosity, and F's are the body forces. The material constitutive laws are:

$$\sigma_{ij}^s = 2\,\mu\,\epsilon_{ij}^s + (\lambda\,e^s + Q_p\,e^f)\,\delta_{ij} \tag{4.3}$$

$$\sigma^f = -\phi_p\,p^f = Q_p\,e^s + R_p\,e^f \tag{4.4}$$

where λ and μ are Lamé's coefficients for the solid phase; Q_p and R_p are fluid phase related material constants; δ_{ij} is the Kronecker symbol; and e is the dilatation; i.e.:

$$e = \epsilon_{ii} = u_{i,i}. \tag{4.5}$$

The material constants for an open cylindrical pore porous material can be completely determined in terms of the following seven solid phase constants and the properties of air [30]: porosity ϕ_p; solid phase Poisson's ratio ν_s; structural shape factor ϵ'; flow resistivity σ_r; solid phase structural dissipation factor η_s; solid phase Young's modulus E_s; the solid phase density ρ_s; the speed of sound in air c_0; and the air density ρ_0. The constants reported by Bolton [30] in the current notation are:

$$\rho_{11} = \rho_s + \phi_p\,\rho_0\,(\epsilon' - 1) \tag{4.6}$$

$$\rho_{22} = \phi_p\,\rho_0\,\epsilon' \tag{4.7}$$

$$\rho_{12} = -\phi_p\,\rho_0\,(\epsilon' - 1) \tag{4.8}$$

The liquid bulk modulus between the cylindrical pores (E_2) is:

$$E_2 = \frac{E_0}{1 + \dfrac{2\,(\gamma_0 - 1)\,J_1\left(\lambda_c\sqrt{-i\,N_{Pr}}\right)}{\lambda_c\,\sqrt{-i\,N_{Pr}}\,J_0\left(\lambda_c\sqrt{-i\,N_{Pr}}\right)}} \tag{4.9}$$

where E_0 is the bulk modulus of air; γ_0 is the specific heats ratio for air (= 1.4); J_i is the Bessel function of order i; N_{Pr} is the Prandtl number (=0.713 at 20 C$^\circ$); $i = \sqrt{-1}$; and λ_c

depends on the angular velocity ω; fluid density ρ_f; structural factor of the pores ϵ'; flow resistivity σ_r; and the porosity ϕ_p as:

$$\lambda_c^2 = \frac{8\,\omega\,\rho^f\,\epsilon'}{\sigma_r\,\phi_p} \tag{4.10}$$

Bulk modulus of air can be expressed in terms of the speed of sound in air and the air density:

$$E_0 = \rho_0\,c_0 \tag{4.11}$$

Finally, the constants used in the governing equation of motion are:

$$Q_p = (1-\phi_p)\,E_2 \tag{4.12}$$

$$R_p = \phi_p\,E_2 \tag{4.13}$$

$$b = -\frac{\sigma_r\,\phi_p^2\,\lambda_c\sqrt{-i}\,J_1(\lambda_c\sqrt{-i})}{4\,J_0(\lambda_c\sqrt{-i})}\left(1-\frac{2\,J_1(\lambda_c\sqrt{-i})}{J_0(\lambda_c\sqrt{-i})}\right)^{-1} \tag{4.14}$$

In the absence of the body forces, harmonic ($e^{i\omega t}$) steady state volumetric strains equations are governed by:

$$Q_p\,\nabla^2 e^f + \omega^2\rho_{12}^*\,e^f = -P\,\nabla^2 e^s - \omega^2\rho_{11}^* e^s \tag{4.15}$$

$$R_p\,\nabla^2 e^f + \omega^2\rho_{22}^*\,e^f = -Q_p\,\nabla^2 e^s - \omega^2\rho_{12}^* e^s \tag{4.16}$$

where the new mass coefficients are defined by:

$$\rho_{ij}^* = \rho_{ij} + \frac{b}{i\omega}\,(-1)^{i+j} \tag{4.17}$$

and $P = \lambda + 2\,\mu$. Equations (4.15) and (4.16) can also be written as:

$$\nabla^2 e^f = \frac{(\rho_{12}^* Q_p - \rho_{22}^* P)\,\nabla^2 e^s + \omega^2\left({\rho_{12}^*}^2 - \rho_{11}^*\rho_{22}^*\right)e^s}{\rho_{22}^* Q_p - \rho_{12}^* R_p} \tag{4.18}$$

$$e^f = \frac{\left(PR_p - Q_p^2\right)\nabla^2 e^s + \omega^2\left(\rho_{11}^* R_p - \rho_{12}^* Q_p\right)e^s}{\omega^2\left(\rho_{22}^* Q_p - \rho_{12}^* R_p\right)} \tag{4.19}$$

The solid phase dilatational wave equation may be consequently derived from (4.18) and

(4.19) as:

$$\nabla^4 e^s + \chi_1 \nabla^2 e^s + \chi_2 \, e^s = 0 \tag{4.20}$$

where

$$\chi_1 = \frac{\omega^2 \left(\rho_{11}^* \, R_p - 2\rho_{12}^* \, Q_p + \rho_{22}^* \, P\right)}{P \, R_p - Q_p^2} \tag{4.21}$$

$$\chi_2 = \frac{\omega^4 \left(\rho_{11}^* \, \rho_{22}^* - \rho_{12}^{*\,2}\right)}{P \, R_p - Q_p^2} \tag{4.22}$$

Two dilatational wave numbers can be found from the characteristic equation of the above differential equation:

$$k_{\substack{1 \\ (2)}} = \sqrt{\frac{\chi_1 \overset{+}{\underset{(-)}{}} \sqrt{\chi_1^2 - 4\chi_2}}{2}} \tag{4.23}$$

The torsional wave number of solid may be found in a similar way:

$$k_t = \frac{\omega}{\sqrt{\mu}} \sqrt{\rho_{11}^* - \frac{\rho_{12}^{*\,2}}{\rho_{22}^{*\,2}}} \tag{4.24}$$

Once the free wave numbers are determined, the velocity potentials of the two dilatational waves ($\Phi_i(x,z,t) = \phi_i(z) \, e^{i(\omega \, t - k_x \, x)}, i = 1,2$) and the divergence free shearing velocity ($\Psi(x,z,t) = \psi_i(z) \, e^{i(\omega \, t - k_x \, x)}$) for a porous layer (with the coordinates shown in figure 4.1) can be computed. To determine the trace wave number, k_x, the general Snell's law must be applied to match the trace speeds. This means that for an incident wave number k_{inc} and an incident angle θ_{inc}:

$$k_x = k_{inc} \, \sin\theta_{inc} \; = k_i \, \sin\theta_i \; , \qquad\qquad i = 1,2,t. \tag{4.25}$$

Since the wave numbers are all complex, Snell's law must be enforced in the complex plane to find the complex angles [32]. The displacements from these two dilatational waves and the torsional waves are superimposed to evaluate the displacement components of the solid phase:

$$\mathbf{u} = \nabla\phi_1 + \nabla\phi_2 + \nabla \times \boldsymbol{\psi} \tag{4.26}$$

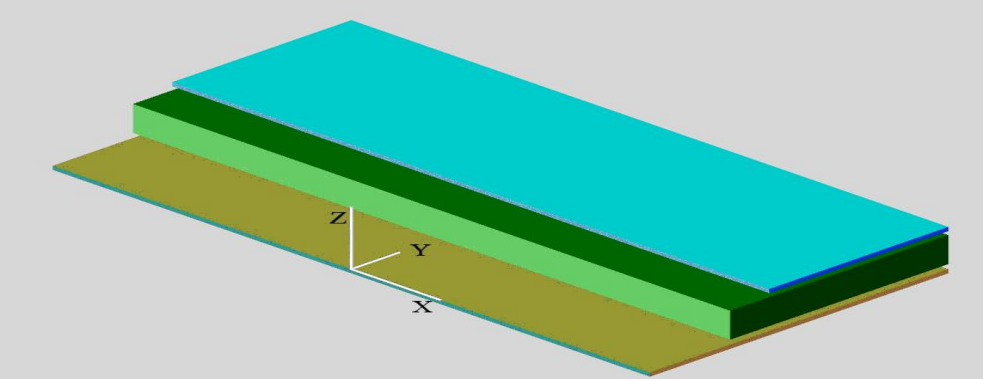

Figure 4.1: Coordinate system chosen for a layer

For a layer structure, the variations along the Y–axis are neglected [31], define:

$$\boldsymbol{\psi}(x,z,t) = (0, \psi_y(x,z,t), 0) \triangleq (0, \phi_t(x,z,t), 0) \tag{4.27}$$

Plane harmonic waves contain both of the incoming and outgoing components. Thus the displacements and the stresses need to be expressed in terms of incoming and outgoing waves of these three wave types. Therefore, the displacement and stress fields of a porous layer can fully be stated in terms of 6 wave amplitudes. Define:

$$\phi_j(x,z) = (C_{j1}\, e^{-i\, k_{jz}\, z} + C_{j2}\, e^{i\, k_{jz}\, z})\, e^{-i\, k_x\, x}, \qquad j = 1,2,t \tag{4.28}$$

$$= (A_{j1}\, \cos k_{jz} z\, + A_{j2}\, i\, \sin k_{jz} z\,)\, e^{-i\, k_x\, x}. \tag{4.29}$$

The displacement vectors are found accordingly as:

$$\mathbf{u} = (\phi_{1,x} + \phi_{2,x} - \phi_{t,z}\,,\, u_y\,,\, \phi_{1,z} + \phi_{2,z} + \phi_{t,x}) \tag{4.30}$$

Fluid displacement components can be determined from the equations of fluid and solid volumetric strains along with the solid phase displacements; however, a smarter way to find the fluid displacement components is by constructing them on the basis of the similarity of the solid and fluid dilatation functions structures. After substituting equation (4.5) into (4.26):

$$e^s = \nabla^2\phi_1 + \nabla^2\phi_2 = -k_1^2\, \phi_1 - k_2^2\, \phi_2 \tag{4.31}$$

The fluid phase dilatational wave function is readily computed via equations (4.19) and (4.31):

$$e^f = -\kappa_1^2\,\phi_1 - \kappa_2^2\,\phi_2 \tag{4.32}$$

where

$$\kappa_i^2 = \frac{2\rho_{11}^*\,R_p - 3\rho_{12}^*\,Q_p + \rho_{22}^*\,P}{\rho_{22}^* Q_p - \rho_{12}^* R_p}\,k_i^2 + \frac{\chi_2}{\omega^2}, \qquad i = 1, 2. \tag{4.33}$$

The z–dependent components of the velocities and stresses are finally computed as:

$$\begin{aligned} v_z^f = &\left(\frac{i\omega b_1 k_{1z}}{k_1^2}\sin k_{1z}z\right)A_{11} + \left(\frac{\omega b_1 k_{1z}}{k_1^2}\cos k_{1z}z\right)A_{12} + \left(\frac{i\omega b_2 k_{2z}}{k_2^2}\sin k_{2z}z\right)A_{21} \\ &+ \left(\frac{\omega b_2 k_{2z}}{k_2^2}\cos k_{2z}z\right)A_{22} + \left(\frac{-\omega g k_x}{k_t^2}\cos k_{tz}z\right)A_{t1} + \left(\frac{-i\omega g k_x}{k_t^2}\sin k_{tz}z\right)A_{t2} \end{aligned} \tag{4.34}$$

$$\begin{aligned} v_z^s = &\left(\frac{i\omega k_{1z}}{k_1^2}\sin k_{1z}z\right)A_{11} + \left(\frac{\omega k_{1z}}{k_1^2}\cos k_{1z}z\right)A_{12} + \left(\frac{i\omega k_{2z}}{k_2^2}\sin k_{2z}z\right)A_{21} + \\ &+ \left(\frac{\omega k_{2z}}{k_2^2}\cos k_{2z}z\right)A_{22} + \left(\frac{-\omega k_x}{k_t^2}\cos k_{tz}z\right)A_{t1} + \left(\frac{-i\omega k_x}{k_t^2}\sin k_{tz}z\right)A_{t2} \end{aligned} \tag{4.35}$$

$$\begin{aligned} v_x^s = &\left(\frac{-\omega k_x}{k_1^2}\cos k_{1z}z\right)A_{11} + \left(\frac{-i\omega k_x}{k_1^2}\sin k_{1z}z\right)A_{12} + \left(\frac{-\omega k_x}{k_2^2}\cos k_{2z}z\right)A_{21} \\ &+ \left(\frac{-i\omega k_x}{k_2^2}\sin k_{2z}z\right)A_{22} + \left(\frac{-i\omega k_{tz}}{k_t^2}\sin k_{tz}z\right)A_{t1} + \left(\frac{-\omega k_{tz}}{k_t^2}\cos k_{tz}z\right)A_{t2} \end{aligned} \tag{4.36}$$

$$\begin{aligned} \sigma_{zz}^f = &\left[(b_1 R_p + Q_p)\cos k_{1z}z\right]A_{11} + \left[i(b_1 R_p + Q_p)\sin k_{1z}z\right]A_{12} \\ &+ \left[(b_2 R_p + Q_p)\cos k_{2z}z\right]A_{21} + \left[i(b_2 R_p + Q_p)\sin k_{2z}z\right]A_{22} \end{aligned} \tag{4.37}$$

$$\begin{aligned} \sigma_{zz}^s = &\left[(\lambda + 2\mu + b_1 Q_p + \frac{2\mu k_{1z}^2}{k_1^2})\cos k_{1z}z\right]A_{11} + \left[i(\lambda + 2\mu + b_1 Q_p + \frac{2\mu k_{1z}^2}{k_1^2})\sin k_{1z}z\right]A_{12} + \\ &\left[(\lambda + 2\mu + b_2 Q_p + \frac{2\mu k_{2z}^2}{k_2^2})\cos k_{2z}z\right]A_{21} + \left[i(\lambda + 2\mu + b_2 Q_p + \frac{2\mu k_{2z}^2}{k_2^2})\sin k_{2z}z\right]A_{22} + \\ &\left(\frac{-2i\mu k_x k_{tz}}{k_t^2}\sin k_{tz}z\right)A_{t1} + \left(\frac{-2\mu k_x k_{tz}}{k_t^2}\cos k_{tz}z\right)A_{t2} \end{aligned} \tag{4.38}$$

$$\begin{aligned} \sigma_{xz}^s = &\left(\frac{-2i\mu k_x k_{1z}}{k_1^2}\sin k_{1z}z\right)A_{11} + \left(\frac{-2\mu k_x k_{1z}}{k_1^2}\cos k_{1z}z\right)A_{12} + \left(\frac{-2i\mu k_x k_{2z}}{k_2^2}\sin k_{2z}z\right)A_{21} \\ &+ \left(\frac{-2\mu k_x k_{2z}}{k_2^2}\cos k_{2z}z\right)A_{22} + \left(\frac{\mu(k_x^2 - k_{tz}^2)}{k_t^2}\cos k_{tz}z\right)A_{t1} + \left(\frac{i\mu(k_x^2 - k_{tz}^2)}{k_t^2}\sin k_{tz}z\right)A_{t2} \end{aligned} \tag{4.39}$$

The above equations can be used to find the matrix which relates the displacement and the stress components to the waves amplitudes vector.

4.3 Isotropic Solid Layer Wave Equations

An isotropic solid layer may be considered as a special case of a homogenous porous layer. Plane wave equations for such a layer can readily be obtained from porous layer wave equations. This is due to the fact that a porous material possesses a more general constitutive material law. As mentioned in section 4.2, three wave types propagate within a porous layer. One of the waves is torsional and the other two are dilatational. A close look at equations (4.21) and (4.23) shows that the longitudinal wave number for a solid medium can be recovered by eliminating the fluid phase as:

$$k_l = k_1 = \sqrt{\frac{\chi_1 + \sqrt{\chi_1^2 - 0}}{2}} = \sqrt{\frac{\omega^2 \left(\rho_{22}^* R_p - 0 + 0\right)}{P R_p - 0}} = \omega \sqrt{\frac{\rho}{\lambda + 2\mu}} \tag{4.40}$$

This coincides with the commonly known longitudinal wave numbers in solids. In fact, the first dilatational wave has a greater correspondence with the solid matrix of the porous material. The shearing wave number can also be found from equation (4.24):

$$k_t = \frac{\omega}{\mu} \sqrt{\rho_{11}^* - 0} = \omega \sqrt{\frac{\rho}{\mu}} \tag{4.41}$$

Again this is the very same result from the classical wave theory.

The equations for the velocities and the stresses of a solid layer can be recovered from those of a porous layer in the same fashion by eliminating the fluid phase related terms and relabeling the first dilatational with subscript “l” instead of “1”.

4.4 Wave Equations of a Plate Like Simple Fluid

A layer of an ideal isentropic non-moving isotropic fluid is often a good model for an acoustic medium. After eliminating the solid phase, equation (4.2) is reduced to Euler’s equation and equation (4.4) will be the constitutive law of a simple fluid. The pressure and

normal velocity of a fluid layer can be computed from a velocity potential in the form of equation (4.28). The following relations hold:

$$
\begin{aligned}
v(x,z,t) &= -\frac{\partial}{\partial z}\Phi(x,z,t) && (4.42)\\
v(z) &= A^{+}k_z\sin(k_z z) - A^{-}ik_z\cos(k_z z) && (4.43)\\
p(x,y,z) &= -i\omega\rho\Phi(x,z,t) && (4.44)\\
\sigma(z) &= A^{+}(-i\omega\rho\cos(k_z z)) + A^{-}(i\omega\rho\sin(k_z z))) && (4.45)
\end{aligned}
$$

The speed of sound in the fluid, c_l, is constant; therefore, the wave number is proportional to frequency:

$$k_l = \frac{\omega}{c_l}. \tag{4.46}$$

4.5 Boundary Conditions

The velocity and stress fields in different layers have several unknown wave amplitudes. The problem of finding the wave amplitudes or the determination of the propagation of waves in layered structures is well-posed. Hence the boundary conditions (BC's) are safely exploited to match the waves inside the layers to one another by determining the wave amplitudes uniquely. In general, the BC's either enforce the kinematics to match (compatibility) or balance the forces (equilibrium). The following BC's are recognized in the analysis of a layered structure:

- Radiation condition: The incident and final transmitted semi-infinite media can bear only one of the in-coming or out-going waves only. The reason is that the energy norm corresponding to a hyperbolic equation solution tends to zero over time [48]. As a result, one of the wave amplitudes must be set to zero.

- Ideal fluid layer contact: An ideal fluid cannot withstand shearing forces. Therefore, at the interface of a fluid layer with another layer, three BC's should be compelled: compatibility of the normal velocities (displacements), equilibrium of the normal stresses (forces), and setting the shearing stresses (forces) to zero.

- Un-bonded (U) solid layers contact: On the surfaces of two adjacent solid layers that can slide with no friction, shearing forces are absent. Hence, four BC's must be satisfied: compatibility of the normal velocities, equilibrium of the normal stresses, and vanishing of the shearing stresses on both surfaces of the contact.

- Bonded (B) solid layers contact: When two solid layers are joint by welding (or being tightly adhered), four BC's must be satisfied: compatibility of the normal velocities, compatibility of the tangential velocities, equilibrium of the normal stresses, and finally equilibrium of the tangential stresses

- Porous layers surface conditions: There are a total of 6 independent components on the surface of a porous layer. Four of these are the normal and tangential of solid phase velocities and stresses; the other two are the normal velocity and stress (pressure) corresponding to the fluid phase. Deresiewicz and Skalak [41] mathematically showed that there are three possible type of contacts for a porous surface. If a porous surface is attached to another porous surface in a way that the solid components are perfectly stuck together; however, the pores of the surfaces will partially cover one another due to porosity difference, a partially bonded contact will results. The other two cases are: when a porous touches another surface so that there exists no flow across the surface and when a porous surface is in contact with another porous surface or an ideal fluid. The latter is considered open pores. In the open pores case, the pressure of the fluid phase is not(necessarily) continuous. Gurevich and Schoenberg[42] demonstrated that Deresiewicz and Skalak conditions can be recaptured by replacing the porous surface with a layer of an ideal fluid whose permeability is proportional to the layer thickness as the thickness tends to zero. This is why the unglued porous surface can be categorized as U no matter if it is in touch with another porous layer, solid layer, or fluid layer. In fact, by considering the flow of the fluid across the open pores interface,

equivalent U surface stress σ_z and velocity v_z can may be defined:

$$\sigma_{zz}^f = \phi_p \, \sigma_{zz} \tag{4.47a}$$

$$\sigma_{zz}^s = (1 - \phi_p)\sigma_{zz} \tag{4.47b}$$

$$v_z = \phi_p \, v_z^f + (1 - \phi_p) v_z^s \tag{4.47c}$$

By considering the combined normal velocity and stress of the surface, the BC's for a U porous surface are: continuity of the equivalent normal stress and velocity, and setting the tangential stress or stresses to zero (if the adjacent layer is a solid layer or another porous layer).

On the other hand, for a closed pores (perfectly bonded) surface, the surface normal stress is simply the sum of the fluid and solid phases stresses.

$$\sigma_{zz} = \sigma_{zz}^s + \sigma_{zz}^f \tag{4.48a}$$

$$v_z = v_z^f \tag{4.48b}$$

$$v_z = v_z^s \tag{4.48c}$$

For a perfectly B porous surface five conditions should be imposed: the surface normal stress of the surface should match the adjacent normal stress, both normal velocities of the solid and fluid phases should be equal to the adjacent layer normal velocity (in the case of a porous layer, again both phases should be considered); compatibility of the tangential velocity of the solid phase and the next layer tangential velocity; and finally, equilibrium of the shearing stresses.

Finally, when two porous layers are connected in such way that the solid phases are bonded perfectly and the pores partially overlap, a partially B contact will result. the BC's will be: compatibility of the solid phases velocity components, equilibrium of the solid phases shearing stresses, balance of the B surface normal stress, matching the in-pores flows of the surfaces and equilibrium of the (inversely scaled with the porosity) fluid phases stresses. Therefore, the following quantities should match at

the interface of the porous surfaces:

$$\phi\,(v_z^f - v_z^s),\ v_z^s,\ v_x^s,\ \frac{1}{\phi}\,\sigma_{zz}^f,\ \sigma_{zz}^f + \sigma_{zz}^s,\ \sigma_{xz}^s \tag{4.49}$$

It should be noted that in reality, such a contact is hard to achieve, since usually the glue that bonds the layers will fill in between the pores and hence results in a (perfectly) B surface contact.

4.6 Direct calculation of multi-layer structure transmission

The transmission of sound waves through a layered structure can be predicted by solving the set of wave equations of the layer along with imposing the boundary conditions to match the waves on the layers interfaces. The problem of solving the set of wave equations with proper BC's on the surfaces, as mentioned earlier, is mathematically well-posed. This means that the number of the equations and the the number of unknowns are equal and under normal conditions the unknowns can be determined uniquely. If the layers are all unbonded, it is possible to use the Brekhovskikh [31] recursive normal impedance formula; however, since this method is based on equating the normal components of the velocities and the stresses, it can not be used when a combination of B and U layers is present.

There are two major methods of analyzing general layered structures; here, they may be called the direct and the transfer function (TF) methods. In the direct method, which is used by Bolton et al [30] and Brouard and Allard [38], the set of equations (in the case of Brouard and Allard, layer matrices) are assembled into a large global system and the wave amplitudes are determined by inverting the aggregated coefficient matrix. Bolton recognized three different situations regarding matching the surfaces of the layers: a) interface between an acoustic medium and a thin panel resulting in 3 equations, b) a free porous surface that gives 4 equations, and c) a bonded thin plate and a porous layer leading to 6 equations. The direct approach has been used successfully; however, when the number of layers increases, its implementation is not very straightforward, specifically because the equations of vibration of the panels are combined with the equations of the porous layer. Further, the application

of this method is not very efficient for sandwich layers made of a larger number of layers, since the final coefficient matrix can have a substantial order and the inversion (or pseudo-inversion)of such a matrix can be cumbersome if not impossible due to singularities. In extreme cases, such as eliminating a layer from a sandwich, i.e. equating the thickness to zero, the matrix will not be full rank. Hence, the linear system has no solution and all of the equations need to be rewritten. Bolton has analyzed three different configurations: BB (a 12×12 linear system), UU (a 14×14 linear system), and BU (a 13×13 linear system).

4.7 Transmission through a Multi-layer Structure- Transfer Matrix Method

A layered structure made of finite numbers of layers as well can be analyzed when each layer is represented by a transfer function (transfer matrix). A TF relates the particle velocity and stress components from one side of the layer to the other side. A TF is alternatively called "matrix propagator" since "it allows propagation of the field" from one point to another point [31]. From a system theory point of view, TF's are like the building blocks of a linear system that can be put together to create a single TF that represents the whole layered structure.

The advantage of using TF's is that it involves only multiplying a set of matrices rather than solving a large set of global equations; moreover, the insertion or elimination of the layers are simply done by taking the corresponding matrix out of the production of the matrices. Another benefit of this method is that linear system theory knowledge may also add to the understanding of the layered systems. An Equivalent network analogy of a solid layer to an electrical block diagram has been depicted by Rudgers [34]. Cerevenka and Challande [35] have also developed a computational algorithm for the matrix method when the layers are comprised of a combination of fluids and or solids (only). Moore and Lyon [37] used the impedance matrix method for analyzing geometrically symmetric panels with and without soft cores, cited that the accuracy is limited when the thickness is (relative to frequency) is large.

Allard and his colleagues ([28, 38, 39, 40]) developed and used the transfer matrix

method to analyze a layered system. Block diagrams of equivalent electrical networks for the layers may be found in their work as well. However, in their analysis, they introduced intermediate joint matrices which depend on both layers being able to use unreduced matrices.

In the following sections the matrices that represent fluid layers, thin plates (panels), solid layers, and porous layers will be given. It should be also noted that the information regarding the angle(s) of incidence must be conveyed to the next matrix; this information along with Snell's law, determine the wave number component in each layer.

4.8 Transfer Matrix Derivation

The typical procedure for extracting a layer matrix from the plane wave equations is explained in this section. First of all, the velocity and stress vectors need to be expressed in terms of the wave amplitudes. As shown in figure 4.1, coordinates system can be set up such that the Z–axis is perpendicular to the layer surface; thus designating the thickness. Also, the X–axis is coincident with the edge of the layer cross section; therefore, the variation of variables along the Y–axis can be neglected. Once the displacement and stress fields are determined, these relations are expressed in the following matrix form:

$$\begin{Bmatrix} \mathbf{v} \\ \boldsymbol{\sigma} \end{Bmatrix} = [\,\Gamma\,] \begin{Bmatrix} A \end{Bmatrix} \tag{4.50}$$

Without the loss of generality, it is possible to set the datum on the input surface (at $z = 0$); hence:

$$\begin{Bmatrix} A \end{Bmatrix} = [\,\Gamma_0\,]^{-1} \begin{Bmatrix} \mathbf{v}_0 \\ \boldsymbol{\sigma}_0 \end{Bmatrix} \tag{4.51}$$

By combining (4.50) and (4.51):

$$[\,TF\,] = [\,\Gamma\,][\,\Gamma_0\,]^{-1}. \tag{4.52}$$

Brekhovskikh and [31] have considered the exponential forms of the wave fields. They

have further broken down [Γ] into product of two matrices, one containing the admissible propagation direction (eigen-vectors) which do not depend on the coordinate along the layer thickness ([Δ] and a diagonal n exponential.

4.9 Fluid layer TF

The simplest plane wave field occurs in an ideal isentropic homogenous, steady state fluid which is at rest. The matrix relation for a layer of a plate like fluid can easily be found via equations (4.43)-(4.45):

$$\begin{Bmatrix} v_z \\ \sigma_{zz} \end{Bmatrix}_z = \begin{bmatrix} \cos(k_z z) & -\dfrac{k_z \sin(k_z z)}{i\omega\rho} \\ -\dfrac{\omega\rho \sin(k_z z)}{i k_z} & \cos(k_z z) \end{bmatrix} \begin{Bmatrix} v_z \\ \sigma_{zz} \end{Bmatrix}_{z=0} \tag{4.53}$$

4.10 BB Solid layer TF

The equations of the longitudinal (dilatational) wave and the transverse (shearing) wave were recovered from those of a porous layer in section 4.3. When the solid layer faces are glued or welded to the neighbor layers, both the normal and tangential components of the velocities and stresses need to be considered in enforcing the BC's. The following matrix relationship for a BB solid layer is obtained:

$$\begin{Bmatrix} v_z \\ v_x \\ \sigma_{zz} \\ \sigma_{xz} \end{Bmatrix}_z = \begin{bmatrix} T^S_{11} & T^S_{12} & T^S_{13} & T^S_{14} \\ T^S_{21} & T^S_{22} & T^S_{14} & T^S_{24} \\ T^S_{31} & T^S_{32} & T^S_{11} & T^S_{21} \\ T^S_{32} & T^S_{42} & T^S_{12} & T^S_{22} \end{bmatrix} \begin{Bmatrix} v_z \\ v_x \\ \sigma_{zz} \\ \sigma_{xz} \end{Bmatrix}_{z=0} \tag{4.54}$$

After expressing the wave number components in terms of the corresponding angles, the entries of the above TF matrix will be:

$$T_{11}^S = \cos 2\theta_t \cos k_{lz} z + 2 \sin^2\theta_t \cos k_{tz} z \tag{4.55a}$$

$$T_{12}^S = 2\,i \sin^2\theta_t \cot\theta_l \sin k_{lz} z - i \cos 2\theta_t \tan\theta_t \sin k_{tz} z \tag{4.55b}$$

$$T_{13}^S = -\frac{i\,k_{lz} \sin^2\theta_t}{\rho\,\omega} \sin k_{lz} z - \frac{i\,k_x \tan\theta_t}{\rho\,\omega} \sin k_{tz} z \tag{4.55c}$$

$$T_{14}^S = -\frac{i\,k_x}{\rho\,\omega} (\sin k_{lz} z - \sin k_{tz} z) \tag{4.55d}$$

$$T_{21}^S = i \cos 2\theta_t \tan\theta_l \sin k_{lz} z - i \sin 2\theta_t \sin k_{tz} z \tag{4.55e}$$

$$T_{22}^S = 2 \sin^2\theta_t \cos k_{lz} z + \cos 2\theta_t \cos k_{tz} z \tag{4.55f}$$

$$T_{24}^S = -\frac{i\,k_x}{\rho\,\omega} \sin k_{lz} z - \frac{i\,k_{tz}}{\rho\,\omega} \sin k_{tz} z \tag{4.55g}$$

$$T_{31}^S = \frac{i\,\rho\,\omega}{k_{lz}} \cos 2\theta_t \sin k_{lz} z - \frac{4i\,\rho\,\omega}{k_t} \sin^2\theta_t \sin k_{tz} z \tag{4.55h}$$

$$T_{32}^S = -\frac{2\,\rho\,\omega}{k_t} \sin\theta_t \cos 2\theta_t (\sin k_{lz} z - \sin k_{tz} z) \tag{4.55i}$$

$$T_{42}^S = \frac{-4\,\rho\,\omega\,k_{lz}}{k_t^2} \sin^2\theta_t \sin k_{lz} z - \frac{i\,\rho\,\omega}{k_{tz}^2} \cos^2 2\theta_t \sin k_{tz} z \tag{4.55j}$$

Folds and Loggins [36], Cerevenka and Challande [35], and Brekhovskikh [31] derived the above matrices for the harmonic convention $e^{-i\,\omega\,t}$. Unfortunately, Allard et al [**?**] reported this matrix for the positive harmonic time convention ($e^{i\,\omega\,t}$) incorrectly.

4.11 UU Solid Layer TF

A solid layer can be inserted between two layers by means of no glue or welding; the adjacent layers may be simple inviscid fluid and or other frictionless solid or porous layers. When both sides are unbonded and frictionless, the solid layer is called UU. The surfaces of a UU layer cannot carry any shearing stress; thus, on these surfaces the input and output vectors may be reduced to only two component vectors. The reduction of the TF of a UU solid layer is possible by substituting for the unwanted tangential velocities of both sides.

The final matrix will be 2×2 and is related to the BB solid layer TF entries as:

$$[T^S_{UU}] = \begin{bmatrix} T^S_{11} - \frac{T^S_{41}T^S_{12}}{T^S_{42}} & T^S_{13} - \frac{T^S_{42}T^S_{12}}{T^S_{42}} \\ \\ T^S_{31} - \frac{T^S_{41}T^S_{32}}{T^S_{42}} & T^S_{11} - \frac{T^S_{42}T^S_{32}}{T^S_{42}} \end{bmatrix} \tag{4.56}$$

A simple investigation shows that the denominator cannot be zero for the positive incident angles less than $\pi/2$ (or tilt mode as is called by Cerevenka and Challande [35])

4.12 BB Thin plate (Panel) TF

A thin plate model also leads to a very simple transfer matrix. A panel is identical to a thin solid layer. The TF of a solid layer is greatly simplified when the thickness is small. In this context, small is relative, meaning that thickness is of an order smaller than the longitudinal wave number. The longitudinal wave number is proportional to the frequency; therefore, as the frequency increases, the thin plate model validity is reduced. As a matter of fact, in the higher frequency ranges, the surface waves need to be accounted for. For the current frequency range of interest (less than 10 kHz) and practical structural panels (less than few centimeters), the thin plate accuracy is acceptable.

A panel TF may be derived in two ways: a) first order expanding of the solid layer TF entries with regard to the thickness; b) considering the plate theories. In this section the latter approach is selected. The plate is assumed to obey the Kirchhoff model. A complete list of the assumptions made for such a model can be sought in a plate book (e.g. [16] or [49]). However, the main assumptions made are the following: a) the points along the thickness sections have the same displacements; b) in-plane deformations of higher orders than the thickness are negligible; c) in-plane forces, except for the shearing stresses on the faces can be ignored. The coordinate system is again chosen as shown in figure 4.1. The mid plane displacement is designated by (η_p, ζ_p, ξ_p). The geometry of the deformation relates the displacements (hence the velocities) of the panel faces. Under the used kinematical

hypothesis:

$$v_z = v_{z0} = \dot{\xi_p} \tag{4.57}$$

$$\begin{aligned} v_x(z) &= \dot{\eta_p} - z\,\dot{\xi_{p,x}} = \dot{\eta_p} - z\,(-i\,k_x)\dot{\xi_p} \\ &= \dot{\eta_p} + i\,z\,k_x\,v_{z0} \end{aligned} \tag{4.58}$$

Equation 4.58 can be used to relate the in-plane velocities of the sides:

$$v_{xL} = i\,k_x\,L\,v_{z0} + v_{x0} \tag{4.59}$$

where L is the thickness of the panel.

The governing equations of motion can be found by writing the variational form of energy. The in-plane vibration equation is obtained as:

$$D_I\,\eta_{p,xx} + \sigma_{xz} - \sigma_{xz0} = \rho\,L\,\ddot{\eta_p} \tag{4.60}$$

ρ is the density of the panel; σ_{xz} and σ_{xz0} are the shearing stresses acting on the input and output faces of the panel respectively; and D_I is the in-plane rigidity of the plate defined as:

$$D_I = \frac{E\,L}{1-\nu^2} \tag{4.61}$$

E is the Young's modulus of the panel; and ν is the Poisson's ratio of the thin plate. The bending vibration of the plate will be:

$$D_B\,\nabla^4\xi_p + \rho\,L\,\ddot{\xi_p} = \sigma_{zz} - \sigma_{zz0} + \frac{L}{2}\,(\sigma_{xz} + \sigma_{xz0})_{,x} \tag{4.62}$$

Equations (4.57), (4.59), (4.60), and (4.62) lead into the following TF for a BB panel:

$$[\,T_{BB}^{Pa}\,] = \begin{bmatrix} 1 & 0 & 0 & 0 \\ i\,z\,k_x & 1 & 0 & 0 \\ Z_B - \frac{1}{4}z^2\,k_x^2\,Z_I & \frac{1}{2}i\,z\,k_x\,Z_I & 1 & i\,z\,k_x \\ \frac{1}{2}i\,z\,k_x Z_I & Z_I & 0 & 1 \end{bmatrix} \tag{4.63}$$

Z_I and Z_B are in-plane and bending impedances of the thin plate respectively. These impedances depend on the thickness as:

$$Z_B = \frac{D_B(z)\, k_x^4 - \rho\, z\, \omega^2}{i\, \omega} \tag{4.64a}$$

$$Z_I = \frac{D_I(z)\, k_x^2 - \rho\, z\, \omega^2}{i\, \omega} \tag{4.64b}$$

Entries $ik_x z$ and $\frac{1}{2} ik_x z Z_I$ are of $O(zf)$ and $O(z^2 f^2)$ respectively. Also, $Z_B - \frac{1}{4} z^2\, k_x^2\, Z_I = C_1^{BB}(zf)^3 + C_2^{BB} zf$; where C's are constant and f is the frequency. Numerical values for a thin steel plate shows that the matrices of a solid layer and a BB panel are practically the same for frequencies under 10 kHz for small practical thicknesses.

4.13 UU Panel TF

A thin plate TF can be derived in two ways. The first method is to combine the commonly known bending vibration of a thin plate with the kinematic hypothesis. The second method is to set the shearing stresses acting on the faces of the panel to zero and substituting for the in-plane velocities. Either method give the same result. This can be considered a recheck for the BB panel TF.

A thin plate layer is equivalent to a layer representing a continuous spring (plate stiffness) and dash pot (by introducing a loss factor to plate Young's modulus) which connect the faces of that layer. The transfer function schematically representing a thin plate, which is shown in figure (4.2), will be derived below. It is assumed that normal velocities of both sides of a vibrating panel are the same; moreover, the plate vibration equation is governed by:

$$(D_B\, k_x^4 - \rho\, L\, \omega^2)(\frac{v_0}{i\, \omega}) = \sigma - \sigma_0 \tag{4.65}$$

Aggregating the above information, the transfer matrix is found as:

$$[\, T^{Pa}\,] = \begin{bmatrix} 1 & 0 \\ \dfrac{D_B\, k_x^4 - \rho\, L\, \omega^2}{i\, \omega} & 1 \end{bmatrix} \tag{4.66}$$

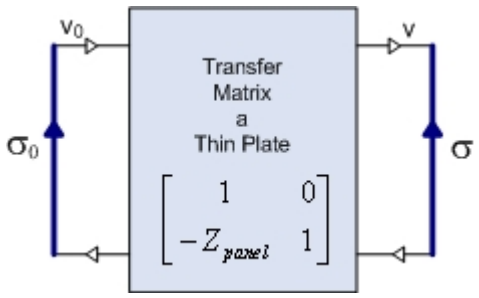

Figure 4.2: TF block diagram for a thin plate

As it mentioned at the beginning of this section, it is possible to check the BB matrix for a solid layer by equating the shear stresses of the input and output surfaces to zero. In fact the thin BB matrix derived in the previous section is an approximation for a solid layer when the thickness is small enough. In other words, if the entries of a solid layer matrix is expanded for small arguments of the sine and cosine functions, the thin BB panel results. One way to quantify the accuracy of the BB panel TF is to find the UU TF of the combination of two panels of thicknesses L and δL and comparing it with UU TF resulting from the Kirchhoff model explained in this section for the perturbed thickness $L+\delta L$. Such an analysis shows that the difference in of the impedances is of $O(zf)$.

4.14 Unreduced Porous Layer TF

The TF representing a porous layer TF can be extracted from the wave equations of the section. This unreduced 6×6 matrix that relates the velocities and stresses of the solid and fluid phases of the surfaces of a porous layer can be determined from the wave equations. Allard et al first derived a 4×4 matrix neglecting the shearing wave [**?**] and then introduced the 6×6 TF in their notation [28] and [**?**]. By means of the wave equations in a porous layer, the matrix relating the wave amplitudes to the normal/tangential stresses and velocities in the current notation can be found. Define:

$$\left\{ v_z^f,\, v_z^s,\, v_x^s,\, \sigma_{zz}^f,\, \sigma_{zz}^s,\, \sigma_{xz}^s \right\}^T = [\,\Gamma\,]_{6\times 6} \left\{ A_1^+,\, A_1^-,\, A_2^+,\, A_2^-,\, A_3^+,\, A_3^- \right\}^T, \tag{4.67}$$

Using the equations of section 4.2, the entries are:

$$
\begin{aligned}
\Gamma_{11} &= \frac{i\omega b_1 k_{1z}}{k_1^2}\sin k_{1z}z,\ \Gamma_{12} = \frac{\omega b_1 k_{1z}}{k_1^2}\cos k_{1z}z,\ \Gamma_{13} = \frac{i\omega b_2 k_{2z}}{k_2^2}\sin k_{2z}z \\
\Gamma_{14} &= \frac{\omega b_2 k_{2z}}{k_2^2}\cos k_{2z}z,\ \Gamma_{15} = \frac{-\omega g k_x}{k_t^2}\cos k_{tz}z, \Gamma_{16} = \frac{-i\omega g k_x}{k_t^2}\sin k_{tz}z \\
\Gamma_{21} &= \frac{i\omega k_{1z}}{k_1^2}\sin k_{1z}z,\ \Gamma_{22} = \frac{\omega k_{1z}}{k_1^2}\cos k_{1z}z,\ \Gamma_{23} = \frac{i\omega k_{2z}}{k_2^2}\sin k_{2z}z \\
\Gamma_{24} &= \frac{\omega k_{2z}}{k_2^2}\cos k_{2z}z,\ \Gamma_{25} = \frac{-\omega k_x}{k_t^2}\cos k_{tz}z, \Gamma_{26} = \frac{-i\omega k_x}{k_t^2}\sin k_{tz}z \\
\Gamma_{31} &= \frac{-\omega k_x}{k_1^2}\cos k_{1z}z,\ \Gamma_{32} = \frac{-i\omega k_x}{k_1^2}\sin k_{1z}z\ ,\ \Gamma_{33} = \frac{-\omega k_x}{k_2^2}\cos k_{2z}z \\
\Gamma_{34} &= \frac{-i\omega k_x}{k_2^2}\sin k_{2z}z,\ \Gamma_{35} = \frac{-i\omega k_{tz}}{k_t^2}\sin k_{tz}z,\ \Gamma_{36} = \frac{-\omega k_{tz}}{k_t^2}\cos k_{tz}z \\
\Gamma_{41} &= (b_1 R_p + Q_p)\cos k_{1z}z, \Gamma_{42} = i(b_1 R_p + Q_p)\sin k_{1z}z, \\
\Gamma_{43} &= (b_2 R_p + Q_p)\cos k_{2z}z, \Gamma_{44} = i(b_2 R_p + Q_p)\sin k_{2z}z, \Gamma_{45} = \Gamma_{46} = 0 \\
\Gamma_{51} &= (\lambda + 2\mu + b_1 Q_p + \frac{2\mu k_{1z}^2}{k_1^2})\cos k_{1z}z, \Gamma_{52} = i(\lambda + 2\mu + b_1 Q_p + \frac{2\mu k_{1z}^2}{k_1^2})\sin k_{1z}z \\
\Gamma_{53} &= (\lambda + 2\mu + b_2 Q_p + \frac{2\mu k_{2z}^2}{k_2^2})\cos k_{2z}z, \Gamma_{54} = i(\lambda + 2\mu + b_2 Q_p + \frac{2\mu k_{2z}^2}{k_2^2})\sin k_{2z}z, \\
\Gamma_{55} &= \frac{-2i\mu k_x k_{tz}}{k_t^2}\sin k_{tz}z, \Gamma_{56} = \frac{-2\mu k_x k_{tz}}{k_t^2}\cos k_{tz}z, \\
\Gamma_{61} &= \frac{-2i\mu k_x k_{1z}}{k_1^2}\sin k_{1z}z \Gamma_{62} = \frac{-2\mu k_x k_{1z}}{k_1^2}\cos k_{1z}z,\ \Gamma_{63} = \frac{-2i\mu k_x k_{2z}}{k_2^2}\sin k_{2z}z \\
\Gamma_{64} &= \frac{-2\mu k_x k_{2z}}{k_2^2}\cos k_{2z}z, \Gamma_{65} = \frac{\mu(k_x^2 - k_{tz}^2)}{k_t^2}\cos k_{tz}z, \Gamma_{66} = \frac{i\mu(k_x^2 - k_{tz}^2)}{k_t^2}\sin k_{tz}z
\end{aligned}
$$

The transfer matrix will be found by means of equation (4.52). $[\,T^{P6}\,]$ is a 6×6 matrix which relates the normal/tangential stresses and velocities of surfaces of the layer as:

$$
\begin{Bmatrix} \mathbf{v} \\ \boldsymbol{\sigma} \end{Bmatrix}_z = \left\{ v_z^f, v_z^s, v_x^s, \sigma_{zz}^f, \sigma_{zz}^s, \sigma_{xz}^s \right\}_z^T = [\,T^{P6}\,] \left\{ v_z^f, v_z^s, v_x^s, \sigma_{zz}^f, \sigma_{zz}^s, \sigma_{xz}^s \right\}_0^T \tag{4.68}
$$

4.15 Partially bonded porous layers TF

Transfer matrix for a porous layer combined of two partially bonded porous layer has also a structure similar to an unreduced porous layer. In fact, such a combined layer is a new porous material and its TF is again a 6×6 matrix. At the interface of two partially

bonded porous layers, the pores are not completely covered; however, the solid phases are assumed to be bonded perfectly. Therefore, the fluid can flow in between the pores from the input surface of the first layer to the output surface of the second layer. This is the reason that such an ideal structure still needs to be considered a porous layer and its TF cannot be reduced yet. In reality, this is not a good model for a layered structure including two glued porous layers, since the gluing material will eventually fill in the pores at the interface of the sub-layers.

In order to apply the BC's for this model, the output vector of the first layer as well as the input vector of the second layer should under linear transformation. The reason is that for such an interface, a linear combination of the stresses and velocities should be equated on the interface as indicated by conditions of (4.49).

A simple linear transformation designated by $[\Upsilon^l]$ can do this job, $l = 1, 2$. $[\Upsilon^l]$ entries are the same as those of the 6×6 identity matrix but for the followings:

$$\Upsilon^l_{1,1} = \phi_l,\ \Upsilon^l_{1,2} = -\Upsilon^l_{1,1},\ \Upsilon^l_{4,1} = \frac{1}{\phi_l},\ \Upsilon^l_{5,1} = 1 \tag{4.69}$$

Therefore:

$$\left\{\phi_l(v^f_z - v^s_z),\ v^s_z,\ v^s_x,\ \tfrac{1}{\phi_i}\sigma^f_{zz},\ \sigma^s_{zz} + \sigma^f_{zz},\ \sigma^s_{xz}\right\}^T = [\Upsilon^i]\begin{Bmatrix}\mathbf{v}\\ \boldsymbol{\sigma}\end{Bmatrix}_l,\ l = 1, 2 \tag{4.70}$$

Hence:

$$\begin{Bmatrix}\mathbf{v}\\ \boldsymbol{\sigma}\end{Bmatrix}_z = [T_2^{P6}][\Upsilon][T_1^{P6}]\begin{Bmatrix}\mathbf{v}\\ \boldsymbol{\sigma}\end{Bmatrix}_0 \tag{4.71}$$

where

$$[\Upsilon] = [\Upsilon^2]^{-1}[\Upsilon^1] \tag{4.72}$$

The entries of $[\Upsilon]$ which are different from those of the identity matrix are:

$$\Upsilon_{1,1} = \frac{\phi_2}{\phi_1},\ \Upsilon_{1,2} = 1 - \Upsilon_{1,1},\ \Upsilon_{4,4} = \frac{1}{\Upsilon_{1,1}},\ \Upsilon_{5,4} = 1 - \Upsilon_{4,4} \tag{4.73}$$

4.16 UU porous layer TF

A porous layer with unglued faces can be represented by a reduced order TF. On the surfaces of such a layer, shearing stresses will diminish. A UU layer is either in contact with two acoustic media and/or with other layers that can bear no shearing stress (e.g. unglued frictionless layers). Hence, as the block diagram in figure (4.3) suggests, the TF can be reduced from order 6×6 to 2×2. Once the UU TF is determined, the UU porous layer can be treated as a fluid layer.

Although it is possible to find the reduced 2×2 UU TF from the original 6×6 matrix, it is better to find an intermediate matrix $[\,T^{PU}\,]$ in which the tangential velocities and the shearing stresses are eliminated. By introducing this matrix, the final TF can be written more elegantly. Define a porosity vector as:

$$\boldsymbol{\phi}^T = \{\phi_p, 1-\phi_p\} \tag{4.74}$$

Equations (4.47) can be expressed in the vector form as:

$$\boldsymbol{\sigma} = \left\{\sigma^f, \sigma^s\right\}^T = \boldsymbol{\phi}^T \sigma \tag{4.75}$$

$$\boldsymbol{\phi}^T \left\{v^f,\, v^s\right\}^T = v \tag{4.76}$$

Elements of this matrix can be determined in terms of $[\,T^{P6}\,]$, as:

$$[\,T^{PU}\,] = \begin{bmatrix} T^{P6}_{11} - \frac{T^{P6}_{13}\,T^{P6}_{61}}{T^{P6}_{63}} & T^{P6}_{12} - \frac{T^{P6}_{13}T^{P6}_{62}}{T^{P6}_{63}} & T^{P6}_{14} - \frac{T^{P6}_{13}\,T^{P6}_{64}}{T^{P6}_{63}} & T^{P6}_{15} - \frac{T^{P6}_{13}T^{P6}_{65}}{T^{P6}_{63}} \\ T^{P6}_{21} - \frac{T^{P6}_{23}\,T^{P6}_{61}}{T^{P6}_{63}} & T^{P6}_{22} - \frac{T^{P6}_{23}T^{P6}_{62}}{T^{P6}_{63}} & T^{P6}_{24} - \frac{T^{P6}_{23}\,T^{P6}_{64}}{T^{P6}_{63}} & T^{P6}_{25} - \frac{T^{P6}_{23}T^{P6}_{65}}{T^{P6}_{63}} \\ T^{P6}_{41} - \frac{T^{P6}_{43}\,T^{P6}_{61}}{T^{P6}_{63}} & T^{P6}_{42} - \frac{T^{P6}_{43}T^{P6}_{62}}{T^{P6}_{63}} & T^{P6}_{44} - \frac{T^{P6}_{43}\,T^{P6}_{64}}{T^{P6}_{63}} & T^{P6}_{45} - \frac{T^{P6}_{43}T^{P6}_{65}}{T^{P6}_{63}} \\ T^{P6}_{51} - \frac{T^{P6}_{53}\,T^{P6}_{61}}{T^{P6}_{63}} & T^{P6}_{52} - \frac{T^{P6}_{53}T^{P6}_{62}}{T^{P6}_{63}} & T^{P6}_{54} - \frac{T^{P6}_{53}\,T^{P6}_{64}}{T^{P6}_{63}} & T^{P6}_{55} - \frac{T^{P6}_{53}T^{P6}_{65}}{T^{P6}_{63}} \end{bmatrix} \tag{4.77}$$

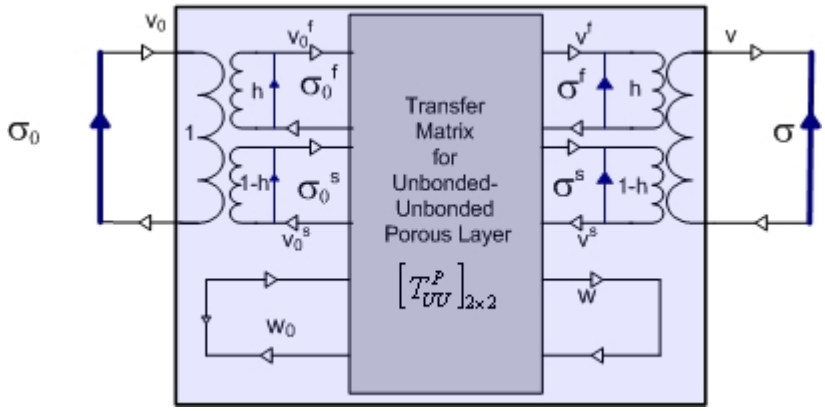

Figure 4.3: A UU porous layer TF block diagram

The above matrix can be partitioned as below:

$$[\,T_{UU}^{P}\,] = \begin{bmatrix} T_1 & T_2 \\ T_3 & T_4 \end{bmatrix} \tag{4.78}$$

where T_i's $(i = 1, 2, 3, 4)$ are all 2×2 matrices; therefore:

$$\begin{Bmatrix} \mathbf{v} \\ \boldsymbol{\sigma} \end{Bmatrix} = \begin{bmatrix} T_1 & T_2 \\ T_3 & T_4 \end{bmatrix} \begin{Bmatrix} \mathbf{v}_0 \\ \boldsymbol{\sigma}_0 \end{Bmatrix} \tag{4.79}$$

Note that $\mathbf{v}$ and $\boldsymbol{\sigma}$ are now vectors and include both normal and tangential components. The above matrix equation can be written in vector form as:

$$\mathbf{v} = T_1\mathbf{v}_0 + T_2\boldsymbol{\sigma}_0 \tag{4.80}$$

$$\boldsymbol{\sigma} = T_3\mathbf{v}_0 + T_4\boldsymbol{\sigma}_0 \tag{4.81}$$

It can be shown that $[\,T_3\,]$ cannot be singular; thus:

$$T_3{}^{-1}\boldsymbol{\phi}\,\sigma = \mathbf{v}_0 + T_3{}^{-1}\,T_4\,\boldsymbol{\phi}\,\sigma_0 \tag{4.82}$$

The total normal stress can be computed after applying the velocity boundary condition

as:

$$\sigma = \frac{v_0}{\boldsymbol{\phi}^T {T_3}^{-1} \boldsymbol{\phi}} + \frac{\boldsymbol{\phi}^T {T_3}^{-1} T_4 \boldsymbol{\phi}}{\boldsymbol{\phi}^T {T_3}^{-1} \boldsymbol{\phi}} \sigma_0 \tag{4.83}$$

Also, equation (4.76) can be used to eliminate the input velocity vector; after multiplying both sides of (4.75) by $\boldsymbol{\phi}^T$, the total normal velocity and stress on the output side can be related to the input side as:

$$v - \boldsymbol{\phi}^T T_1 {T_3}^{-1} \boldsymbol{\phi} \sigma = \boldsymbol{\phi}^T (T_2 - T_1 {T_3}^{-1} T_4) \boldsymbol{\phi} \sigma_0 \tag{4.84}$$

The transfer function $[\, T^P_{UU} \,]$ for UU porous layer finally will be:

$$[\, T^P_{UU} \,] = \begin{bmatrix} \dfrac{\boldsymbol{\phi}^T T_1 {T_3}^{-1} \boldsymbol{\phi}}{\boldsymbol{\phi}^T {T_3}^{-1} \boldsymbol{\phi}} & \dfrac{\boldsymbol{\phi}^T T_1 {T_3}^{-1} \boldsymbol{\phi} \boldsymbol{\phi}^T {T_3}^{-1} T_4 \boldsymbol{\phi}}{\boldsymbol{\phi}^T {T_3}^{-1} \boldsymbol{\phi}} \\ \\ \dfrac{1}{\boldsymbol{\phi}^T {T_3}^{-1} \boldsymbol{\phi}} & \dfrac{\boldsymbol{\phi}^T T_1 {T_3}^{-1} \boldsymbol{\phi}}{\boldsymbol{\phi}^T {T_3}^{-1} \boldsymbol{\phi}} \end{bmatrix} \tag{4.85}$$

It should be noted that the inverse of the above 2×2 matrices can easily be computed in closed form. Moreover, if before the tangential components are eliminated velocities and the stresses of the phases are combined, the very same matrix will result.

4.17 TF of a BB porous layer

Fluid cannot flow across the faces of a BB porous layer. To enforce the boundary conditions, equivalent normal velocity and stress can be calculated in accordance with equation (4.48) to reduce the 6×6 TF of a porous layer for a BB configuration. Similar to the open pores porosity vector, a closed pore vector may be defines as:

$$\boldsymbol{\phi_c} = \{1, 1\}^T \tag{4.86}$$

The unreduced TF of a porous layer (4.68) can be partitioned as:

$$T_1^{P6} \triangleq \begin{bmatrix} T_{11}^{P6} & T_{12}^{P6} \\ T_{21}^{P6} & T_{22}^{P6} \end{bmatrix}, \mathbf{T}_2^{P6} \triangleq \begin{bmatrix} T_{13}^{P6} \\ T_{23}^{P6} \end{bmatrix}, T_3^{P6} \triangleq \begin{bmatrix} T_{14}^{P6} & T_{15}^{P6} \\ T_{24}^{P6} & T_{25}^{P6} \end{bmatrix}, \mathbf{T}_4^{P6} \triangleq \begin{bmatrix} T_{16}^{P6} \\ T_{26}^{P6} \end{bmatrix}$$

$$\mathbf{T}_5^{P6} \triangleq \begin{bmatrix} T_{31}^{P6} \\ T_{32}^{P6} \end{bmatrix}, \mathbf{T}_7^{P6} \triangleq \begin{bmatrix} T_{34}^{P6} \\ T_{35}^{P6} \end{bmatrix}, T_9^{P6} \triangleq \begin{bmatrix} T_{41}^{P6} & T_{42}^{P6} \\ T_{51}^{P6} & T_{52}^{P6} \end{bmatrix}, \mathbf{T}_{10}^{P6} \triangleq \begin{bmatrix} T_{43}^{P6} \\ T_{53}^{P6} \end{bmatrix}$$

$$T_{11}^{P6} \triangleq \begin{bmatrix} T_{44}^{P6} & T_{45}^{P6} \\ T_{54}^{P6} & T_{55}^{P6} \end{bmatrix}, \mathbf{T}_{13}^{P6} \triangleq \begin{bmatrix} T_{61}^{P6} \\ T_{62}^{P6} \end{bmatrix}, \mathbf{T}_{15}^{P6} \triangleq \begin{bmatrix} T_{64}^{P6} \\ T_{65}^{P6} \end{bmatrix}$$

Expansion of the first row of the matrix equation (4.68) in terms of the sub-matrices, leads to the following vector equation:

$$\mathbf{v}_z = \boldsymbol{\phi}_c \, v_z = T_1^{P6}(\boldsymbol{\phi}_c \, v_{z_0}) + \boldsymbol{T}_2^{P6} v_{x_0} + T_3^{P6} \boldsymbol{\sigma}_{zz_0} + \boldsymbol{T}_4^{P6} \sigma_{xz_0} \tag{4.87}$$

Therefore:

$$\boldsymbol{\sigma}_{zz_0} = T_3^{P6^{-1}} \left[\, \boldsymbol{\phi}_c \, v_z - T_1^{P6}(\, \boldsymbol{\phi}_c \, v_{z_0}) - \boldsymbol{T}_2^{P6} v_{x_0} - \boldsymbol{T}_4^{P6} \sigma_{xz_0} \right] \tag{4.88}$$

$$\begin{aligned} v_z = {} & \frac{\boldsymbol{\phi}_c{}^T T_3^{P6^{-1}} T_1^{P6} \boldsymbol{\phi}_c}{\boldsymbol{\phi}_c^T T_3^{P6^{-1}} \boldsymbol{\phi}_c} v_{z_0} + \frac{\boldsymbol{\phi}_c^T T_3^{P6^{-1}} \boldsymbol{T}_2^{P6}}{\boldsymbol{\phi}_c^T T_3^{P6^{-1}} \boldsymbol{\phi}_c} v_{x_0} \\ & + \frac{1}{\boldsymbol{\phi}_c^T T_3^{P6^{-1}} \boldsymbol{\phi}_c} \sigma_{zz_0} + \frac{\boldsymbol{\phi}_c^T T_3^{P6^{-1}} \boldsymbol{T}_4^{P6}}{\boldsymbol{\phi}_c^T T_3^{P6^{-1}} \boldsymbol{\phi}_c} \sigma_{xz_0} \end{aligned} \tag{4.89}$$

And the third row expansion:

$$\boldsymbol{\sigma}_{zz} = T_9^{P6}(\, \boldsymbol{\phi}_c \, v_{z_0}) + \boldsymbol{T}_{10}^{P6} v_{x_0} + T_{11}^{P6} \boldsymbol{\sigma}_{zz_0} + \boldsymbol{T}_{12}^{P6} \sigma_{xz_0} \tag{4.90}$$

Equations (4.88) and (4.90) can be used to relate the equivalent normal stress of the output side to the input side as:

$$\begin{aligned} \sigma_{zz} = {} & \left[\boldsymbol{\phi}_c^T T_9^{P6} \boldsymbol{\phi}_c - \boldsymbol{\phi}_c^T T_{11}^{P6} T_3^{P6^{-1}} T_1^{P6} \boldsymbol{\phi}_c + \frac{\boldsymbol{\phi}_c^T T_{11}^{P6} T_3^{P6^{-1}} \boldsymbol{\phi}_c \boldsymbol{\phi}_c{}^T T_3^{P6^{-1}} T_1^{P6} \boldsymbol{\phi}_c}{\boldsymbol{\phi}_c{}^T T_3^{P6^{-1}} \boldsymbol{\phi}_c} \right] v_{z0} \\ & + \left[\boldsymbol{\phi}_c^T \boldsymbol{T}_{10}^{P6} - \boldsymbol{\phi}_c^T T_{11}^{P6} T_3^{P6^{-1}} \boldsymbol{T}_2^{P6} + \frac{\boldsymbol{\phi}_c^T T_3^{P6^{-1}} \boldsymbol{T}_2^{P6^{-1}}}{\boldsymbol{\phi}_c{}^T T_3^{P6^{-1}} \boldsymbol{\phi}_c} \right] v_{x0} + \frac{\boldsymbol{\phi}_c^T T_{11}^{P6} T_3^{P6^{-1}} \boldsymbol{\phi}_c}{\boldsymbol{\phi}_c{}^T T_3^{P6^{-1}} \boldsymbol{\phi}_c} \sigma_{zz_0} \\ & + \left[\boldsymbol{\phi}_c^T \boldsymbol{T}_{12}^{P6} - \boldsymbol{\phi}_c^T T_{11}^{P6} T_3^{P6^{-1}} \boldsymbol{T}_4^{P6} + \frac{\boldsymbol{\phi}_c^T T_{11}^{P6} T_3^{P6^{-1}} \boldsymbol{\phi}_c \boldsymbol{\phi}_c^T T_3^{P6^{-1}} \boldsymbol{T}_4^{P6}}{\boldsymbol{\phi}_c{}^T T_3^{P6^{-1}} \boldsymbol{\phi}_c} \right] \sigma_{xz_0} \end{aligned} \tag{4.91}$$

Similarly, the shearing components of the output surface velocity and the stress can be expressed in terms of the input surface quantities as:

$$v_x = \left[\boldsymbol{T}_5^{P6^T} \boldsymbol{\phi}_c - \boldsymbol{T}_7^{P6^T} T_3^{P6^{-1}} T_1^{P6} \boldsymbol{\phi}_c + \frac{\boldsymbol{T}_7^{P6^T} T_3^{P6^{-1}} \boldsymbol{\phi}_c \boldsymbol{\phi}_c{}^T T_3^{P6^{-1}} T_1^{P6} \boldsymbol{\phi}_c}{\boldsymbol{\phi}_c{}^T T_3^{P6^{-1}} \boldsymbol{\phi}_c} \right] v_{z0} + \left[T_{33}^{P6} - \boldsymbol{T}_7^{P6^T} T_3^{P6^{-1}} \boldsymbol{T}_2^{P6} + \frac{\boldsymbol{T}_7^{P6^T} T_3^{P6^{-1}} \boldsymbol{\phi}_c \boldsymbol{\phi}_c{}^T T_3^{P6^{-1}} \boldsymbol{T}_2^{P6^T}}{\boldsymbol{\phi}_c{}^T T_3^{P6^{-1}} \boldsymbol{\phi}_c} \right] v_{x0} + \frac{\boldsymbol{T}_7^{P6^T} T_3^{P6^{-1}} \boldsymbol{\phi}_c}{\boldsymbol{\phi}_c{}^T T_3^{P6^{-1}} \boldsymbol{\phi}_c} \sigma_{zz_0} + \left[T_{36}^{P6} - \boldsymbol{T}_7{}^T T_3^{P6^{-1}} \boldsymbol{T}_4^{P6} + \frac{\boldsymbol{T}_7{}^T T_3^{P6^{-1}} \boldsymbol{\phi}_c \boldsymbol{\phi}_c^T T_3^{P6^{-1}} \boldsymbol{T}_4^{P6}}{\boldsymbol{\phi}_c{}^T T_3^{P6^{-1}} \boldsymbol{\phi}_c} \right] \sigma_{xz_0} \quad (4.92)$$

$$\tau_{xz} = \left[\boldsymbol{T}_{13}^{P6^T} \boldsymbol{\phi}_c - \boldsymbol{T}_{15}{}^T T_3^{P6^{-1}} T_1^{P6} \boldsymbol{\phi}_c + \frac{\boldsymbol{T}_{15}^{P6^T} T_3^{P6^{-1}} \boldsymbol{\phi}_c \boldsymbol{\phi}_c{}^T T_3^{P6^{-1}} T_1^{P6} \boldsymbol{\phi}_c}{\boldsymbol{\phi}_c{}^T T_3^{P6^{-1}} \boldsymbol{\phi}_c} \right] v_{z_0} + \left[T_{63}^{P6} - \boldsymbol{T}_{15}^{P6^T} T_3^{P6^{-1}} T_2^{P6} + \frac{\boldsymbol{T}_{15}^{P6^T} T_3^{P6^{-1}} \boldsymbol{\phi}_c \boldsymbol{\phi}_c{}^T T_3^{P6^{-1}} \boldsymbol{T}_2^{P6^T}}{\boldsymbol{\phi}_c{}^T T_3^{P6^{-1}} \boldsymbol{\phi}_c} \right] v_{x0} + \frac{\boldsymbol{T}_{15}{}^T T_3^{P6^{-1}} \boldsymbol{\phi}_c}{\boldsymbol{\phi}_c{}^T T_3^{P6^{-1}} \boldsymbol{\phi}_c} \sigma_{zz_0} + \left[T_{66}^{P6} - \boldsymbol{T}_{15}^{P6^T} T_3^{P6^{-1}} \boldsymbol{T}_4^{P6} + \frac{\boldsymbol{T}_{15}{}^T T_3^{P6^{-1}} \boldsymbol{\phi}_c \boldsymbol{\phi}_c^T T_3^{P6^{-1}} \boldsymbol{T}_4^{P6}}{\boldsymbol{\phi}_c{}^T T_3^{P6^{-1}} \boldsymbol{\phi}_c} \right] \sigma_{xz_0} \quad (4.93)$$

4.18 Closure

The transfer matrix for a plate like fluid layer, and for a thin plate, a solid layer, and a porous layer with bonded bonded and unbonded unboded face have been derive so far. In next chapter, it will be shown how to use this library of functions to deal with the modeling of a sandwich layer.

TF of a transversely solid layer has been derived by Brekhovskikh and Godin [31]. Unfortunately two entries of their matrix is incorrect. A correction of the matrix using their notation is given in the appendix. An anisotropic layer is not the topic of this research, the TF for such a layer with the current time convention which is different from the convention used by Brekhovskikh and Godin can easily be derived.

CHAPTER 5

Reduction and Homogenization of Layered Structures

5.1 Introduction

The response of complex structures are usually found by means of the traditional finite element method. However, as it was argued earlier, the application of the FEA is limited in the higher frequencies. As mentioned before, the EFEA can more efficiently capture the dynamic behavior of the structures and acoustic media computationally with less sensitivity to the details of the structure in the higher frequency range.

Like FEA, EFEA requires the structure to be discretesized. Meshing the individual layers of a sandwich structure by 3-D elements, is computationally very expensive and probably impossible (for FEA) and inaccurate for EFEA. The often used two dimensional shell elements, however are not accurate enough to account for the displacement and stress fields across the elements. This motivates the attempt to find an equivalent layer to reduce the computational hassle.

In this chapter, first the matrices for individual layers derived in the previous section are augmented into a 2 by 2 system transfer matrix between two acoustic media. An equivalent approximate layer with a virtual material properties will then be found to be used for the EFEA method.

5.2 Systematic reduction of a layered system

In the previous chapter, the TF for individual layers of common materials has been found. These matrices can be multiplied in the appropriate order to find the overall 2×2 matrix of the sandwich structure located between two acoustic media. To the best knowledge of the author's, the systematic treatment of a combination of layers has not been done when the layers include a porous material.

The procedure is as follows: After the structure sub-layers matrices are found, the system needs is separated into appropriate sub-systems. Second the equivalent BB TF's of these subsystems is found. Third these matrices are reduced to 2×2 matrices. Finally, the equivalent system TF is computed from the intermediate reduced matrices.

To determine the appropriate subsystems of a layered structure, as suggested in the first step, the set of layers which are bonded together with the first layer being UB and the last layer being BU, are bundled together as one subsystem. Suppose that there are p of these subsystems, each containing q_p bonded layers, in the layered structure.

Following the second step, consider bundle l of these subsystems. This batch contains q (for simplicity q is chosen instead of q_l)BB layers. When the compatibility and equilibrium conditions are applied, the 4×4 BB matrix for this subsystem is obtained as:

$$\begin{Bmatrix} \mathbf{v}_{l,2} \\ \boldsymbol{\sigma}_{l,2} \end{Bmatrix} = [\, T_{l,1} \,] \begin{Bmatrix} \mathbf{v}_{l} \\ \boldsymbol{\sigma}_{l} \end{Bmatrix}_{input} \tag{5.1}$$

$$\vdots$$

$$\begin{Bmatrix} \mathbf{v}_{l,q} \\ \boldsymbol{\sigma}_{l,q} \end{Bmatrix} = [\, T_{l,q-1} \,] \begin{Bmatrix} \mathbf{v}_{l,q-1} \\ \boldsymbol{\sigma}_{l,q-1} \end{Bmatrix} \tag{5.2}$$

$$\begin{Bmatrix} \mathbf{v}_{l,q} \\ \boldsymbol{\sigma}_{l,q} \end{Bmatrix}_{output} = [\, T_{l,q} \,] \begin{Bmatrix} \mathbf{v}_{l,q} \\ \boldsymbol{\sigma}_{l,q} \end{Bmatrix} \tag{5.3}$$

Combining the above relations leads to:

$$\begin{Bmatrix} \mathbf{v}_l \\ \boldsymbol{\sigma}_l \end{Bmatrix}_{output} = [\,T_{l,q}\,]\,[\,T_{l,q-1}\,]\,\ldots[\,T_{l,1}\,] \begin{Bmatrix} \mathbf{v}_l \\ \boldsymbol{\sigma}_l \end{Bmatrix}_{input} \tag{5.4}$$

Therefore:

$$[\,T_{l^{BB}}\,] = [\,T_{l,q}\,]\,[\,T_{l,q-1}\,]\,\ldots[\,T_{l,1}\,] \tag{5.5}$$

This means that the equivalent BB matrix for a subsystem is computed by left multiplying the consequent layer matrices, starting from the first layer.

Information regarding the absence of the shearing stresses on the input and output faces of this bundle can be employed to reduce the order of the BB matrix, as suggested in the third step. The last row of the subsystem equivalent BB matrix can be expanded as:

$$0 = T_{l\,(4,1)}\,v_{z_{(l,input)}} + T_{l\,(4,2)}\,v_{x_{(l,input)}} + T_{l\,(4,3)}\,\sigma_{zz_{(l,input)}} + T_{l\,(4,4)} \times 0 \tag{5.6}$$

If $T_{l\,(4,2)} = 0$, the normal velocity and stress on the input surface will be proportional and this is not necessarily compatible with the previous layer since each layer depends on the previous layers. Consequently, this system is not mathematically solvable. For well-posed problems, it is reasonable to assume that $T_l(4,2) \neq 0$; therefore:

$$v_{x_{(l,input)}} = -\frac{T_{l\,(4,1)}}{T_{l\,(4,2)}}\,v_{z_{(l,input)}} - \frac{T_{l\,(4,3)}}{T_{l\,(4,2)}}\,\sigma_{zz_{(l,input)}} \tag{5.7}$$

Hence:

$$\begin{Bmatrix} v_z \\ \sigma_{zz} \end{Bmatrix}_{l,out} = \begin{bmatrix} T_{l\,(1,1)} - \dfrac{T_{l\,(1,2)}\,T_{l\,(4,1)}}{T_{l\,(4,2)}} & T_{l\,(1,3)} - \dfrac{T_{l\,(1,2)}\,T_{l\,(4,3)}}{T_{l\,(4,2)}} \\ T_{l\,(3,1)} - \dfrac{T_{l\,(3,2)}\,T_{l\,(4,1)}}{T_{l\,(4,2)}} & T_{l\,(3,3)} - \dfrac{T_{l\,(3,2)}\,T_{l\,(4,3)}}{T_{l\,(4,2)}} \end{bmatrix} \begin{Bmatrix} v_z \\ \sigma_{zz} \end{Bmatrix}_{l,in} \tag{5.8}$$

At this point, the system is reduced to q 2×2 sub-matrices. Following the same logic of the second step, the final equivalent system matrix is obtained by left multiplication of the

consequent sub-layers matrices, starting from the first reduced subsystem, as:

$$[\,T_{sys}\,] = [\,T_p^{UU}\,]\,[\,T_{p-1}^{UU}\,]\,\ldots\,[\,T_1^{UU}\,] \tag{5.9}$$

where the right hand matrices are computed by means of the equation (5.8) for each subsystem.

5.3 Transmission loss calculation

A layered material structure that separates two half spaces of acoustic media can be reduced to an overall matrix $[T_{sys}]$ of the order 2×2. Considering equation (4.28), it is usual to assume that the incident velocity potential has a unit amplitude; i.e. $C^+ = 1$; denote the reflection by R_{ref}; i.e.: $R_{ref} \triangleq C^-$. Due to the radiation condition, there is no incoming wave from the transmitted side: $C^- = 0$; $T_{tr} \triangleq C^+$. The following simple relationship can be exploited to find R and T:

$$\begin{Bmatrix} T_{tr} \\ R_{ref} \end{Bmatrix} = \left[\begin{Bmatrix} i\,k_z \\ -i\,\omega\,\rho \end{Bmatrix}_{tr} e^{-i\,k_z\,L} \quad \vdots \quad [T_{sys}] \begin{Bmatrix} i\,k_z \\ i\,\omega\,\rho \end{Bmatrix}_{inc} \right]^{-1} [T_{sys}] \begin{Bmatrix} i\,k_z \\ -i\,\omega\,\rho \end{Bmatrix}_{inc} \tag{5.10}$$

In above equation, L is the total thickness of the structure. Subscripts "tr", "ref" "inc" and "tr" indicate transmitted, reflected, incident and transmitted sides respectively. Obviously the inverse of the 2×2 matrix can readily be determined in closed form.

The transmitted velocity pressure wave amplitude is a function of angle of incident. For a diffusive (random) acoustic media, it is customary to average the quantities over the solid angles by means of Paris law [50].When a probability distribution (weight function in averaging integral), $\mathcal{P}(\theta)$ for the incident waves is assumed, the transmission loss is computed as:

$$\overline{\tau} = \frac{\int_0^{\theta_{lim}} |T(\theta)|^2\,\mathcal{P}(\theta)\,\sin 2\theta\,d\theta}{\int_0^{\theta_{lim}} \mathcal{P}(\theta)\,\sin 2\theta\,d\theta} \tag{5.11}$$

$$TL = 10\log_{10}\frac{1}{\overline{\tau}} = -10\log_{10}\overline{\tau} \tag{5.12}$$

As an example Kang et al [51] used a Gaussian distribution to calculate the transmission

loss. If the directional distribution of the waves in is considered to be uniform, the averaging weight function in the integrand is simply 1.

5.4 A numerical example

To verify that the method proposed here is consistent with the available results in the literature, the transmission loss calculations for a UU panel consisting of an aluminum (a density of 2700 kg/m^3, a Young's modulus of 70 GPa, a Poisson's ratio of 0.33) of 1.27 mm thickness on the incident side, a 2.7 cm thick foam layer (solid phase density: 30 kg/m^3,solid phase Young's modulus: 0.8 MPa, damping loss factor: 0.265, solid phase Poisson's: 0.4; flow resistivity: 25000 $MKSRayls/m$; structural factor: 7.8; and porosity: 0.90) and an inner aluminum thin panel of thickness 0.762 mm is considered. This trim panel has been modeled by Bolton et al [30]. The transmission loss calculations are carried out by both of the direct method and the matrix method. As it is seen in figure 5.1 the results obtained by both methods are identical to the results reported by Bolton et al [30].

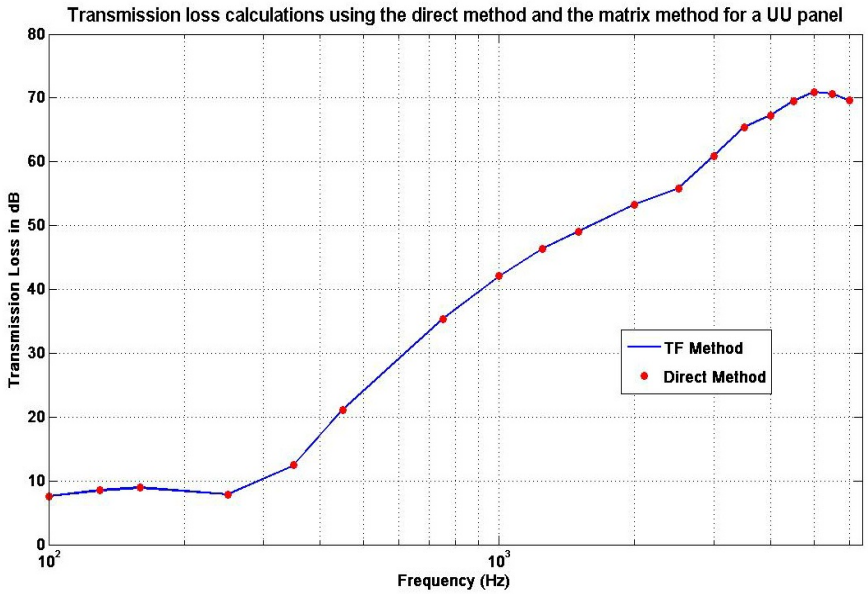

Figure 5.1: Verification of the matrix method for the UU panel reported by [30]

5.5 A comment on surface waves

The current work is not concerned with the surface waves since the individual layer responses are of no interest; however, the analysis can be used to study the surface waves as well. Surface waves are of great importance when guided and point sources are studied. Such studies have vast applications mainly in electro-acoustic devices, nondestructive testing and crack detection and seismic wave studies [31]. Mathematically, the TF for a system is a complex function of the individual layer material properties (e.g. density, wave speeds) and frequency. Therefore, such a function is discontinuous. The dispersion relation of the surface waves are determined by finding the poles and the discontinuities of TF. In fact by setting the determinant of the matrix for a layer, the admissible wave numbers for surface waves can be found. Usually the surface waves decay fast and are dispersive (however Gulyaev-Bluestien surface wave are nondispersive [31]). Some of the common surface waves are: Rayleigh waves (free solid layer surface), Stoneley waves (surface of a solid layer and a fluid layer), leaky waves (interface of two solid layers).

5.6 Homogenization and equivalent material

Finding an equivalent or effective layer replace to a sandwich structure enables one to break the complex structure into simpler elements and find the response by means of the traditional or energy finite elements.

5.6.1 Replacing the foam layer by an equivalent fluid

In the constitutive law of a porous layer material, one of the properties is flow resistivity. For common man made foam materials, this property is one of the most important parameters which characterizes the material. Flow resistivity is an indication of how air flows in between the pores of the porous material. To measure flow resistivity, a steady state flow of fluid (for the treatment materials air) is passed through a sample of the porous material. and the ratio of the pressure difference for the unit thickness is calculated as flow resistivity [47]. It has been shown empirically that in the commonly used foam material treatments,

flow resistivities and the surface impedances are related through some power laws Delany [43], Fellah [53], Tomilson [52]. Like any other empirical model, the validity of the model for different ranges of frequency is not clear. In such a model a fibreous foam layer can be replaced by an equivalent fluid layer. This equivalent fluid is characterized by adding an imaginary function that indicates a complex deviation of the density and wave speed from the values of air Cox [47]. It worths to note that the added complex parts differ from those of a dissipative model of fluids. The wave number of the equivalent fluid for foam has the following form (Delany [43] and Cox [47]):

$$k = \frac{\omega}{c_0}\left(1 + a_1\left(\frac{f}{\sigma}\right)^{n_1} - ia_2\left(\frac{f}{\sigma}\right)^{n_2}\right) \tag{5.13}$$

where a_1,a_2,n_1,n_2 are empirical constants and f and σ are frequency and the flow resistivity respectively. While the wave number of a dissipative fluid in the absence of thermal conductivity is obtained from:

$$k_{_I} = \frac{\omega}{c}\frac{1}{\sqrt{1 + \frac{i\omega(\zeta + 4/3\eta)}{\rho c_T^2}}} \tag{5.14}$$

where η and ζ are the first (shear) and second (volume) viscosities; c and $c_{_T}$ are the speed of sound for adiabatic and isothermal propagations respectively as derived by Brekhovskikh [?].

Replacing the foam layer by an equivalent fluid has been previously employed to model a treated panel. In particular, Lee and Kim [45] have adapted a similar approach to determine an equivalent fluid that defines the equivalent element properties for their FE analysis. They retained only one of the existing waves of the porous layer which dominates the other two waves. They chose the dominating wave according to some energy criteria. With the current approach, this equivalent layer can be adapted without going through their cumbersome calculations.

5.6.2 Equivalent layer for a layered structure

In this section, a very simple approach is considered in order to replace the layer structure with a simpler equivalent model.

As an example, the transfer matrix for a structure consisting of a thin plate (with impedance Z_1), a fluid layer (thickness z, wave number k_f and density ρ) and a second thin plate (with impedance Z_2) is found by multiplying the transfer matrices of the layers as:

$$\begin{bmatrix} \cos k_f z + \dfrac{ik_f \sin k_f z Z_2}{\omega \rho} & \dfrac{ik_f \sin k_f z}{\omega \rho} \\ i(Z_1+Z_2)\cos k_f z + \dfrac{i\rho\omega}{k_f}\left(1+\dfrac{Z_1 Z_2 k_f^2}{\rho^2\omega^2}\right)\sin k_f z & \cos k_f z + \dfrac{ik_f \sin k_f z Z_1}{\omega \rho} \end{bmatrix}$$

As can be seen the diagonal entries are not necessarily equal. This means that in general a combined panel cannot be replaced by one layer.

As a special case Brekhovskikh and Godin [31] have shown that a system of layers with periodicity can be replaced by an anisotropic transversely isotropic layer. Such a material has invariant properties along the planes parallel to the half space. The constitutive law of the material involves 5 different constants. Unfortunately, their matrix has some incorrect entries. The correct matrix is given in the appendix in their notation.

They analytically derived an "effective" layer for a periodic system of isotropic layer. The effective layer is now transversely isotropic with 5 Lamè's constants. These constants are computed as average of some functions of individual layers Lamè's constants [31].

As a good candidate to replace a layered structure, a transversely isotropic layer can be considered to replace a layered structure; however, further calculations show that even for such a layer, reducing the TF for this extended material model will produce the same entries on the diagonal entries. The calculations are omitted for the sake of brevity. Hence, mathematically, it is impossible to replace a layered structure even by a single layer of a transversely isotropic material.

If a set of equivalent material properties are found that minimizes the error of the entries of the equivalent layer TF and the reduced system to an admissible value, there is no guarantee that these properties (such as $\rho = \rho(\theta, f)$, $E = E(\theta, f)$,$\eta = \eta(\theta, f)$) after

averaging over the incident angle, give the same transmission loss as the reduced system for a particular frequency. Therefore, to find equivalent properties, one can solve an optimization problem which minimizes the difference between the transmission losses resulting from the chosen model and the layered structure. It should be noted that the existence of the solution of the optimization problem is not known a priori. Most likely there is not a unique answer to such problems and the models need to be studied case by case.

To find equivalent properties, here an optimization problem is proposed to be solved for each frequency. The following steps are necessary:

- Find the TF for the layered system for a particular frequency.
- Consider an appropriate equivalent model. For instance, two thin panels with a plate like fluid in between.
- Determine the properties. For example, for a thin plate/fluid/thin plate equivalent system, a typical set of parameters for the panels are: Young's modulus, damping loss factor, thickness, and density; the fluid properties will be the complex numbers speed of sound and the density.
- Fix some of the parameters accordingly. For instance, if the equivalent system is a single thin panel, the thickness and the Young's modulus can be fixed so that the equivalent captures the original structure behavior. For a thin plate/fluid/thin plate system, the plates properties can remain unchanged as the original outer and inner panels.
- Find a set of properties which minimize the transmission losses difference error. In other words, the cost function of the optimization problem is the absolute value of the difference in the transmission loss of the equivalent system and the original system. Commercially available programs like Matlab can handle the optimization problem.
- If a set of the properties is not found for a very complex structure, repeat the process by changing the unknown set of parameters.

5.6.3 A numerical example

(Rayl is the derived SI unit for acoustic impedance [54]); As mentioned, the optimization problem needs to be solved for each case separately. Acoustic and plate elements already are available in EFEA. To deal with the porous layer, an equivalent fluid or plate model needs to be found. In this section the following structure which is also considered by Bolton is reconsidered:

A trim panel consisting of an outer aluminum (a density of 2791.5 kg/m^3, a Young's modulus of 72.4 GPa, a Poisson's ratio of 0.33) of 0.02", a 2.7 cm foam layer (solid phase density: 30 kg/m^3,solid phase Young's modulus: 0.8 MPa, damping loss factor: 0.265, solid phase Poisson's: 0.4; flow resistivity: 25000 $MKSRayls/m$ structural factor: 7.8; and porosity: 0.90) and an inner aluminum thin panel of thickness 0.03 in.

It is possible to find the transmission loss of the structure by left multiplying the transfer matrix of the inner thin plate to the UU porous layer transfer matrix of the layer and finally by the out thin plate transfer matrix. In fact a replication of the Bolton's results and the matrix method shows that the methods calculate the identical results.

As discussed earlier, a single panel model is not proper for finding the equivalent element to be used by EFEA. Replacing the foam by the empirical equivalent fluid layer model is simply done by replacing UU porous layer matrix by a fluid plate like with the wave speed and density modified according to the empirical equivalent wave speed and density [52] from:

$$\rho^* = \rho_0 + \sqrt{-\frac{0.364}{(\rho_0 f/\phi)^2} - i\frac{0.1144}{\rho_0 f/\phi}} \tag{5.15}$$

$$c^* = \sqrt{\frac{101320}{\rho^*}\frac{29.64i + X^*}{21.17i + X^*}} \tag{5.16}$$

$$X^* = \sqrt{2.82\left(\frac{\phi}{\rho_0 f}\right)^2 + 24.9i\frac{\phi}{\rho_0 f}} \tag{5.17}$$

Finding the transmission loss for the panel by replacing the middle layer by a plate like fluid layer in the matrix method is now very easy. Figure (5.2)shows that in fact by replacing the foam layer by such equivalent layer,

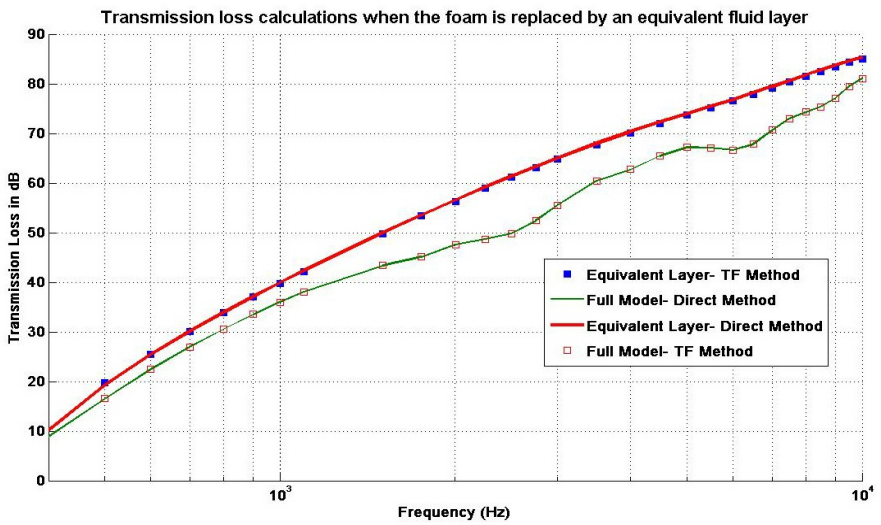

Figure 5.2: Equivalent fluid layer replacement for a UU panel

For this particular problem the equivalent layer properties to be found are considered the real and imaginary parts of the wave speed and the imaginary part of the filling layer density. The transfer matrix is now obtained by left multiplying the outer panel matrix, the equivalent layer (with 3 unknown properties) matrix and the inner panel matrix. The cost function of the optimization problem is defined as the difference between the transmission loss from the model of the layered system and the transmission loss calculated for this new system. For each frequency, the properties of the equivalent layer is found. The optimization results show that the difference between the transmission loss calculated from the porous layer model and the equivalent layer can be minimized to less than 1.2 dB if the add density is kept in [-200,-2] and the real part of the wave speed is kept in [65,300] and the imaginary part is kept within [1,50].

In other words, the foam is replaced by an air like gap. The optimization process adds damping properties to air and readjusts the wave speed and density so the final transmission loss of the new layer will be within an acceptable range of the treated layer.

CHAPTER 6

Conclusions and Future Work

6.1 Conclusions

The modeling of a trim panel in EFEA is divided into two parts: finding the vibrational power transmission coefficient for the connection between the outer and inner panel and the transmission loss through the layers directly.

To account for the power exchange through the connections or mounts, first the waves propagating in simple structural elements are represented by two dynamic matrices: one relating the wave amplitude vector to the displacements and one relating the forces to the wave amplitudes. A matrix method is proposed to solve for the outgoing wave fields. Using the wave solution, the corresponding vibrational power terms are found accordingly. The problem of a beam connected perpendicularly to an infinite plate is analyzed. Furthermore, the power exchange between two plates connected through a beam is find by setting up a system of equations. A closed formula for the power exchange is derived for the case when the plate have identical properties. Numerical examples showed that the new model is more sophisticated than the simple impedance method and at higher frequencies, the higher order modes and other wave types then bending (longitudinal and shearing waves) may also be important. The power transmission coefficients summed up to unity with a high order accuracy which indicates that the energy conservation in the system is maintained.

To calculate the transmission loss of the direct path through layers, layers are presented as matrices and a procedure for finding the transfer matrix for the layered structure is

proposed. It is concluded that a single isotropic layer cannot replace a system of layers with accuracy. An optimization procedure is proposed to replace the structure with a suitable model. For a numerical example, it is shown that a foam layer can be replaced by a viscous fluid plate (air like) layer if proper modifications to air properties are applied through the optimization process.

6.2 Future work

The following problems can be further investigated:

- The wave matrices for an anisotropic plate can be found. Finding such matrices are necessary to find the energy exchange of point connected anisotropic (like composite) plates.
- The rigid inclusion in the plate can be replaced with a flexible disk. This may have some influence on the power coefficients.
- The problem of a beam connected perpendicularly to another beam which is reinforcing a plate is another extension of the point connected structures.
- Derivation of the transfer matrices for different layers in cylindrical coordinate system can be useful in modeling layered curved panels.
- The transfer matrices for anisotropic layer can be derived and studied in order to find an equivalent layer replacing a layered structure. Such layers probably are good candidates for replacing a layered structure.
- It is worth to attempt to find an equivalent layer transfer matrix for a reinforced beam. Although the existence of such equivalent layer is not guaranteed.

APPENDIX

Appendix

The following is the correct [L] matrix for the transfer matrix of a transversely isotropic solid layer in Brekhovskikh's notation (see Brekhovskikh [31] page 153).

$$[L] = \begin{bmatrix} i\xi & i\xi & -i\alpha_2 & i\alpha_2 \\ v_3^{(1)} & -v_3^{(1)} & v_3^{(3)} & v_3^{(3)} \\ L_{3,1} & L_{3,1} & L_{3,3} & -L_{3,3} \\ \mu''\xi(iv_3^{(1)} - \alpha_1) & -\mu''\xi(iv_3^{(1)} - \alpha_1) & \mu''(i\xi v_3^{(3)} + \alpha_1^2) & \mu''(i\xi v_3^{(3)} + \alpha_1^2) \end{bmatrix}$$

where

$$\begin{aligned} L_{3,1} &= i(\lambda' + 2\mu')\alpha_1 v_3^{(1)} - \xi^2\lambda' \\ L_{3,3} &= i(\lambda' + 2\mu')\alpha_2 v_3^{(3)} + \xi\alpha_2\lambda' \end{aligned}$$

The incorrect $L_{3,3}$ in [31] is:

$$L_{3,3} = i(\lambda' + 2\mu')\alpha_2 v_3^{(3)} - \xi^2\lambda'$$

BIBLIOGRAPHY

BIBLIOGRAPHY

[1] Woodhouse, J.; "An introduction to statistical energy analysis of structural vibration"; Applied Acoustics, v.14; pp 455-469; 1981.

[2] Lyon, R.H. and Dejong, R.G. "Theory and Application of Statistical Energy Analysis"; Lyon Corp.; 1995

[3] Craik, R. J. M.; "Sound transmission through buildings: using statistical energy analysis"; Brookfield, Vt.: Gower, 1996.

[4] Bouthier, O.M. and Bernhard, R.J. ; "Models of space-averaged energetics of plates", American Institute of Aeronautics and Astronautics Journal v. 30 n.3 pp 34-44 1992

[5] Zhang, W.; Wang, A. and Vlahopoulos, N.; "An alternative energy finite element formulation based on incoherent orthogonal waves and its validation for marine structures"; Finite Elements in Analysis and Design v. 38; pp. 10951113; 2002.

[6] Vlahopoulos, N.; Garza-Rios, L. O. and Mollo, C.; "Numerical implementation, validation, and marine applications of an energy finite element formulation"; Journal of Ship Research, v 43, n 3; p 143-156; 1999.

[7] Hong,S. B. and Wang A. and Vlahopoulos, N.; "A hybrid finite element formulation for a beam-plate system"; Journal of Sound and Vibration Volume v. 298, n 1 pp 233-256 2006

[8] Cho, P.; "Energy 4ow analysis of coupled structures"; Ph.D. Dissertation, Mechanical Engineering Department, Purdue University, Lafayette, IN, 1993.

[9] Graff, K. F.; "Wave Motion in Elastic Solids"; Dover Publications, 1991.

[10] Redwood, M.; Mechanical Waveguides; Pergamon Press, New York 1960.

[11] Achenbach J.D.; "Wave Propagation in Elastic Solids". North-Holland, 1987.

[12] Cremer, L.; Heckl, M. and Petersson B.A.T. ;"Structure-Borne Sound: Structural Vibrations and Sound Radiation at Audio Frequencies Structure-Borne Sound: Structural Vibrations and Sound Radiation at Audio Frequencies"; 3rd edition; Springer, 2005.

[13] Banerjee, J.R.; "Development of an exact dynamic stiffness matrix for free vibration analysis of a twisted Timoshenko beam"; Journal of Sound and Vibration, v 270, n 1-2, p 379-401; 2004.

[14] Langley, R.S. and Shorter, P.J.; Diffuse wavefields in cylindrical coordinates; Journal of the Acoustical Society of America, v 112, n 4, 2002, pp 1465-1470.

[15] Leissa R.W.; "Vibration of Plates"; Acoustical Society of Ameirca; 1993.

[16] Szilard, R.; Theories and applications of plate analysis: classical, numerical, and engineering methods; John Wiley, Hoboken, N.J.; 2004.

[17] Morfey, C.L.; "Cylindrical in-plane waves in an elastic plate"; Journal of Sound and Vibration, v 173, n 4, p 557-60, 1994.

[18] Ljunggren, S.; Generation of waves in an elastic plate by a vertical force and by a moment in the vertical plane; Journal of Sound and Vibration, v 90, 1983, pp. 559-584.

[19] Ljunggren, S.; Generation of waves in an elastic plate by a torsional moment and horizontal force; Journal of Sound and Vibration, v 93, n 2, 1984, pp 161-187.

[20] Leung, R.C.N. and Pinnington, R.J.; "Point inertance of an infinite plate with respect to a force acting in its plane"; Journal of Sound and Vibration, v 111, n 1, 1986, pp 125-129.

[21] Pinnington, R.J; "Point inertance of an infinite plate with respect to a force acting in its plane"; Journal of Sound and Vibration, v 111, n 1, 1986, pp 125-129.

[22] Dyer, I.; Moment impedance of plates; Journal Acoustical Society of America , v 32, n 10, 1960, pp 1290-1297.

[23] Thomas, D.A.; Mechanical impedances for thin plates; Journal of Acoustical Society of America, v 32, n 10, 1960, pp 1302-1304.

[24] Langley, R.S. and Shorter, P.J.; "The wave transmission coefficients and coupling loss factors of point connected structures"; Journal of the Acoustical Society of America, v 113, n 4, p 1947-64,2003.

[25] Attenborough,K.; "Acoustical characteristics of porous materials"; Physics Reports v. 82, n. 3 pp 179-227; 1982.

[26] Cederbaum, G.; Li, L. and Schulgasser, K.; Poroelastic structures; Elsevier, Amsterdam, New York; 2000.

[27] Biot, M. A.; "Theory of propagation of elaastic waves in a fluid saturated porous solid, part I and II; Journal of Acoustical Society of America; v. 28; n; pp 156-191; 1956

[28] Allard, J.-F. Propagation of sound in porous media: modeling sound absorbing materials; Elsevier Applied Science, London, New York, 1993.

[29] Theodorakopoulos D.D. and Beskos, D.E.," Flexural vibrations of poroelastic plates"; Acta mechanica; v 103, n1, pp 191 -203.

[30] Bolton, S. J.; Shiau, N.M., and Kang, Y.J.; "Sound transmission through multi-panel structures lined with elastic porous materials"; Journal of Sound and Vibration; v 191 n. 3, pp 317-347, 1996

[31] Brekhovskikh, L.M. and Godin, O.A. Acoustics of Layered Media I Plane and Quasi-Plane Waves; Springer-Verlag Berlin Heidelberg; 1990

[32] Nayfeh, A. H.; "Wave Propagation in Layered Anisotropic Media with Application to Composites" Elsevier Sceinces B.V., The Netherlands, 1995.

[33] Allard, J.-F., Brouard, B., and Lafarge, D. "Reciprocity and antireciprocity in sound transmission through layered materials including elastic and porous media"; Wave Motion; v 17, pp 329 -335.

[34] Rudgers, A.J., "Equivalent networks for representing the two-dimensional propagation of dilatatitaional and shear waves in infinite elastic plates and in startified elastic media" Journal of Acoustical Society of America, v. 91, n. 1, pp 28-38.

[35] Cerevenka, P. and Challande, P., "A new efficient algorithm to compute the exact reflection and transmission factros for plane waves in layered absoring media (liquids and solids)" Journal of Acoustical Society of America, v. 89, n. 4, pp 1579-1589

[36] Folds, D.L. and Loggins, C.D., "Transmissiom and reflection of ultrasonic waves in layered media" Journal of Acoustical Society of America, v. 62, n. 5, pp 1102-1109.

[37] Moore, J. A., Lyon, R. H."Resonant porous materials absorbers"; Journal of Acoustical Society of America; v 72, n6 pp 1989 -1999; 1982.

[38] Brouard, B.; Lafarge, D. and Allard, J.-F."A general method of modelling sound propagation in layered media"; Journal of Sound and Vibration, v 183, n 1, pp 125-142; 1995.

[39] Allard, J-F, Bourdier,R, and Depollier, C.; "Biot waves in layered media"; Journal of Applied Physics; v 60, n15, pp 1926 -1929.

[40] Allard, J-F, Depollier, C., and Rebillard, P.; "Inhomogenous Biot waves in layered media"; Journal of Applied Physics; v 66, n6, pp 2278 -2284.

[41] Deresiewicz, H. and Skalak, R.; On uniqueness in dynamic poroelasticity; Bulletin of Seismological Society of America, v 53, 1963, pp 783-788.

[42] Gurevich ,B. and Schoenberg ,M.; Interface conditions for Biot's equations of poroelasticity; Journal of the Acoustical Society of America, v 105, n 5, pp. 2585-2589.

[43] M. E. Delany M.E. and Bazley E. N.; "Acoustical properties of fiberous absorbent materials"; Applied Acoustics, v3 pp 105-116, 1970.

[44] Cox, T. J. and D'Antonio, Acoustic Absorbers and Diffusers: Theory, Design, and Application; Taylor and Francis 2004

[45] Lee, J. and Kim, J.; "Simplified method to solve sound transmission through structures lined with elastic porous material"; Journal of the Acoustical Society of America, v 110, n 5, pp. 2282-2294.

[46] Lyon, R.H. and Eichler, E.; Random vibration of connected structures; Journal of Acoustical Society of America, v 36, n 7, 1964, p 1345.

[47] Cox, T. J. and D'Antonio, Acoustic Absorbers and Diffusers: Theory, Design, and Application; Taylor and Francis 2004

[48] Fritz, J.; "Partial Differential Equations" 4th ed. Springer, 1991

[49] Wang, C.M., Reddy, J.N., and Lee, K.H. ; Shear deformable beams and plates; Elsevier Sciences, UK; 2000.

[50] Mulholland, K.A., Parbrook, H.D. and Cummings, A.; The transmission loss of double panels; Journal of Sound and Vibration, v 6, n 3, 1967, pp 324-334.

[51] Kang, H.-J. , Ih, J.-G., Kim, J.-S., and Kim, H.-S.; Prediction of sound transmission loss through multilayered panels by using Gaussian distribution of directional incident energy; Journal of the Acoustical Society of America, v 107, n 3, 2000, pp 1413-1420

[52] Tomilson, D.; Craik R.J.M. and Wilson,R. "Acousti c radiation from a plate into a porous medium"; Journal of Sound and Vibration; v. 273, n1 pp 33-49, 2004.

[53] Fellah, Z.E.A.; Mitri, F.G.; Depollier, C.; Berger, S.; Lauriks, W. and Chapelon, J.Y.; "Characterization of porous materials with a rigid frame via reflected waves"; Journal of Applied Physics. v. 94, n15 ppp 7914-7922; 2003.

[54] Mills, N.; "Polymer Foams Handbook: Engineering and Biomechanics Applications and Design"; Butterworth-Heinemann; 2007.